universität wien

MASTERARBEIT / MASTER'S THESIS

Titel der Masterarbeit / Title of the Master's Thesis

„The role of the SR-BI receptor in 3D cell culture models of melanoma invasion "

verfasst von / submitted by

Maria Vallianou, BSc

angestrebter akademischer Grad / in partial fulfilment of the requirements for the degree of

Master of Science (MSc)

Wien, 2018 / Vienna 2018

Studienkennzahl lt. Studienblatt / degree programme code as it appears on the student record sheet:	A 066 834
Studienrichtung lt. Studienblatt / degree programme as it appears on the student record sheet:	Masterstudium Molekulare Biologie
Betreut von / Supervisor:	Assoc. Prof. Mag. Dr. MAS Mario Mikula

Acknowledgements

Firstly, I would like to express my gratitude to Assoc. Prof. Dr. MAS Mario Mikula for giving me the opportunity to work in his research group and for his endless patience, advice and guidance during this project.

My deepest thanks go to Msc. Katharina Kinslechner for supervising me during my practical work in the laboratory and for her help and constructive advice.

I also owe a great thank you to my colleagues at the Institute for Medical Genetics and most of all to the other lab members David, Birgit, Jelena for always answering my questions and for their help. I would like to also thank Assoc. Prof. Dr. Helmut Dolznig and his research group for the support they provided on the 3D cell culture topic.

Last but not least, I owe my deepest gratitude to my parents and my family. I would have never come so far without them.

Table of Contents

Abstract

New melanoma cases are being diagnosed every year with increasing frequency. Despite the therapeutic advances in skin cancer, mortality rates of patients with metastatic melanoma have not been significantly decreased. Recently, the association between the HDL receptor SR-BI and cancer progression has been reported in breast and prostate tumors. Accordingly, this study aimed to investigate the role of SR-BI expression in melanoma progression and invasion. In order to mimic the *in vivo* setting of solid melanoma tumors, six melanoma cell lines were taken to generate 3D cell culture models. Cells expressing the SR-BI receptor demonstrated significantly increased invasion into a collagenous matrix when compared to cells with SR-BI knock-down. SR-BI gene ablation also resulted in altered expression of crucial genes involved in cancer development and in the EMT process. More specifically, our results indicated a positive correlation between VEGFA, SNAIL2 and SR-BI expression. Protein glycosylation, which has been reported to be elevated in metastatic cells in the process of EMT, was also reduced upon SR-BI gene ablation. Furthermore, expression of cell adhesion- and ECM synthesis-associated genes like E-Cadherin and *CTGF* was shown to increase in SR-BI knock-down cells. These findings thus led to the conclusion that SR-BI expression might promote melanoma invasion and metastasis by upregulating the EMT process, by suppressing cell adhesion and by remodeling ECM components. In summary, this study provides significant evidence proposing a role for SR-BI expression in melanoma tumor progression. Future studies could provide more conclusive data about the HDL receptor as a promoting factor in malignancy and thus render SR-BI a promising diagnostic tool or therapeutic target.

Zusammenfassung

Neue Melanomfälle werden jedes Jahr mit zunehmender Häufigkeit diagnostiziert. Trotz der therapeutischen Fortschritte bei Hautkrebs sind die Mortalitätsraten von PatientInnen mit metastasierendem Melanom nicht reduziert. Vor kurzem wurde über den Zusammenhang zwischen dem HDL-Rezeptor SR-BI und der Krebsprogression bei Brust- und Prostatakrebs berichtet. Dementsprechend zielte diese Masterarbeit darauf ab, die Rolle der SR-BI-Expression in der Melanom-Progression und Invasion zu untersuchen. Um die *in-vivo* Verhältnisse von soliden Melanomtumoren nachzuahmen, sechs verschiedene Melanom-Zelllinien wurden verwendet um 3D-Zellkulturmodelle zu generieren. Zellen, die den SR-BI-Rezeptor exprimierten, zeigten im Vergleich zu Zellen mit SR-BI knock-down eine signifikant erhöhte Invasion in eine Kollagenmatrix. Die SR-BI Genablation führte auch zu einer veränderten Expression wichtiger Gene, die an der Krebsentwicklung und am EMT-Prozess beteiligt sind. Insbesondere zeigten unsere Ergebnisse eine positive Korrelation zwischen der VEGFA-, SNAIL2- und SR-BI-Expression. Die Glycosylierung von Proteinen, die in metastatischen malignen Zellen im Verlauf von EMT erhöht ist, wurde ebenfalls durch die SR-BI Genablation verringert. Darüber hinaus wurde gezeigt, dass die Expression von Zelladhäsions- und ECM-Synthese-assoziierten Genen wie E-Cadherin und CTGF in SR-BI knock-down Zellen zunimmt. Diese Ergebnisse führten zu der Schlussfolgerung, dass die SR-BI Expression die Melanom-Invasion und Metastasierung durch Hochregulierung des EMT-Prozesses und durch Unterdrückung der Zelladhäsion und Modulierung der ECM-Synthese fördern könnte. Zusammengefasst liefert diese Studie signifikante Beweise, die die Rolle der SR-BI-Expression bei der Melanom-Tumorprogression bekräftigen. Zukünftige Studien könnten weitere schlüssige Daten über die Rolle des HDL-Rezeptors als pro-malignen Faktor liefern und somit SR-BI zu einem vielversprechenden Molekül in der Diagnostik und/oder Therapie des malignen Melanoms machen.

1. Introduction

1.1 Malignant melanoma

1.1.1 Epidemiological data

Melanoma is a skin cancer type, which is considered as a deadly disease when not diagnosed in an early stage. [1] Although considered a rare form of cancer, the incidence of melanoma has significantly increased over the past decades. [2] An annual number of 232,000 newly diagnosed melanoma cases are reported by the World Health Organization and despite the emergence of new enhanced therapeutic methods, melanoma accounts in its advanced form for 55,000 deaths per year worldwide. [3]

One of the most important triggers of melanoma development is ultraviolet radiation (UV). UV radiation has also been officially classified by the International Agency for Research on Cancer (IARC) as a Group 1 carcinogen to humans. Extended exposure to UV radiation through solar radiation often resulting in sunburns has been confirmed to increase the risk of melanoma development. Other factors such as pale skin type (Fitzpatrick skin types I and II), melanocytic naevi number, dysplastic naevi presence on the skin and occurrence of melanoma within a family can also contribute to a high risk of melanoma development in humans (Figure 1). [4]

1. INTRODUCTION

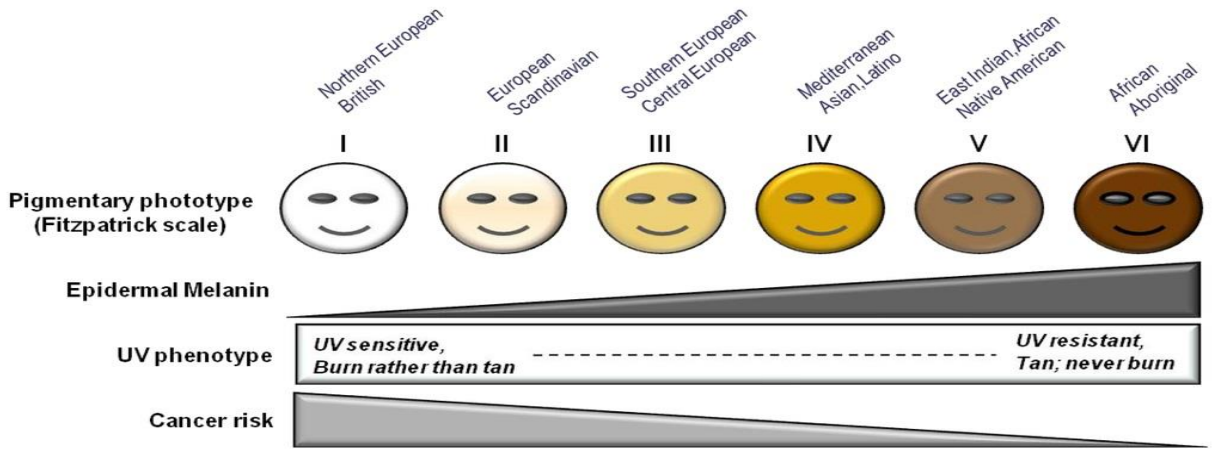

Figure 1: Pigmentation level and skin cancer risk; picture taken from [5] with permission. (Creative Commons Attribution License-CC BY: https://creativecommons.org/licenses/by-nc-nd/3.0/) Melanin levels define the UV phenotype of each individual. Northern European individuals with fair skin are susceptible to sunburn and skin damage leading to skin cancer while dark-skinned individuals display UV radiation resistance with lower skin cancer risk.

However, the recent facts about melanoma and the crucial role of UV radiation in melanoma epidemiology highlighted the importance of public health standards such as sun protection and sunburn avoidance (Figure 2). Campaigns involving public health messages about sun avoidance and melanoma risk were thus subsequently further improved and promoted. [4, 6]

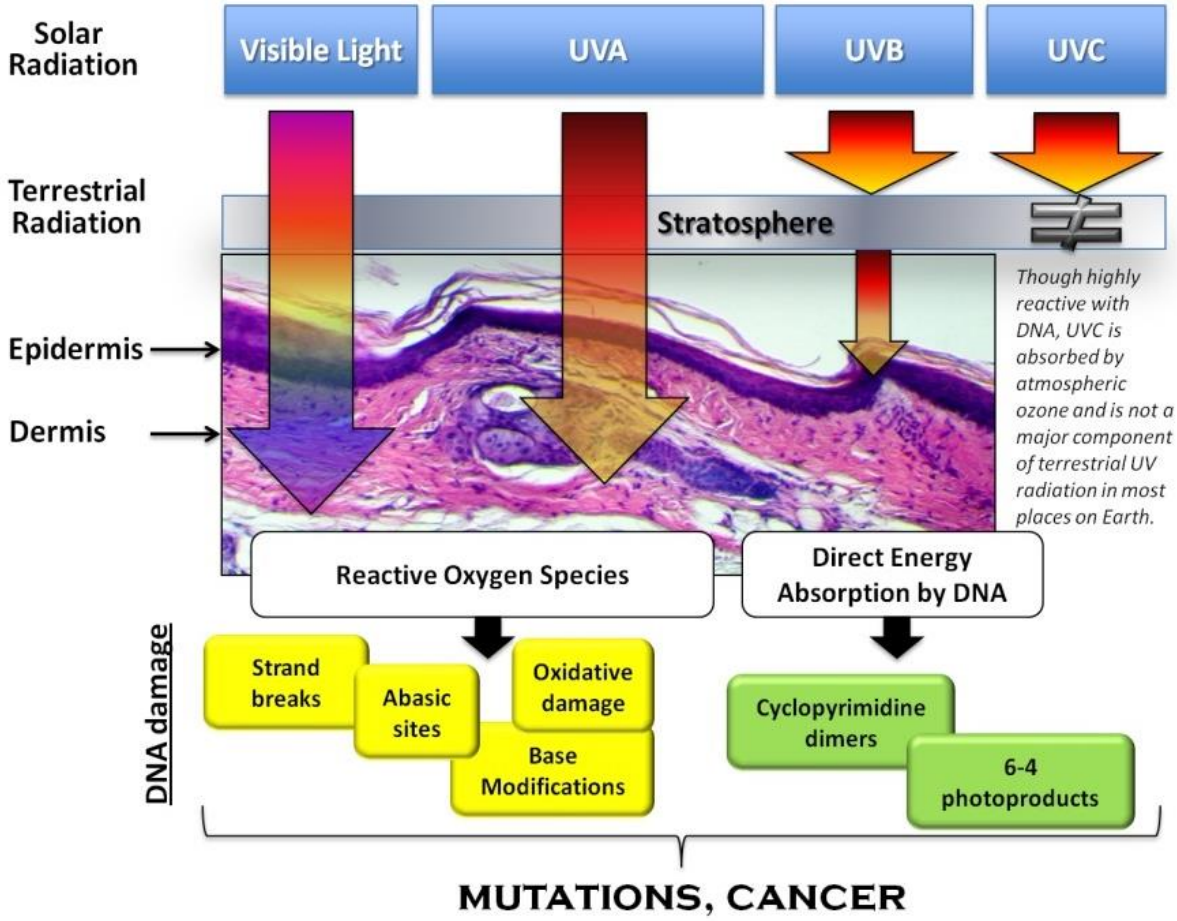

Figure 2: Solar radiation and its biologic effect on human skin; picture taken from [7] with permission.(© 2013 D'Orazio JA, Jarrett S, Marsch A, Lagrew J, Cleary L. Published in [7] under CC BY 3.0 license. Available from:http://dx.doi.org/10.5772/55172.)
Solar radiation is divided into visible light, UVA, UVB and UVC radiation. Visible light and UVA have a higher skin penetration potential reaching the derma stratum papillare with the ability to damage the DNA by reactive oxygen species generation. UVB radiation cannot reach further than the epidermis but can directly affect the DNA causing molecular alteration. All solar radiation components reaching the skin can thus be responsible for mutations and skin cancer development.

The mortality of malignant melanoma is mostly attributed to a high metastatic rate compared to other skin tumors, thus detection at an early stage of the disease followed by appropriate treatment are of crucial importance. [2]

In order to evaluate the potential of a melanocytic neoplasm to develop into a malignant lesion, samples are usually examined by histopathological techniques, which are the most common diagnostic tools (Figure 3). However, the accuracy of these techniques is limited when it comes to

an accurate assessment of the malignant potential and the classification of the lesions. The recent emergence of biomarkers may present a solution to this problem, as their integration in diagnostic processes could reveal further information about the development of malignant lesions in each individual case. [6]

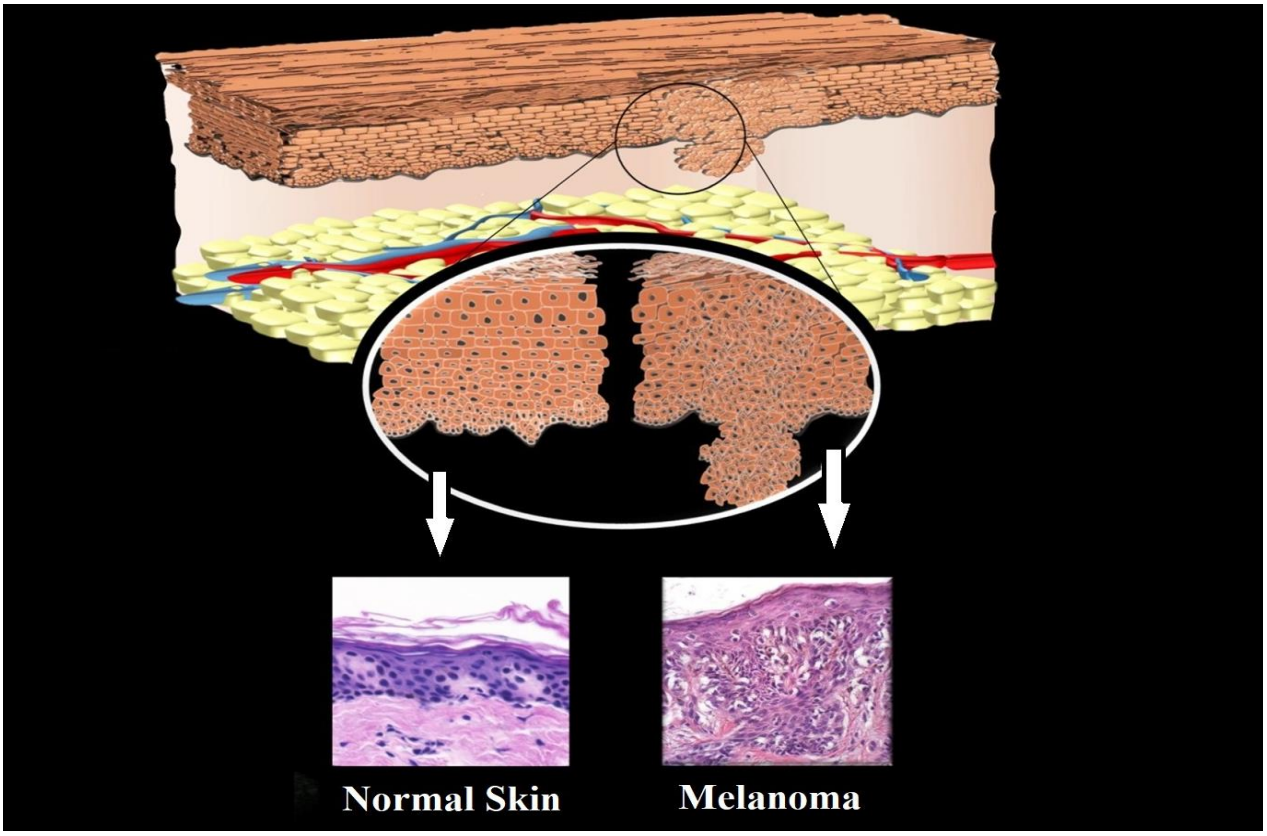

Figure 3: Hematoxylin and eosin (H&E) histopathological staining technique in melanoma diagnosis; picture adapted from [8] with permission from the National Institute of Biomedical Imaging and Bioengineering.

Distinct morphological patterns can be observed in a stained sample of healthy skin (left) while melanoma samples display asymmetrical patterns of cell layers consisting of cells with an atypical form (right).

1.1.2 Development of melanoma-classification and stages

Malignant melanocytic neoplasms, described as melanomas stem from the neural crest-derived cells called melanocytes. Melanocytes are located in the basal epidermis, where they divide

infrequently while providing the pigment molecule melanin to keratinocytes. The stimulating factor of melanin production as well as melanocyte proliferation is the damage in keratinocytes caused by UV radiation, which causes the secretion of an α-melanocyte stimulating hormone (αMSH) in a p53-dependent manner. [9] The role of melanin is to absorb the UV radiation and to protect the keratinocytic nucleus from UV radiation damage. Melanocytes constitute therefore a pivotal part of the defense mechanism protecting the organism from DNA damage, which is induced by UV radiation. However, after the acquisition of certain initiating mutations, melanocytes can proliferate creating a naevus. After a naevus is formed, melanocytes usually enter a senescence-like state, where they rarely proliferate. [6] Yet, it has been reported that some melanocytes that are present in naevi maintain their proliferative ability and can undergo mitosis [10] when exposed to specific stimuli such as UV radiation [11], pregnancy [12] and immunosuppression [13].

Benign naevi can subsequently give rise to dysplastic naevi, a reported intermediate melanocytic neoplasm with a malignant potential between that of common naevi and that of unequivocal melanoma. Dysplastic naevi can also arise *ex novo* in a new location and consist of lesions sharing benign and malignant histopathological features, which usually prevent a clear pathological diagnosis leading to diagnostic variation between observers. Regardless of their unclear malignant potential, it has been observed that dysplastic naevi demonstrate a higher overall mutational burden than common naevi. [6]

As described in the Clark model for development of malignant melanoma (Figure 4), the progression of melanoma principally includes the stepwise transformation of a benign naevus to dysplastic naevus followed by its transformation to melanoma *in situ* and then into invasive and metastatic melanoma. [6, 14]

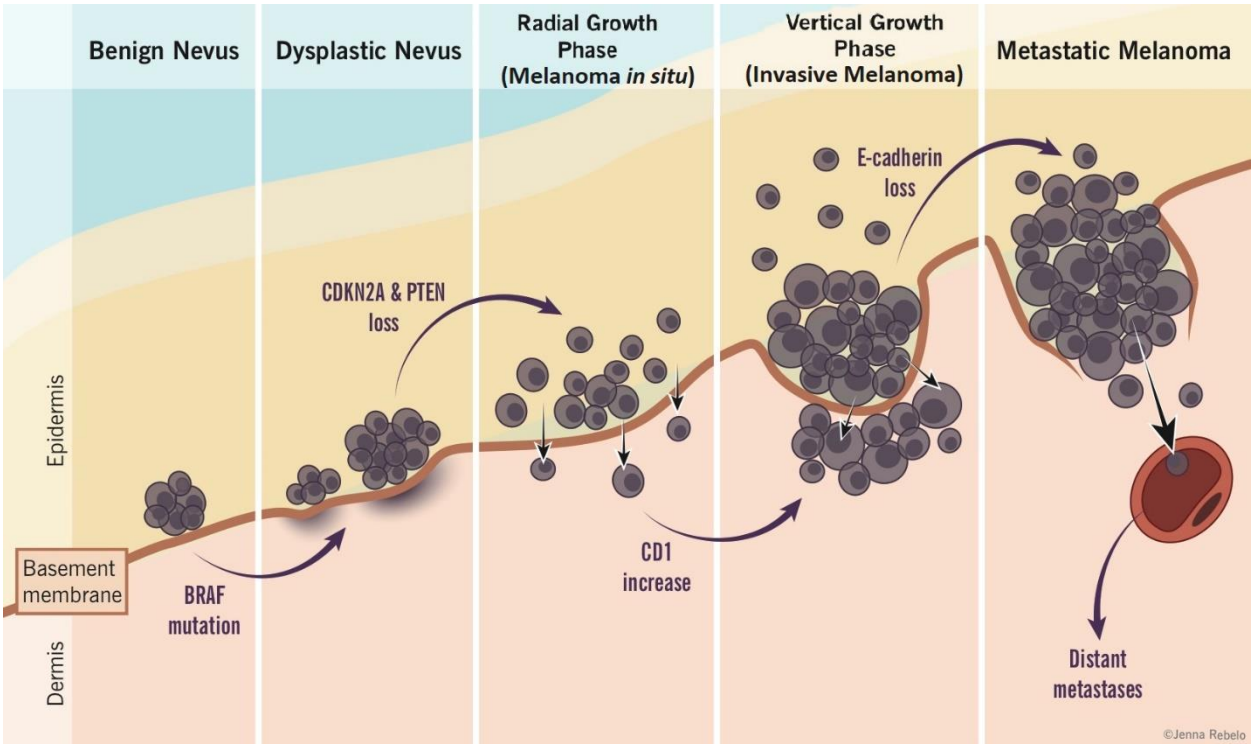

Figure 4: Melanoma progression stages based on Clarks' model; picture adapted from [15]. (Modified with permission from Jenna Rebelo, Eric Wong, and Sultan Chaudhry. McMaster Pathophysiology Review, www.pathophys.org.)
According to Clark's model, melanoma development is initiated by the transformation of a benign naevus to a dysplastic naevus. Following steps include the superficial growth (melanoma in situ), vertical growth (invasive form of melanoma) and distant spreading of melanoma cells, resulting in metastases.

Clark's classification of malignant melanoma (Figure 5), established in the 1970s and officially applied in the current World Health Organization (WHO) classification of skin tumors, divides melanoma in four main types: 1) superficial spreading melanoma (SSM) 2) lentigo maligna melanoma (LMM) 3) nodular melanoma (NM) 4) acral lentiginous melanoma (ALM) [16].

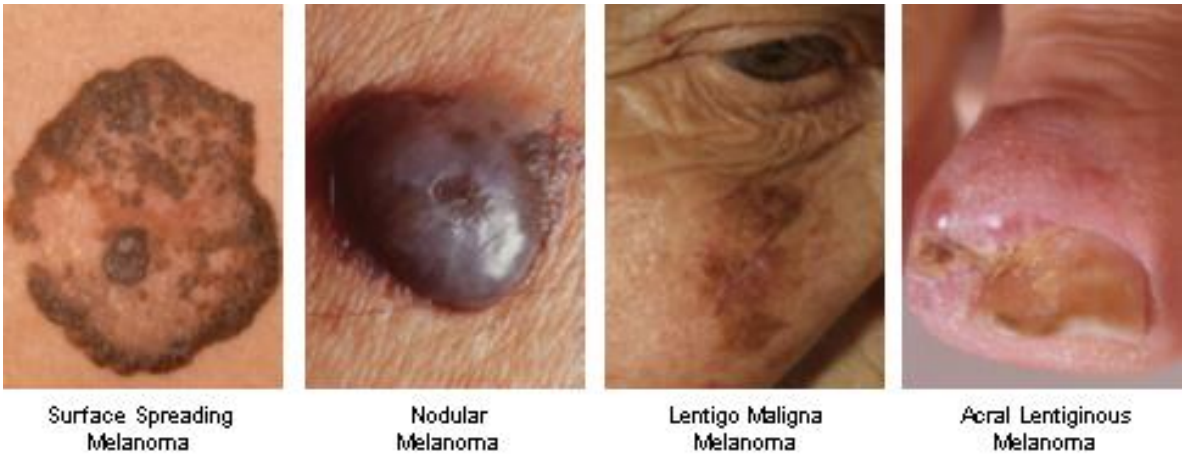

Figure 5: Clark's malignant melanoma classes; picture takem from [17].
The four classes of melanoma, as described by the Clark's model consist of the most common cutaneous melanoma class named superficial spreading melanoma (SSM), the second most common cutaneous melanoma class described as nodular melanoma (NM), the lentigo maligna melanoma (LMM), which is most commonly found on sun-exposed skin in the elderly and the acral lentiginous melanoma (ALM), which occurs on palms, soles, and subungual regions.

This classification model, which relies on microscopic growth patterns and clinical features of the disease (anatomical site of primary tumor, patient age) was revised by Boris Bastian and his colleagues in their effort to include somatic genetic alterations into a new melanoma classification system [18]. In their classification system a pattern of genetic mutations and chromosomal abnormalities in the *BRAF*, *NRAS* and *KIT* oncogenes was reported correlating with the primary tumor site as well as with the chronic sun-induced skin damage degree. Subsequently four melanoma groups were established based on the reported facts. [16] Melanoma was classified by Boris Bastian and his colleagues into the four groups depending on its presence on: skin with chronic sun-damage (CSD melanoma), skin without chronic sun-damage (non-CSD melanoma), skin on palms, soles and nail bed (acral melanoma), and mucous membrane (mucosal melanoma). [18]

The new classification system of Boris Bastian shows a correlation to Clark's classification system. The most common types of melanoma: CSD and non-CSD melanoma, practically correspond to the LMM and SMM melanoma classes, respectively. Similarly, acral melanoma according to Boris Bastians' system corresponds to Clark's ALM. The NM class was not included in Boris Bastians' system since the nodular melanoma (NM) class shows no specific features such as characteristic anatomical sites and distinct genetic alterations. [16]

1. INTRODUCTION

Depending on the origin of melanoma from chronically sun damaged (CSD) or non- chronically sun damaged (non-CSD) skin, melanoma lesions can greatly vary in aspects including: the site of origin on the human body, the degree of overall exposure to ultraviolet (UV) radiation, patient age, mutational burden and mutation types [19-21]. As illustrated in Figure 6, the most common origin sites of CSD melanoma are usually the dorsal part of distal extremities as well as upper body parts of individuals exceeding 55 years of age with skin exhibiting signs of long-term exposure to UV radiation (such as solar elastosis). The mutational burden of such lesions is quite high and often associated with *NF1*, *NRAS*, $BRAF^{nonV600E}$ and *KIT* mutations. On the contrary, non-CSD melanoma is of a lower mutational burden with mainly $BRAF^{V600E}$ mutations and located on body areas with decreased sun-exposure of younger individuals. [6] (Figure 6)

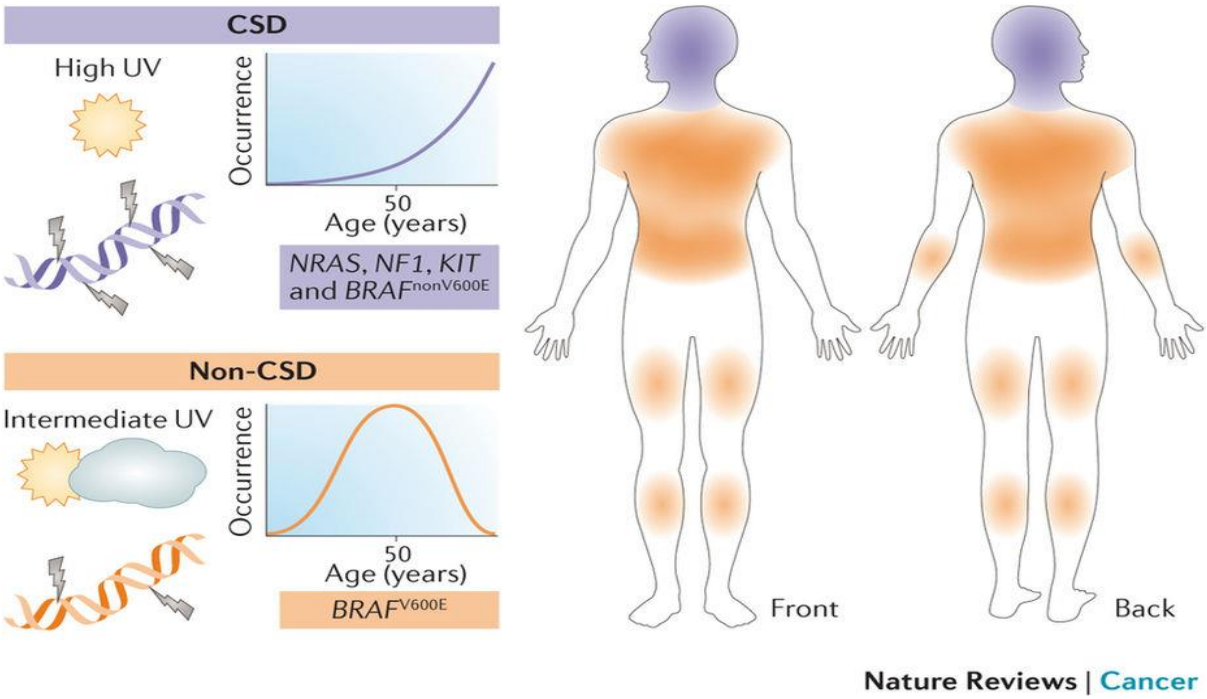

Figure 6: Chronically sun damaged (CSD) and non- chronically sun damaged (non-CSD) skin melanoma and its properties; picture taken from [6] with permission (License Number: 4312040032727).

Sun-induced damage on skin plays a crucial role in induction of genetic mutations and subsequently in the development of the specific melanoma types. CSD melanoma is associated with NRAS, NF1, KIT and BRAF^{nonV600E} mutations, late age onset and typically appears on the head and neck skin areas. In contrast, non-CSD melanoma appears on skin with intermediate sun exposure and damage, has an onset in younger age of the individuals and is associated with BRAF^{V600E} mutations.

1.1.3 Melanoma in situ

The invasive forms of CSD and non-CSD melanoma is usually preceded by the *in-situ* melanoma, however non-CSD melanomas display a strong evolutionary relationship to common naevi [22, 23]. The *in-situ* melanoma consists of melanocytes with increased nuclei size, which proliferate and expand irregularly in the epidermis. Its growth pattern can be sub-divided into: the pagetoid pattern and the lentiginous pattern, each growth pattern correlating with either the non-CSD or CSD melanoma form as well as with different genetic mutations in the affected melanocytes. While the genetic mutation *BRAF*^{V600E} is mainly associated with the pagetoid growth pattern and

subsequently with the non-CSD melanoma class that spreads superficially, lesions spreading in a lentiginous growth pattern are never associated with the *BRAF*^{V600E} mutation and progress to form a CSD-type melanoma with single melanocyte groups dispersed in the basilar epidermis area. Melanoma *in situ* of the acral and mucosal melanoma group also grows in a lentiginous pattern. [6] The lentiginous type of *in situ* melanoma, also named lentigo maligna melanoma, unlike the non-CSD melanoma, is rarely preceded by a naevus, as it usually emerges *ex novo* on sun damaged skin (CSD type melanoma) [24]. It can superficially spread on skin for several years before it enters the invasive state. On the contrary, when originating from naevi, melanoma *in situ* grows from an intra-epidermal source and expands in a pagetoid pattern. Its formation is induced by melanocytes located superficially on naevi and which primarily acquire their malignant potential after undergoing mutations caused by UV radiation. [6] Genetic alterations that are usually observed in *in situ* melanoma lesions include mutations in the *TERT* promoter, heterozygous alterations in the *CDKN2A* gene and mutations interfering with the MAPK pathway most commonly in the *BRAF*, *NF1* and *NRAS* genes (Figure 7) [25].

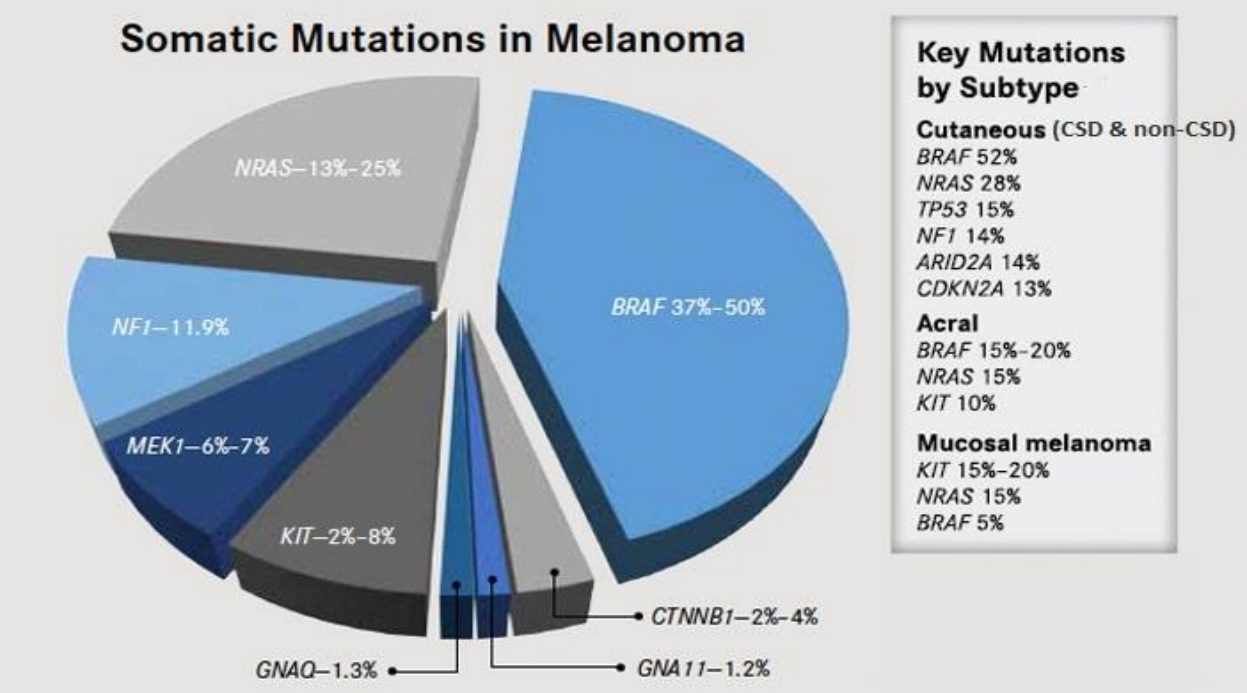

Figure 7: Genetic mutations associated with the cutaneous, acral and mucosal melanoma subtypes; picture adapted from [26] with permission from OncLive.com.
BRAF and NRAS mutations are the most frequent mutations occurring in all melanoma subtypes followed by NF1 mutations. The CSD and non-CSD types of cutaneous melanoma are also mostly correlated to BRAF, NRAS, TP53, NF1, ARID2A and CDKN2A mutations while the acral melanoma subtype is mostly associated with BRAF, NRAS and KIT mutations. Most cases of mucosal melanoma exhibit KIT and NRAS mutations.

Pathogenic genetic mutations are induced and increase in their number over an extended time frame [27] resulting into the slow development of *in situ* melanoma, which usually arises when the affected individuals have reached a late age [6]. Melanoma can be present for many years in its *in situ* form before transforming into invasive melanoma [28]. This fact can confirm the assumption that the invasive potential of melanoma is only acquired through essential mutations, which are additionally induced over time (Figure 8) [6].

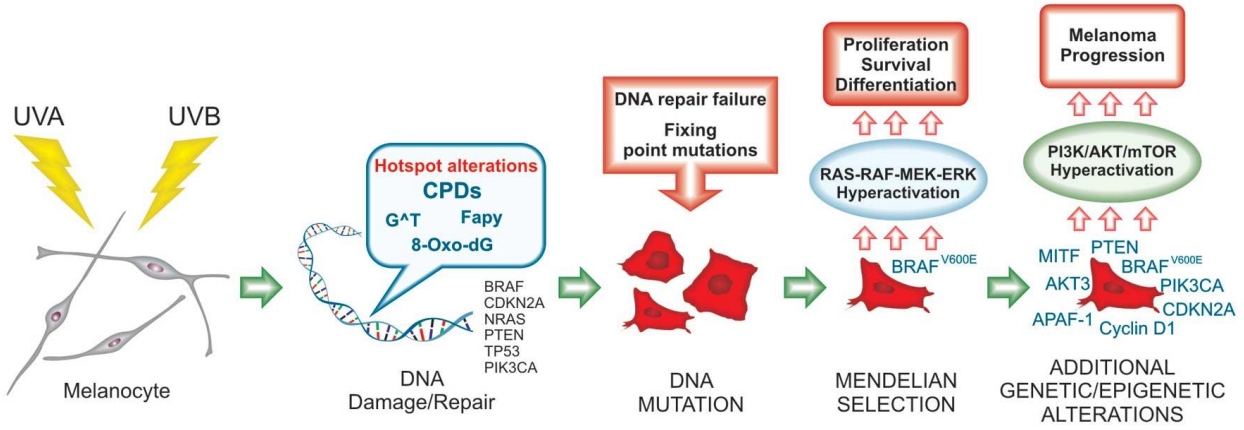

Figure 8: Genetic alterations induced by UV-radiation and potentially involved in melanoma development and progression; picture taken from [29] with permission. ***(Creative Commons Attribution License-CC BY: https://creativecommons.org/licenses/by-nc-nd/3.0/)***
Mutations in oncogenes such as BRAF, NRAS, CDKN2A are a result of UV-radiation and failed DNA repair mechanisms resulting into an increased activation of proliferative pathways. Cells with increased proliferation and survival rates thus prevail and acquire additional genetic and epigenetic alterations leading to melanoma progression.

1.1.4 Invasive melanoma

Melanoma cells are described as invasive when they succeed in entering the mesenchymal tissue after detaching from the epidermis where they are located on the epithelium [30] (Figure 4). With the exception of nodular melanoma, which is never preceded by another lesion, most melanomas *in situ* give rise to highly invasive melanoma forms [6]. Invasion depth can be clinically used as an indication for metastasis and death risk [31]. Parallel to the transition of melanoma cells into the invasive state, the mechanisms inducing genetic alterations in melanoma cells begin to change and evolve. Invasive melanoma cells possess mutations that were already formed in their pre-invasive state such as driver mutations which activate the *MAPK* pathway and mutations in the *TERT* gene. Additionally, bi-allelic inactivation of the *CDKN2A* gene as well as mutations in the *SWI/SNF* chromatin remodeling complex typically occur in the invasive state of melanoma cells [25]. At a progressed melanoma stage, melanoma cells are also reported to acquire *TP53* (Figure 7) [32] and *PTEN* [33] gene mutations.

1.1.5 Metastatic melanoma

At a progressed stage, melanoma cells begin migrating and expanding to other body tissues and organs after detaching from the primary tumor (Figure 9). This process is called metastasis and initially appears in the lymph nodes located in the proximal area of the primary tumor. It is believed that after local metastases are formed, migration and metastatic spreading of cancer cells gradually progresses to distant metastasis. [6] However, there is also data that supports the theory that distant site metastases may be formed in parallel, rather than gradually following the formational of regional metastases [34]. According to that theory, regional lymph nodes do not constitute a borderline for spreading cancer cells [35] but are merely a direct connection to the primary tumor and thus metastatic tumor cells are most likely to spread into lymph nodes. Dissemination to distant sites may simultaneously take place, yet with a slower progression rate due to the physical distance and subsequently due to the lower percentage of melanoma cells reaching the same distant site. [6]

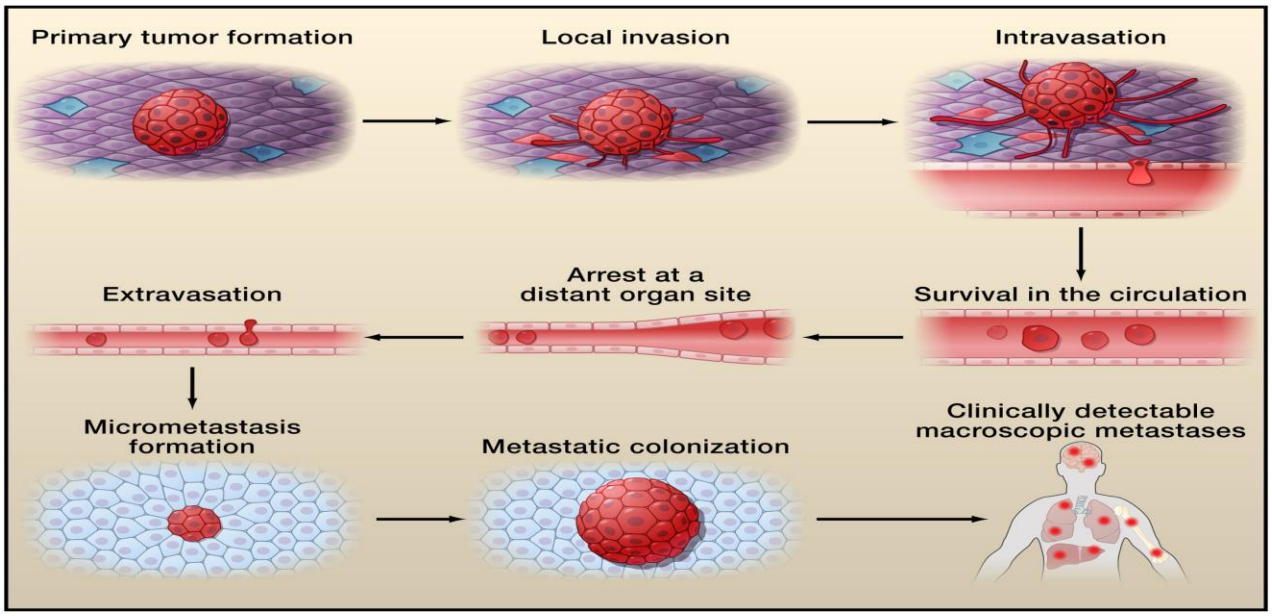

Figure 9: The process of invasion and metastasis of a primary tumor; picture taken from [36] with permission (License Number: 4312100697444).

Cancer cells enter the bloodstream by intravasation after invading cell layers and extracellular matrix (ECM). They circulate in the blood vessels and subsequently arrest at distant organs and extravasate into their distant tissues forming micrometastases. After adapting and surviving in the foreign microenvironment, they produce macroscopic metastases with enhanced proliferative capacities.

Another form of metastasis is named benign metastasis and the term describes the process of cell dissemination of a benign tumor. Benign metastasis is however not exclusively observed in melanoma tumors. [37] Metastasis also generates 4% of melanomas, which are reported to appear without having a primary tumor as a source. This melanoma type is termed MUP, an abbreviation standing for melanomas of unknown primary. [6] Similar to melanoma cells with a primary tumor site, MUP cells carry mutations that are induced by UV-radiation and possess a high mutational burden thus leading to the assumption that their source of origin is sun- damaged skin [38]. 70% of MUPs can be located in lymph nodes while the rest is formed spontaneously on various body sites [39]. It can be also assumed that a part of MUPs is the result of spontaneous regression of primary lesions or they could also partly arise out of primary lesions that were removed due to a false diagnosis. Yet, there is the strong assumption that the main origin of MUPs are melanocytes, which were detached from naevi. This fact can be supported by evidence proposing the early onset of metastatic processes in melanoma lesions, even in the stages preceding the melanoma formation. However, in order to form clinically relevant metastases with a high proliferative potential, further genetic mutations in melanocytic cells are of crucial importance. [6]

Despite the missing evidence about the exact mutations that constitute the driver mutations initiating the metastatic process, there is data suggesting the WNT signaling pathway as an effector of metastasis [40] when activated by various mutated forms of β-catenin [34]. Conclusive data about genetic mutations, which are connected to the development of melanoma metastasis, has still to be clarified.

Melanoma metastases consist of melanoma cell subpopulations with heterogenous genetic make-up [6]. Their genetic consistence is less diverse than that of the primary source of metastases due to the prevalence of a limited number of subpopulations of the founding disseminated melanoma cells [34]. Some of the subpopulations are carrying resistance to targeted therapies against mutated proteins such as the mutant BRAF-V600E protein, thus possibly contributing to the concurrent presence of resistant melanoma cell populations in various body sites [41]. Metastases formation by seeding and reseeding of cancer cells from primary tumor sites to different body sites subsequently contributes to the complex nature of the metastatic cell subpopulation’s diversity and supports the development of therapy resistance. Nevertheless, recent scientific development in the understanding of genetic

mechanisms involved in melanoma formation as well the establishment of different melanoma classes and the respective precursor lesions have contributed to improvements in diagnostic and therapeutic approaches for preventing the progression of melanoma. [6]

An important mechanism, which also strongly contributes to the initiation of metastasis in melanoma, is considered to be the epithelial–mesenchymal transition (EMT) process [42]. During this process, melanoma cells undergo a phenotypic change from the epithelial cell phenotype to that of a mesenchymal cell. The EMT process is accompanied by reduced E-cadherin expression while a shift in adhesion molecule classes results into the loss of melanoma cell contact to proximal cells such as keratinocytes. [43] Melanoma cells subsequently initiate attachment to stromal fibroblasts and endothelial cells and acquire a migratory phenotype [43, 44]. These cancer cells are thus, through the EMT process, supported in their capacity to invade dermal and vascular tissues, forming metastases in remote tissues. [43]

Metastasis formation in different body parts leads to complications in therapeutic approaches (surgical resection, chemotherapy, radiotherapy) and can prevent remission often leading to death. Cancer metastasis is thus the major contributor in cancer-associated mortality. Cells of primary tumors with highly increased proliferative rates require certain metabolic reprogramming, such as increased aerobic glycolysis (Figure 10) and glutamine metabolism, which appear in the malignant cells in order to enable survival in nutrient deficiency and acquisition of metastatic properties. Additional metabolic processes that are also affected in malignant cells and promote cancer progression include the lipid metabolism (Figure 10). [45]

1.2 Lipid metabolism in cancer cells

Lipid metabolism, which involves the synthesis, storage and degradation of lipids, is crucial to rapidly growing malignant cells that proliferate and expand at a very high rate. Lipids are essential elements of the cell membrane, while they also play a major role in energy storage, energy production (ATP synthesis) and in the creation of signaling molecules.[45] Several studies have reported that important enzymes involved in lipid metabolism, such as ATP citrate lyase (*ACLY*) [46], acetyl-CoA carboxylase (*ACC*) [47], fatty acid synthase (*FASN*) [48], stearoyl-CoA desaturase (*SCD*) [49] and phosphatidate phosphatase (*PAP*) [50] can contribute to cancer progression and metastasis as the respective genes are overexpressed in malignant tissues (Figure 10). In addition, lipid rafts also play a major role in tumor aggressiveness acting as signaling platforms [45]. An abnormal triggering of *de novo* lipidogenesis was reported in cancerous tissues. This was not observed in healthy tissues, where the fatty acid and cholesterol synthesis are mainly present in the liver and adipose cells. [51] These data were confirmed by another study, which describes a significant increase of fatty acids, phospholipids and cholesterol in malignant cells and tumor tissue [52].

Moreover, a crucial enzyme for phosphatidylcholine synthesis, choline kinase is presumably activated by the Ras protein coded by the *RAS* oncogene and is thus in abundance in several malignant cell lines and tumors [53]. Additional evidence is available showing that high levels of cholesterol biosynthesis and cholesterol efflux are present in neoplasms and proliferating non-malignant tissues which further supports the fact that cell proliferation is highly depended on cellular production of sterol lipids [54]. This finding was functionally verified by data demonstrating that cholesterol inhibition led to decreased cell growth [55].

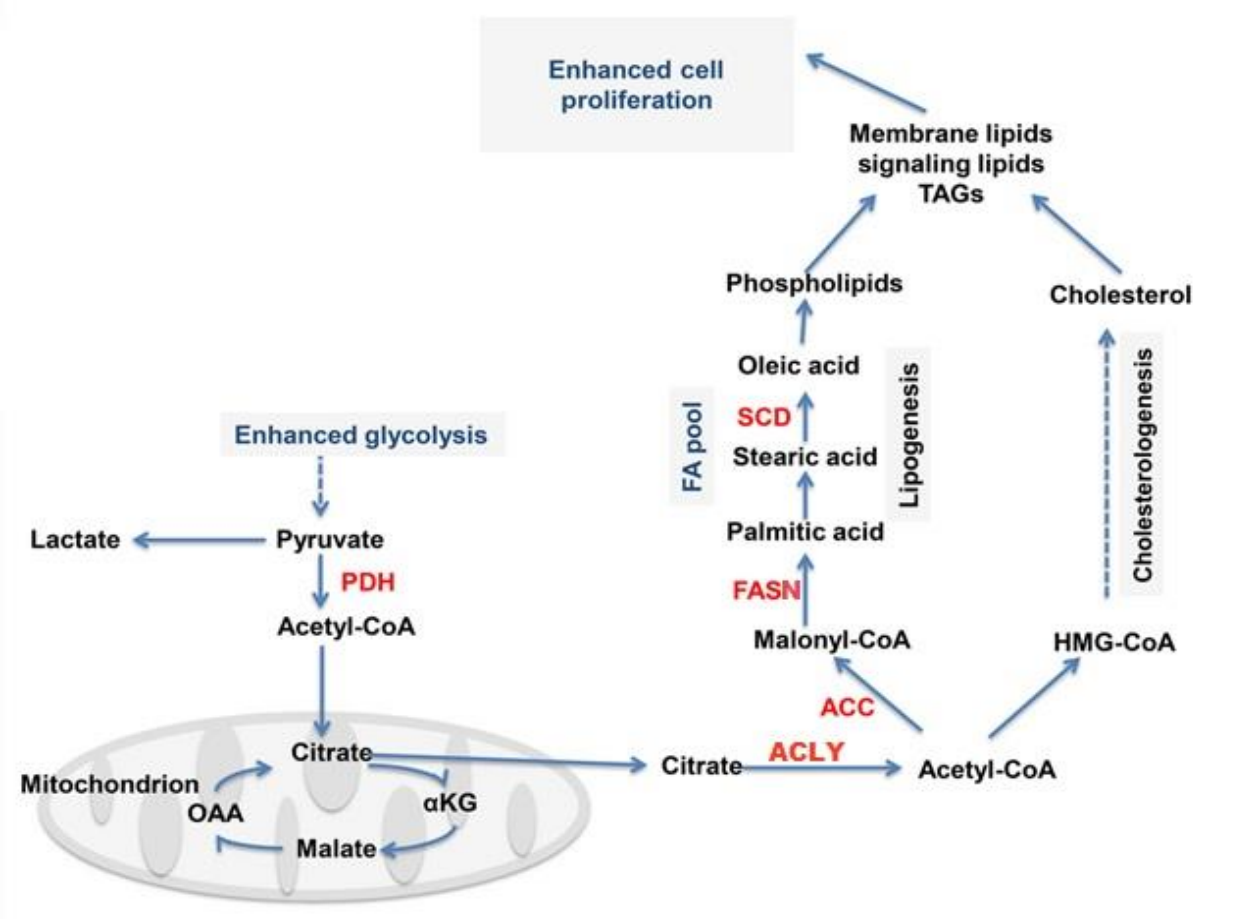

Figure 10: The effect of malignancy on lipid metabolism; picture adapted from [56] with permission (License Number: 4312111410833) .

Due to increased glycolysis in cancerous cells, the elevated concentration of citrate and acetyl-CoA leads to increased lipidogenesis and cholesterologenesis, which accounts for higher membrane and signaling lipid levels and subsequently enhanced cell proliferation. Several enzymes affected in their expression pattern in cancer cells such as ATP citrate lyase (ACLY), acetyl-CoA carboxylase (ACC), fatty acid synthase (FASN) and stearoyl-CoA desaturase (SCD) are involved in the process of lipidogenesis, while the enzyme 3-methyl-glutaryl-coenzyme A (HMG-CoA) is responsible for cholesterol production.

1.2.1 The role of cholesterol in cancer

The role of cholesterol, a trivial lipid type, extends beyond maintaining the stability and structure of the cell membrane, as it constitutes an important precursor for bile acids and steroid hormones regulating various signaling cascades. Its homeostatic regulation is achieved by *de novo* synthesis, dietary uptake and efflux from peripheral tissues. [57] Data of several studies have highlighted the importance of cholesterol in the development and progression of malignant lesions, as it is reportedly involved in carcinogenesis as well as in oncogenic processes such as angiogenesis and cell migration [58]. Cholesterol is also reported to disrupt the binding of CD44 glycoprotein to integrin and thus affect cell adhesion, consequently supporting the migration process. [59]

Research on malignant cells revealed increased cholesterol synthesis compared to healthy cells, while high cholesterol levels in lipid rafts stimulate Akt signaling leading to better cell survival rates [60]. Cellular synthesis of cholesterol depends on the mevalonate pathway, which has been recently identified as a potential therapeutic anti-cancer target [58]. Inhibition of this pathway with statin drugs and bisphosphonates prevented tumor growth and cell proliferation [61] while inhibition of the HMG-CoA reductase, an enzyme which is required for cholesterol synthesis, led to a cell-cycle arrest in breast cancer cell lines [62] . Despite the lack of specific knowledge about the exact mechanisms involved in reprogramming cholesterol metabolism in malignant cells, there is a clear dependency of neoplastic cells and tissues on products of the cholesterol biosynthetic pathway [63].

Uptake of cholesterol is carried out by lipoproteins, which transport cholesterol to peripheral tissues. However, lipoproteins can also eliminate excess cholesterol from peripheral tissues and liver [58]. It is thus assumed that the role of lipoproteins is also pivotal in the progression of cancer, as they constitute the cholesterol supplying mechanism for tumor cells. [64] Two major types of lipoprotein particles are the high- and low-density lipoproteins HDL and LDL, respectively, which supply cells with cholesterol, utilizing specific receptor mechanisms. The LDL particle delivers cholesterol mediated by the LDL receptor as endocytosed particle, while HDL lipoproteins act in the process of cholesterol removal from peripheral tissues, facilitating its delivery to the liver and its excretion (=reverse cholesterol transport). [58]

The HDL type lipoprotein concentration in blood appeared evidently modulated in patients with a malignant tumor as demonstrated by lipid analysis of cancer patients [65]. Decreased blood HDL levels are frequently detected in patients with cancerous tumors while elevated cholesterol levels were identified in tumor cell membranes [58]. Additional studies also demonstrated enhanced proliferation of breast cancer cells upon HDL addition [66].

Recently, analysis of cancer samples indicated the abundant presence of important molecules involved in cholesterol transport, such as the HDL receptor, known as scavenger receptor class B type I (SR-BI) and the LDL receptor [67]. Taken together, overexpression of the HDL receptor SR-BI in cancer cells combined with the evidence of lower HDL blood levels in cancer patients indicate utilization of the HDL mediated efflux of cholesterol from peripheral tissues to support the elevated cholesterol demand of malignant cells and tissues. [58]

1.2.2 The HDL receptor SR-BI and cancer association

Recently, a potentially strong relationship between the HDL receptor SR-BI and essential processes in malignant cells such as signaling, proliferation, motility and cholesterol metabolism has been revealed. The receptor SR-BI has been reported to be up-regulated in the majority of tumor cells compared to non-malignant cells. [68] Additional studies presented a direct correlation between SR-BI expression and aggressiveness as well as poor survival rates. Patients with high SR-BI levels exhibit a significantly decreased 10-year survival rate compared to patients with low SR-BI levels (Figure 11). [69]

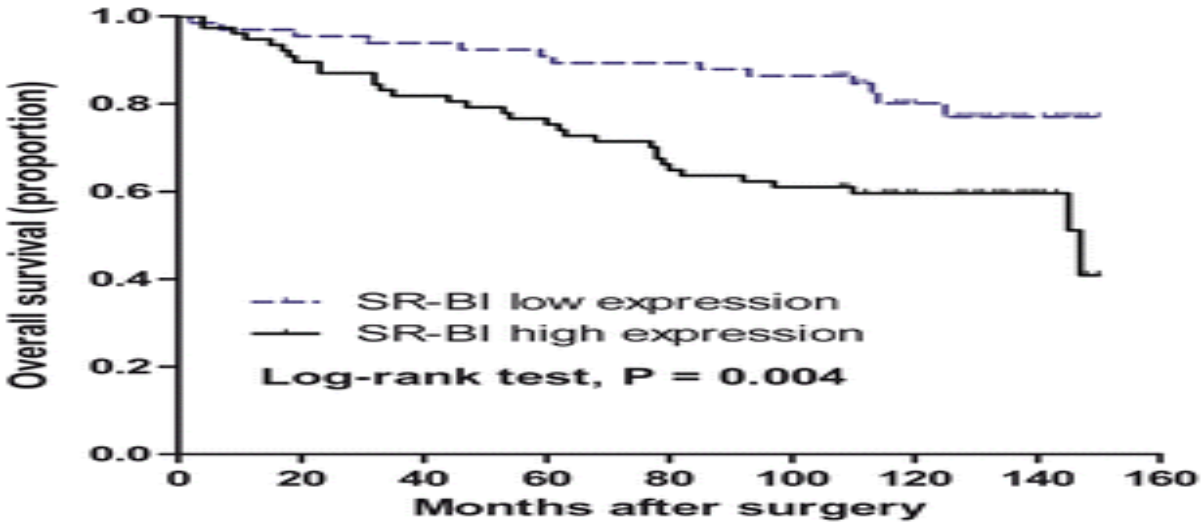

Figure 11: Overall survival rates of breast cancer patients; picture taken from [69] with permission (License Number: 4312101037254).
The Kaplan-Meier survival curve of patients with high SR-BI expression demonstrate only a 60% 10-year survival rate for this patient group. Patients with low SR-BI expression indicated a significantly increased 10-year survival rate of 80% compared to breast cancer patients with high SR-BI expression. (log-rank test p = ***0.004)***

The important role of the receptor in cholesterol delivery was shown in malignant cells with a high proliferative rate [58], as well as in the development of breast cancer xenografts [70], and breast cancer cells [71]. A strong association between human prostate cancer progression and SR-BI expression was also documented. Histological analyses of prostate cancer biopsies revealed high SR-BI expression levels in 53.6% of the malignant specimens, while none of the benign samples demonstrated a high degree of SR-BI staining. In parallel SR-BI expression positively correlated with metastasis and poor clinical prognosis. [72] Despite the ambiguous role of SR-BI in the development of malignancy, there is ample evidence presenting SR-BI as a promising diagnostic and prognostic tool [73]. The HDL receptor could thus serve as a novel therapy target [72] for patients with specific cancer types [68].

1.2.3 HDL receptor SR-BI: Function & Structure

The HDL receptor SR-BI is a scavenger multi-ligand receptor of class B type I, which facilitates the selective uptake of lipoproteins such as cholesteryl ester (CE) derived of high density lipoprotein (HDL) (Figure 12). SR-BI expression is mainly detected in tissues highly involved in cholesterol metabolism such as the liver and steroidogenic tissue. The physiological environment affecting the expression of SR-BI is influenced by other proximal proteins, plasma lipids, hormones, cytokines and by the expression levels of proximate genes. [74]

The role of SR-BI, located in the plasma membrane, is mainly the selective lipid uptake from HDL lipoproteins into cells of the steroidogenic and liver tissues [75] (Figure 12). It thereby facilitates hormone production and biliary cholesterol secretion while enabling the reverse transport of cholesterol from peripheral tissues and macrophages to the liver (cholesterol efflux) (Figure 12). [74, 76] Studies including mouse models with reduced SR-BI expression demonstrated increased plasma levels of HDL as well as increased size of HDL particles. Moreover, these mice exhibited advanced atherosclerosis while the excreted bile contained low cholesterol levels. These results highlighted the role of SR-BI in cholesterol transport as the physiological, active HDL receptor. [77]

Additional to its function as HDL-cholesterol level regulator in the plasma membrane, SR-BI also enables the selective uptake of soluble vitamins and various dietary lipophilic molecules, such as vitamin E and carotenoids [78], while its can also facilitate the entry of viral particles into host cells [79]. As a result, various physiological processes and pathological conditions such as apoptosis, platelet function, female fertility, vasculature inflammation, myocardial infarction and diet-induced atherosclerosis can thus be affected by the activity of the SR-BI receptor. [76]

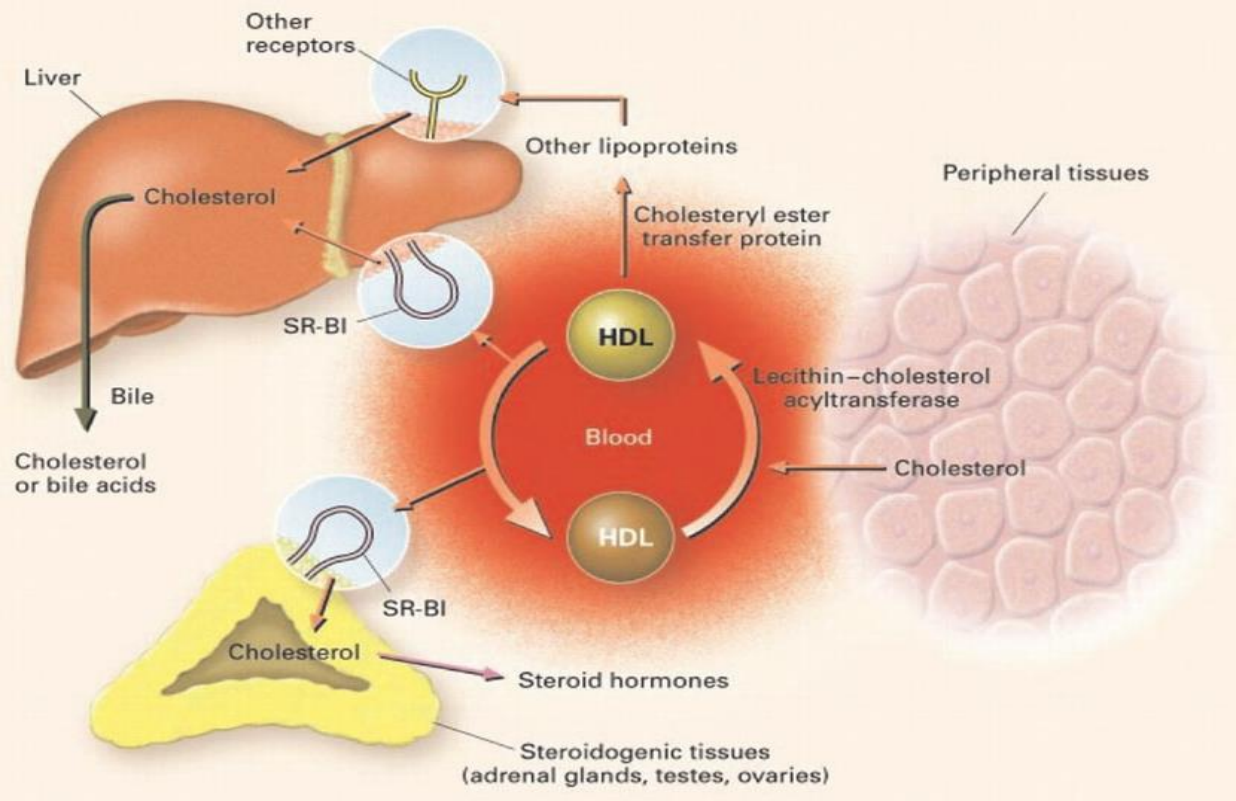

Figure 12: Main function of HDL receptor SR-BI in vivo; picture taken from [75] with permission (License Number: 4312101299437).

The receptor mediates cholesterol efflux from peripheral tissues to HDL in the blood stream. HDL-cholesterol in blood, which is present in the form of cholesterol ester after esterification by the lecithin-cholesterol acyltransferase enzyme (LCAT), is then taken up in the liver directly by the SR-BI receptor or indirectly by other receptors. Uptake by other receptors however requires its transformation to non-HDL lipoprotein. HDL cholesterol is subsequently used by the hepatic cholesterol metabolism in the form of cholesterol or bile acid for bile secretion (reverse cholesterol transport). SR-BI also facilitates the uptake of cholesterol ester by steroidogenic tissues (adrenal glands, testes, ovaries) for steroid hormone production.

Due to its involvement in a key biological process, the *SR-BI* gene is evolutionary well conserved among species [80]. The gene that codes for the human SR-BI protein, named CLA-1, is present on chromosome 12, consisting of 13 exons. The human SR-BI protein consists of 509 amino-acids with a molecular weight of 57 kDa. Human and murine SR-BI protein are reported to contain nine *N*-glycosylation sites (Figure 13) that cause variation in the protein's molecular weight when glycosylated. [74] The protein also exhibits one phosphorylation site and it can be detected in human liver tissues in its phosphorylated form [81].

Studies of the SR-BI protein sequence revealed that the protein consists of two transmembrane domains and two cytoplasmic tails, while the C- and N- terminus are localized intracellularly (Figure 13). The extracellular domain (ectodomain) is situated between the transmembrane domains and contains six cysteines, which enable the formation of disulfide bridges. [74]

Of these cysteines, four are essential for main functions of the SR-BI receptor as they are involved in its transportation to the cell surface, in the selective uptake of CE and in its dimerization and binding activity [82]. The cysteine on position 384 (Cys384) was shown to be a key residue involved in lipid transport, as data indicate its function as the binding site for a synthetic small-molecule inhibitor, named blocker of lipid transport 1 (BLT-1). BLT-1 binding on this residue and subsequent lipid transport inhibition results into a 60% reduction of lipid uptake by SR-BI. [83]

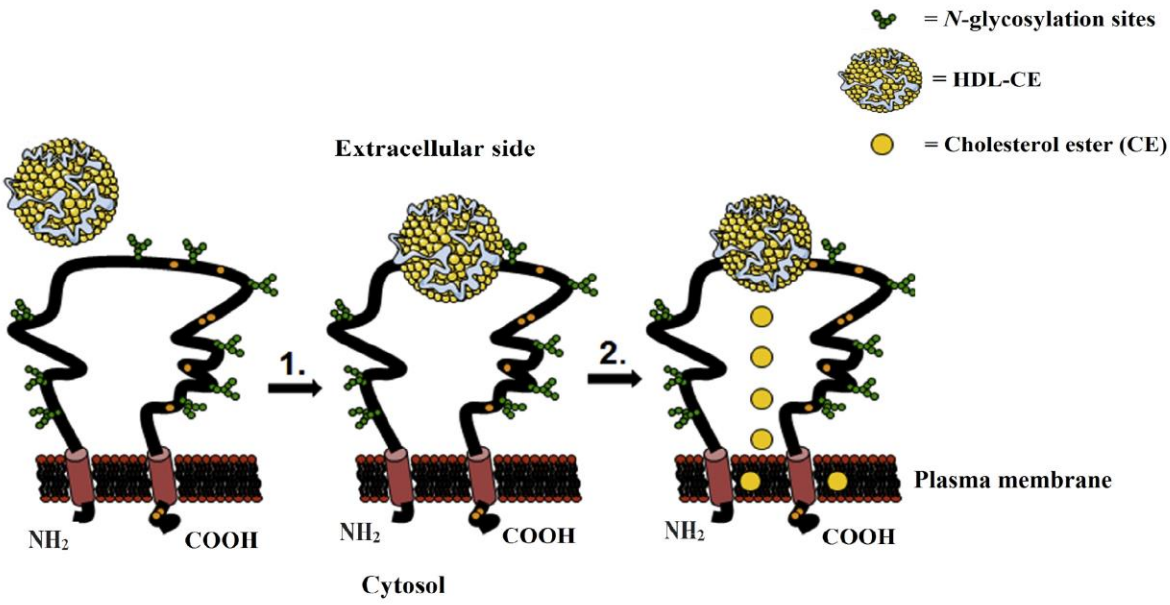

Figure 13: SR-BI structure and HDL uptake process; picture adapted from [84] with permission. (Creative Commons Attribution License -CC BY: https://creativecommons.org/licenses/by/4.0/)
(1) The putative structure of the SR-BI receptor displays an extracellular domain with nine N-glycosylation sites, where cholesterol ester-rich HDL binds. (2) After binding, the HDL-derived cholesterol ester particles are transported to the plasma membrane, from where they can be further delivered to intracellular sites.

1.3 Three-dimensional cell culture models

The cultivation of cells on two-dimensional (2D) surfaces has provided major insights into basic cell biology and tumorigenesis. 2D monolayer cell culture models are easy to handle and convenient for experimental assays [85] involving parameters such as cell growth and apoptosis [86]. Despite the advantages that 2D cell cultures provide, main drawbacks of this culture system exist, such as lack of structural architecture and lack of ability to replicate the tumor complexity in vivo.[87] In order to study metastatic melanoma efficiently, there is a need for screening models which have the ability to simulate the disease. These models, which enable the application of experimental findings from the basic cellular level to the clinical setting, can contribute to the development of new approaches to melanoma therapy. [88] Therefore, new three-dimensional (3D) cell culture systems were developed by utilizing the self-aggregation tendency and ability of tumor cells to form viable multicellular aggregates, described as 3D spheroids. [89] 3D cell culture systems are capable of imitating the *in vivo* microenvironment of the tumor as they are composed of proliferating, non-proliferating, well-oxygenated, hypoxic and necrotic cells, mimicking avascularized tumor regions (Figure 14) [90]. 3D growth of cells in spheroids also influences cell behavior, cell shape, polarity, [91] gene expression [92], proliferation [91], cell motility [93] and differentiation [94] effectively representing the *in vivo* situation in a tumor.

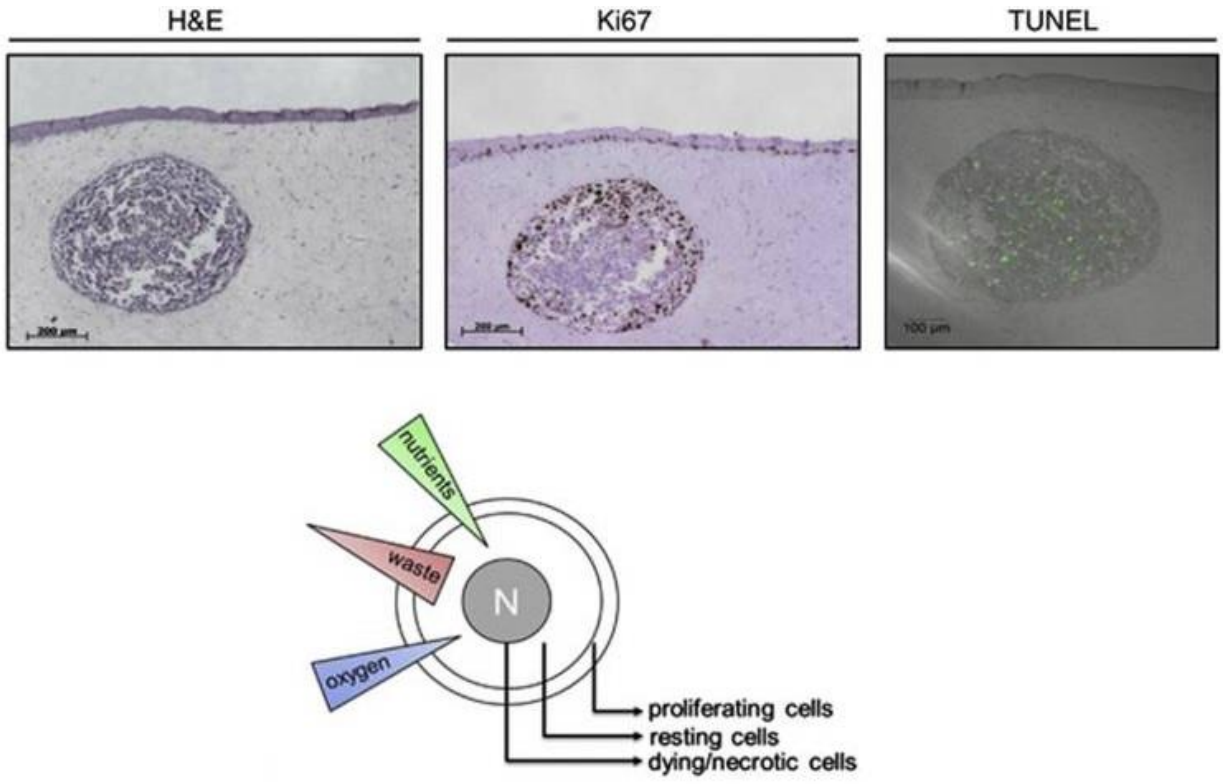

Figure 14: 3D melanoma spheroids and their features resembling an in vivo tumor; picture adapted from [88] with permission. (Creative Commons Attribution License-CC BY: https://creativecommons.org/licenses/by-nc-nd/3.0/)
Consecutive 3D spheroids stained with H&E (left), the antibody Ki67 (middle) for proliferative cells and the TUNEL assay (right). Ki67 staining highlights the proliferating cells, which are located on the peripheral layers of the spheroid while TUNEL staining represents apoptotic and necrotic cells, which are mostly located in the central part of the spheroid. The illustration in the lower panel of the figure describes the different cell subpopulations of an avascularized spheroid or tumor as well as the oxygen, waste and nutrient concentration for each subpopulation.

Tumor properties such as cell invasion and metastasis can also be analyzed by 3D cell culture systems grown on or embedded in matrices consisting of fibrin or collagen [95]. These matrices are physiologically closely related to the extracellular matrix (ECM) of solid cancers, thus partly enabling the simulation of the stromal microenvironment, which surrounds the tumor *in vivo* [87]. The reciprocal crosstalk between the tumor cells and stromal cells has profound influence on tumor development and outcome, as it can modify drug response [96] and is consequently considered as a hallmark of cancer [97]. Replicating the structure and setting of an *in vivo* solid tumor can

subsequently provide more accurate information about cell-cell interaction [98], anti-cancer drug efficiency and the anti-cancer drug effect on the invasive and metastatic potential of the tumor cells [95].

Taken together, 3D *in vitro* culture models are more efficient for elucidating tumor biology than 2D cell cultures. They constitute highly suitable systems for identification, evaluation and optimization of potential target-specific treatments and for further therapeutic development [99]. Due to their advanced physiological and clinical relevance, 3D cell culture models are also efficiently utilized for anti-cancer drug sensitivity prediction *in vivo* [87].

2. Hypothesis and aim of this study

Studies mentioned in 1.1.5 highlighted the important role of the SR-BI receptor in cancer development, as SR-BI was identified to be overexpressed in breast and prostate cancer. Based on these findings, my study aimed to examine the hypothesis that SR-BI expression and the subsequent HDL-derived lipid transport is contributing to the metastatic potential of various metastatic melanoma cell lines.

In particular, the aim of this study was to analyze whether SR-BI expression is crucial for the invasive potential of melanoma. To achieve this aim, methods were used that included *SR-BI* gene silencing via siRNA. In the first experiments SR-BI mediated lipid uptake was also blocked using the small molecule compound BLT-1, which is a SR-BI receptor blocker combined with statin treatment that simultaneously inhibited cholesterol synthesis in melanoma cell lines. Of note, experiments were carried out with 3D cell culture models mimicking the *in vivo* situation of solid tumors. For this, several metastatic melanoma cell lines, harboring $BRAF^{V600E}$ mutations (MCM1DLN, 1205Lu and 451Lu) as well as NRAS mutations (WM3854), were used to analyze phenotypes in a 3D collagenous matrix in order to observe invasion into the ECM *in vivo*. Two isogenic non-metastatic cell lines have also been used for this study (MCM1G, WM793B). 2D monolayers were prior transfected with *SR-BI*-targeting or control siRNA. Subsequently 2D cells were formed into spheroids or 3D cell layers. Transfected spheroids and cell layers as well as spheroids treated with BLT-1 and lovastatin (single or combined treatment) were allowed to invade matrices resembling the ECM. Results were compared to results of wild type (control) melanoma cells. We evaluated histological stainings, mRNA and protein expression as well as viability assays for invasion studies.

We hypothesized that SR-BI ablation or treatment with the above-mentioned inhibitors would disturb cholesterol homeostasis in the cells. Subsequently, it was expected that the invasion rates would decrease and mRNA and protein expression of genes contributing to malignancy of melanoma cells would hypothetically decline. Genes that are involved in cell adhesion and other anti-oncogenes were expected to show increased expression.

3. Materials and Methods

3.1 Cell Culture Methods

3.1.1 Cell material

Isogenic human melanoma cell lines named MCM1DLN and MCM1G as well as 1205Lu and WM793B were used during this study. Cell lines MCM1DLN and MCM1G are primary cells isolated from human patient tumors, injected in mice where they formed tumors and expanded in cell culture [100]. Isogenic cell lines 1205Lu and WM793B as well as the cell line 451Lu were obtained from the American Type Cell Culture Collection (ATCC). Melanoma cell line WM3854 was acquired from Wistar Institute.

3.1.2 Culture media

The above-mentioned cell lines were cultured in melanoma isolation media (MIM) enriched with 2% of fetal calf serum (FCS) (Thermo Scientific). For the preparation of the melanoma isolation media, 80% MCDB 153 powder (Sigma Aldrich) was resuspended in destilled H_2O, 1.3% sodium bicarbonate (Sigma Aldrich) was added and the pH was adjusted to 7.4. After pH adjustment the mixture was filter-sterilized in the lamina hood and 20% Leibovitz's L-15 solution (Sigma Aldrich) was added. The media was further supplemented with 1.68 mM $CaCl_2$ (Sigma Aldrich), 2% fetal calf serum (FCS), 5 µg/mL human insulin (Sigma Aldrich), 5 µg/L epidermal growth factor (EGF) (Thermo Scientific), 0.1% ciprofloxacin (Sigma Aldrich), 50 mg/L streptomycin sulphate and 30 mg/L penicillin (Sigma Aldrich).

3.1.3 Cell passaging

Cells were grown on a 6 cm culture dish (CytoOne) to 90% confluency and split in a 1/3 - 1/4 ratio. Cells were washed with 1x sterile PBS (Lonza) and incubated with 200 µL of 0.25% trypsin/EDTA (Sigma Aldrich) until cell detached. Trypsin was deactivated by adding fresh growth media and cells were then transferred to an appropriate amount to a new culture dish after being resuspended with a pipette (Pipetman, Gilson). Cell lines were cultured at 37°C in 5% CO_2 atmosphere (CO_2 Incubator, Binder).

3.1.4 Cell freezing

Cells that reached 90% confluency were washed with 1x sterile PBS and trypsinized as described at 3.1.3. When cells were detached, 2 mL of media were added and cells were collected in a 15 mL centrifuge tube (Sarstedt) where they were centrifuged for 3 minutes at 1.300 rpm (Heraeus Multifuge, Thermo Scientific). The supernatant was then discarded and the cell pellet was resuspended in serum-free cell culture media containing 10% DMSO (Sigma Aldrich) and 10% FCS. The cell suspension was then aliquoted into 1 mL CryoTubes (VWR) and cells were put on ice for 10 minutes and stored at -80°C in a box made of polystyrene for short term storage.

3.1.5 Cell thawing

CryoTubes containing frozen cells were thawed for 3 minutes in the water bath (Memmert) at 37°C. Thereafter, cells were transferred into a 15 mL centrifuge tube, containing 6 mL of the appropriate media. The cells were then centrifuged at 1,300 rpm for 3 minutes. The supernatant was discarded and the cells were resuspended in 3 mL of the appropriate media and were further platted on a 6 cm culture dish that was previously coated with 0.5% gelatin solution (Sigma Aldrich). Cells were allowed to attach on the 6 cm culture dish at 37°C in the incubator.

3.1.6 Cell counting

Cells were trypsinized as described at 3.1.3 and 25 μL of the cell suspension was mixed with 10 mL of Casy Ton solution in Casy cups (OLS OMNI Life Science). Cells were then counted with the Casy Cell Counter (Roche Innovatis). Information such as cell size, viability and number of living cells were obtained using a specific predefined analyzing software provided by the same company.

3.1.7 Methylcellulose preparation (1.2% w/v)

3 g of methylcellulose powder (4000 centipoises, Sigma) and a magnetic stirrer were added to a 500 mL flask (SCHOTT DURAN) and autoclaved (Autoclave CertoClav) at 121°C for approximately 20 minutes. 125 mL of serum-free media were preheated to 60°C and were added to the autoclaved methylcellulose powder followed by stirring for 20 minutes at room temperature until the powder was dissolved. Additional 125 mL of serum free media was then added at room temperature and the solution was mixed for 2 hours at 4°C. Afterwards the liquid was aliquoted into 50 mL centrifuge tubes and centrifuged at 4,000 rpm for 2 hours at room temperature. Only the clear supernatant was transferred into fresh 50 mL centrifuge tubes and was stored at -20°C for further use. Thawed methylcellulose was stored at 4°C.

3.2 Transient transfection with siRNA

3.2.1 Cell preparation

Cells plated either in a 6 cm dish, 6-well or 12-plate were allowed to grow until 70-80% confluency. The media was removed and replaced with antibiotic-free media and cells were incubated therein for at least 1 hour.

3.2.2 siRNA material preparation

Targeting siRNA stock solution (20 µM) and non-targeting control siRNA solution (20 µM), both obtained from GE Healthcare Dharmacon, were thawed in a laminar flow. Depending on the amount of culture dishes or wells used for transfection the appropriate amount of targeting and non-targeting siRNA at a 5 µM concentration was calculated (Table A). The targeting and non-targeting siRNA stock solutions were each diluted in 1.5 mL micro-centrifuge tubes (VWR) to a 5 µM concentration with the 5x concentrated siRNA Buffer (Dharmacon, Thermo Scientific) that was previously diluted to a 1/5 ratio with RNase-free water (Dharmacon, Thermo Scientific). In a third 1.5 mL micro-centrifuge tube the respective DharmaFECT volume (Table A) was pipetted and subsequently the respective amount of serum-free media (Table A) was added in all 1.5 mL micro-centrifuge tubes, which were then incubated in room temperature for 5 minutes. After incubation the tube containing the DharmaFECT and serum-free media mixture was split into two parts, each mixed with either the tube containing the targeting or non-targeting siRNA. The two tubes were then incubated for another 20 minutes in room temperature.

3.2.3 siRNA transfection

After incubation the respective amount of antibiotic free media (Table A) was added into two 15 mL centrifuge tubes and the content of each tube containing the siRNA was mixed with the antibiotic-free media. After aspiration of the cell media, the transfection media was distributed to the respective wells or culture dishes. Cells were incubated with the transfection media for at least 24 hours at 37°C and after incubation the transfection media was replaced with the appropriate culture media.

Table A: Volumes of siRNA transient transfection material used for each plate type

Volumes of following substances per plate or well	6 cm plate	6-well plate	12-well plate
targeting siRNA (5 µM)	32.5 µL	15 µL	11 µL
non-targeting siRNA (5 µM)	32.5 µL	15 µL	11 µL
DharmaFECT	23 µL	10 µL	8.4 µL
serum-free media added to DharmaFECT	667 µL	490 µL	411.6 µL
serum-free media added to siRNA	345 µL	285 µL	209 µL
antibiotica-free media	2,760 µL	2,000 µL	1,680 µL

3.3 Three-dimensional cell culture methods

3.3.1 Cell Spheroid formation

3.3.1.1 96-well round bottom plate method

Cells at 90% confluency were trypsinized as described at 2.3.1 and counted with the Casy Cell Counter. Thereafter a specific amount of cell suspension (depending on the cell number used for one spheroid and on the spheroid number) was mixed with the appropriate amount of media containing 20% methylcellulose. After resuspending the mixture, 60-100 µL of the mixture containing the desired cell number/spheroid (500-10,000 cells) was pipetted into each wells of a 96-well round bottom plate (SPL Life Sciences) with a multichannel pipette (VWR) and the plate was then centrifuged at 1,200 rpm for 5 minutes at room temperature. After centrifugation the cells were aggregated in the center of each well and were left to grow further at 37°C for 4 to 5 days (depending on the cell line) in order to form spheroids (Figure 15).

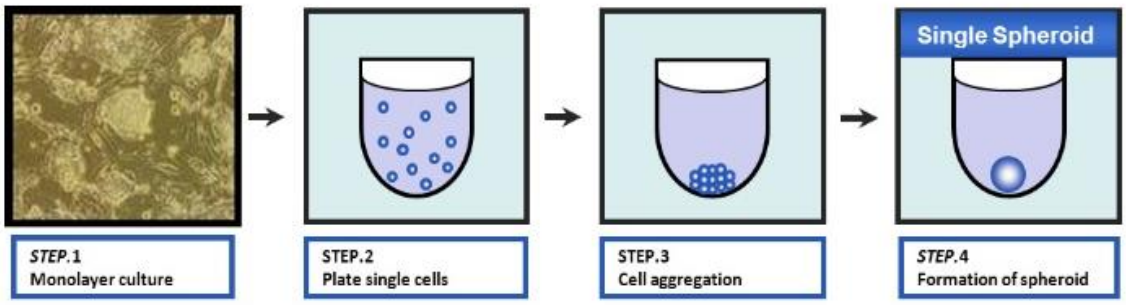

Figure 15: Cell spheroid formation in a 96-well round bottom plate; picture taken from [101] with permission from the company AMS Biotechnology Ltd.
After 2D cultures cells are trypsinized and seeded into round well ultra-low attachment plates. Cells aggregate and form spheroids within 1 to 3 days.

3.3.1.2 Hanging drop method

Cells were trypsinized and mixed with 20% methylcellulose as described at the 96-well round bottom plate method. After mixing with methylcellulose the cell suspension was carefully distributed with the pipette in drops of 35 µl volume on the inside area of the lid of a 10 cm culture dish (CytoOne). The culture dish was filled with 3 mL of 1x sterile PBS and the lid was carefully but rapidly placed on top with the drops hanging towards the bottom. The culture plate with the

hanging drops was carefully placed in the incubator and left there for 3-5 days in order to form spheroids.

3.3.1.3 Centrifuge tube method

This method was used for formation of spheroids with a size exceeding 80,000 cells/spheroid. Cells were trypsinized as described at 2.3.1 and the cell suspension was mixed with 0.5-1 mL 20% methylcellulose in a 15 mL centrifuge tube and centrifuged at 1,000 rpm for 5 minutes. The centrifuge tubes with the cells were then placed in a rack (Dynalon) and left for incubation at 37°C for 5 to 7 days with a slightly open lid until round shaped spheroids of approximately 1.5 mm were formed.

3.3.2 Three-dimensional collagen I spheroid assay

3.3.2.1 Spheroid formation

Cells were formed as described in 3.3.1.1. 25 spheroids each containing 2,500 cells were seeded for every experimental condition in 100 μL methylcellulose-cell suspension mixture per well and were incubated for 4 days for proper spheroid formation.

3.3.2.2 Spheroid harvesting

96-well round bottom plates containing spheroids were put on ice in a sterile environment. 25 spheroids were harvested with a multichannel pipette, were collected initially in a 6 cm culture dish and were transferred in 1 mL growth media into 1.5 mL micro-centrifuge tubes. The tubes containing the spheroids were centrifuged at 1,000 rpm for 2 minutes at room temperature and the supernatant was discarded. The tubes with the spheroids were then put on ice in a sterile environment.

3.3.2.3 Collagen I gel preparation

All materials used as well as the centrifuge were pre-cooled at 4°C and were kept on ice. A collagen I mixture was prepared for the sum of all collagen I gels (300 μL used for each condition) in a 5 mL polystyrene round bottom tube (Falcon). The collagen I mixture consists of 1.5% (w/v) methylcellulose, collagen I stock solution (Corning), 10x sterile filtered PBS (Sigma Aldrich) and

1 M sterile filtered NaOH (Merck Millipore). The collagen I solution was adjusted to a 2 mg/mL concentration and the 10x sterile filtered PBS was diluted in a 1/10 ratio in the mixture prepared. For neutralization and proper polymerization of the collagen I gel the 1M sterile filtered NaOH was added in the mixture in a 7 µL/mL ratio. The whole procedure was performed on ice. After mixing all materials the mixture was thoroughly shaken and centrifuged at 1,200 rpm for 1 minute at 4°C.

3.3.2.4 Spheroid embedding in collagen I gel

300 µl of the collagen I mixture and the spheroids were transferred into a 1.5 mL micro-centrifuge tubes and carefully mixed avoiding air bubbles. The mixture was poured into a round shaped casting device containing a hole with 1 cm diameter. The casting device was made of silicon foil (Gel dryer sealing gasket, 3 mm thickness, Biorad). The spheroids in the casting device, which were placed on the bottom side of a 6 cm culture dish lid, were evenly distributed with a pipette tip and the lid was turned upside down after 1 minute to avoid that spheroids sat down to the bottom surface. The gel was then incubated for 20 minutes at 37°C with the lid on the bottom side again until the collagen was fully polymerized.

3.3.2.5 Transfer of collagen I gel into media containing wells

After collagen I gel polymerization, the casting device was carefully removed with forceps and 1 mL of the appropriate media was pipetted onto the collagen I gels. Further the gel was transferred with the use of ring shaped nylon mesh inserts (Bückmann, Mönchengladbach) into wells of a 12-well plate (one collagen I gel/well) (CytoOne) containing 1 mL of the appropriate media. Sprouting of spheroids into the gel was documented at different time points with the use of the Zeiss Primo Vert microscope and the AxioCam ERc 5s camera. The sprouting area on the images was evaluated with the Image J software.

3.3.3 Vertical three-dimensional gel invasion assay (Organotypic skin model assay)

3.3.3.1 Collagen I gel preparation

The collagen I gel was prepared as described at 3.3.2.3 and was poured into casting devices (diameter: 5 mm, height: 3 mm) made of silicon foil attached on the plastic surface of a 6 cm culture dish lid. Collagen gel was incubated for 20 minutes at 37°C in order to polymerize.

3.3.3.2 Seeding of the cells on collagen I

Cell lines were trypsinized as described at 3.1.3 and resuspended in 1 mL of fresh media. Cells in the suspension were counted as described at 3.1.6 and the appropriate amount of cell suspension with 300,000 cells/replicate was pipetted into a 1.5 mL micro-centrifuge tube. The tube was centrifuged at 1,200 rpm for 2 minutes in room temperature and the supernatant was discarded. Thereafter 300,000 cells were seeded in a volume of 55 μL on top of the collagen gel plug surface in the form of a liquid drop. Cells were allowed to attach on the collagen I gel surface overnight at 37°C.

3.3.3.3 Creation of air/liquid interface

After cell attachment, a thick cell layer was visible under the microscope. A grid in the form of a tripod made of stainless steel mesh (Sigma Aldrich), which was previously autoclaved at 121°C, was placed in each well of a 6-well plate (CytoOne). The casting device was removed from the polymerized collagen gel plugs with the cell layer on top and the plugs were transferred with the use of ring shaped nylon mesh inserts onto the tripod grid leaving the nylon mesh beneath the collagen I plug. The appropriate amount of media was then added into the wells in order to create the air/liquid interface. This was achieved by adding an adequate amount of media to allow contact of the collagen I plug bottom with the media through the grid but avoiding submerging the whole plug. The air/liquid interface creates a gradient which supports invasion of the layer cells into the gel (Figure 16). The gels were incubated in the air/liquid interface for 5 (120 hours) days at 37°C and sufficient media was added every other day in order to maintain the air/liquid interface. After incubation for 5 days the collagen I gel was either fixed with 4% formaldehyde for 2 hours and further used for histological methods or was used for mRNA isolation (as described at 3.9.1).

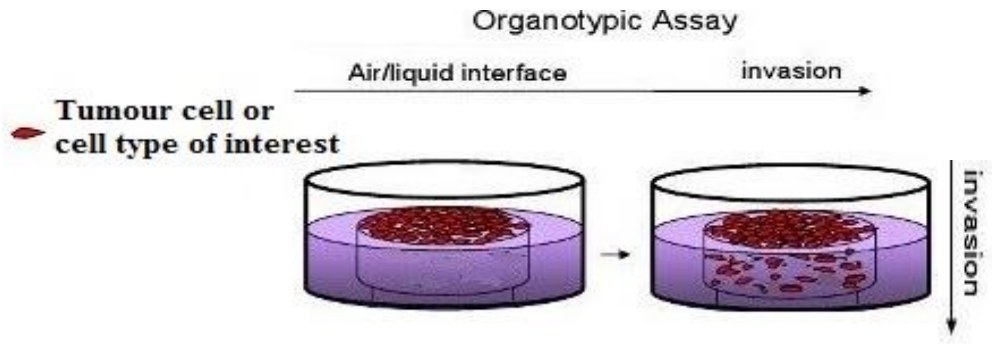

Figure 16: Illustration of the organotypic assay experimental setup; picture adapted from [102] with permission. (Creative Commons Attribution License-CC BY: https://creativecommons.org/licenses/by-nc-nd/3.0/) Cylindrical collagen gels are seeded on top with tumor cells and incubated at the air/liquid interface. Cells start to invade the gels from above and after several days.

3.4 Pharmacological treatment of cell spheroids

Cell spheroids were either treated with lovastatin (statin, inhibits HMG-CoA enzyme) or with the blocker of lipid transport 1 (BLT-1) (inhibits specific HDL-derived lipid uptake via SR-BI). Combinations of treatments were also applied. Pharmacological substances lovastatin (Sigma Aldrich) and BLT-1 (Sigma Aldrich) were dissolved in DMSO with a stock concentration of 10 mM.

3.4.1 Treatments used for the three-dimensional collagen I spheroid assay

Pharmacological substances lovastatin and BLT-1 were diluted in the appropriate cell media (2% MIM) to a final concentration of 5 µM and 1 µM, respectively. 1 mL of each pharmacological substance was used at these dilutions as single treatment or in a combination with each other and was pipetted in the respective 12-well plate well shortly after the collagen I embedded spheroids were transferred in these wells. Control cells were treated with DMSO.

3.4.2 Treatments used for the viability assay

Cells were trypsinized as described at 3.1.3 and seeded with 20% methylcellulose as described at the 2.3.1.1 '96-well round bottom plate method' to form spheroids. The pharmacological substances lovastatin and BLT-1 were used at various concentrations (Table B) and were diluted from the stock concentration of 10 mM in the same media mixture used for spheroid formation (2% MIM media containing 20% methylcellulose). Lovastatin and BLT-1 were each used as a single treatment or in combination of their various concentrations (Table B) and were added to the respective wells of the 96-plate containing the spheroids. After cell spheroid formation cultivation media was replaced by treatments. The cell spheroids (three spheroid replicates per treatment condition) were incubated in the media containing the pharmacological treatments for 72 hours prior to cell spheroid viability evaluation.

Table B: Concentration of pharmacological treatments used for the viability assay

Concentrations of pharmacological substances	Lovastatin	BLT-1
	5 μM	1 μM
	10 μM	3 μM
		9 μM
Combinations of pharmacological treatments	5 μM + 1 μM	
	5 μM + 3 μM	
	5 μM + 9 μM	
	10 μM + 1 μM	
	10 μM + 3 μM	
	10 μM + 9 μM	

3.5 Viability assay

Cell spheroids were formed as described at 3.3.1.1. with 100 µL medium containing 25,000 cells/well and were treated in triplicates with pharmacological substances as described at 2.4.2. for 72 hours. Cell viability was analyzed with the CellTiter-Glo® 3D Cell Viability Assay (Promega). The CellTiter-Glo® 3D reagent was equilibrated to room temperature and 100 µL of the reagent were added to each well. Spheroids were resuspended in the reagent and the 96-well plate was shaken on a microplate shaker (Grant Instruments) at 1,100 rpm for 5 minutes. The plate was then incubated at room temperature for 30 minutes and the luminescent signal of each well was recorded with the Synergy™ HT Multi-Detection Microplate Reader (BioTek). The recorded values of the plate were further processed and evaluated with the Microsoft Excel software.

3.6 Histological methods

3.6.1 Sample fixation

Samples included the three-dimensional collagen I spheroid assay or the organotypic skin model assay and were fixed in 4% formaldehyde solution (Roti-Histofix, Carl Roth). After fixation samples were washed with 70% ethanol (VWR) and were horizontally aligned in liquid 1% (w/v) agarose gel, which was consisting of agarose (Biozyme) dissolved in 0.5% TBA buffer. After polymerization of the agarose gel containing the samples, the area of the gel containing the collagen I samples was cut with a scalpel (Swann-Morton) and was inserted into plastic cassettes (Rotilabo-embedding cassettes, Carl Roth) for further fixation in 4% formaldehyde solution overnight.

3.6.2 Sample staining

The agarose gel was stained for 30 minutes with eosin solution (Carl Roth, 1:5 diluted in 70% ethanol) at room temperature to make the samples visible within the gel. Thereafter stained samples were washed with 70% ethanol to remove the remaining eosin solution.

3.6.3 Dehydration of samples

Samples were dehydrated by incubation in following solutions and in following order (Table C):

Table C: Solutions with the respective incubation time and temperature used for sample dehydration

Incubation order	Solution	Incubation Time	Temperature
1)	70% ethanol	8-12 hours	4°C
2)	80% isopropanol (Carl Roth)	1 hour	room temperature
3)	90% isopropanol	1 hour	room temperature
4)	100% isopropanol	1 hour	room temperature
5)	fresh 100% isopropanol	overnight	room temperature
6)	xylene (Carl Roth)	30 minutes	room temperature
7)	fresh xylene	1 hour	room temperature
8)	molten paraffin wax (Sigma Aldrich)	1 hour	65°C
9)	fresh molten paraffin wax	3 hours	65°C

Samples were then left to solidify at room temperature for 30 minutes.

3.6.4 Paraffin embedding and sectioning

Solidified samples were preheated at 65°C for 1.5 hours in the pre-warming module MPS/W (SLEE medical) and samples were then cut with a scalpel into appropriate portions that fitted the embedding cassettes. Sample portions were placed in vertical position into embedding cassettes of the appropriate size and were embedded into paraffin blocks with preheated liquid paraffin wax located in the dispensing module MPS/P (SLEE medical). Embedded samples were then solidified on a cold plate (cold plate MPS/C, SLEE medical GmbH) at -15°C. With the use of the rotary

microtome (CUT2511A, MicroTec) paraffin sections of 3 µm were cut. The paraffin sections were then transferred with the use of two wet brushes into a water basin with cold water, where single paraffin sections were separated from each other. The sections were transferred with the use of a non-adhesive standard microscope slide (Carl Roth) into a paraffin elongation bath (1052, GFL) in 40°C warm water, where sections were allowed to expand. Subsequently paraffin sections were collected with the super frost adhesive microscope glass slides (Thermo Scientific) and were left to dry at room temperature overnight.

3.7 Histological stainings

3.7.1 Immunofluorescence staining with fixed spheroids embedded in collagen I gel

1) Sample fixation

The collagen I gel embedded spheroids were fixed with 4% formaldehyde solution for 1 hour. After fixation the samples were washed with 1x PBS (Sigma Aldrich) and were maintained in 1x PBS at 4°C.

2) Spheroid cell membrane permeabilization

Each sample was transferred into a well of a 48-well plate (CyteOne) were it was washed with 1x PBS and incubated in 300 µL of 1% Triton X-100 (Sigma Aldrich) (1/100 dilution with 1x PBS) for 15 minutes.

3) Immunofluorescence staining

Samples were washed with 1x PBS three times and were blocked for 1 hour at room temperature with 300 µL of bovine serum albumin (BSA) powder (Sigma Aldrich) dissolved in 1x PBS at a 1% (w/v) ratio. The blocking solution was replaced with 200 µl of the primary antibody diluted in 1% BSA (recommended dilution ratio for each antibody: Table D) including DAPI (1/500 dilution) and the samples were incubated therein overnight at 4°C in a light protected environment. The respective secondary antibody was diluted at a 1/400 ratio with 1% BSA and the samples were subsequently washed with 1x PBS and incubated in 200 µL of the dilution for 1.5 hours at room

temperature in a light protected environment. Samples were washed with 1x PBS three times and were mounted with the Fluoroprep mounting medium (BioMérieux) on superfrost plus glass slides. Covered with Menzel coverslips (Thermo Scientific) the mounted samples were dried overnight at room temperature and in a light protected environment.

3.7.2 Haematoxylin and eosin staining (H&E staining) on paraffin sections

1) Deparaffinization of sections

Slides were pre-heated at 60°C for 20 minutes and were submerged twice in xylene for 10 minutes at each time at room temperature.

2) Rehydration of sections

Slides were incubated for 5 minutes in 100% isopropanol and consequently for 2 minutes each in 96% -, 70% -, 50% - ethanol at room temperature. Slides were then washed in distilled H_2O.

3) Haematoxylin staining

Slides were incubated in filtered haematoxylin (Carl Roth) for 2 minutes. Subsequently slides were washed with tap H_2O for 5 minutes twice.

4) Dehydration and eosin staining of sections

Slides were submerged in each 50% - and 70% - ethanol for 2 minutes and subsequently in the filtered eosin solution for 45 seconds. The slides were then submerged into 70% ethanol for 30 seconds and thereafter in 96% ethanol and 100% isopropanol for 5 minutes each. The slides were further incubated in xylene twice for 5 minutes.

5) Mounting of H&E slides

The slides were mounted with Entellan mounting medium (Merck Millipore) and with microscope cover glasses (VWR). Mounted slides were dried overnight.

For evaluation a Zeiss microscope was used.

3.7.3 Immunohistochemical (IHC) staining with paraffin sections on slides

1) Deparaffinization and rehydration

Slides were deparaffinized and rehydrated as described at 3.7.2 with the exception of the distilled H_2O wash step. Slides were washed with 1x PBS after incubation in 50% ethanol.

2) Epitope unmasking

Various epitope unmasking solutions were used depending on the primary antibody used (Table D). Paraffin sections were autoclaved at 120°C or heated on a heating plate at 80-90°C in citrate buffer with pH 6 (Target Retrieval Solution, Low pH, Dako Agilent) or EDTA buffer with pH 9 (Target Retrieval Solution, High pH, Dako Agilent), which were diluted at a 1/10 ratio with distilled H_2O.

3) Blocking of endogenous peroxidase activity and cell membrane permeabilization

Slides were washed with 1x PBS three times and were incubated in H_2O diluted 1% H_2O_2 (Sigma Aldrich) for 10 minutes in room temperature. Washing with 1x PBS was repeated three times and slides were submerged in a 1/1,000 dilution of Triton X-100 with 1x PBS for 5 minutes at room temperature.

4) Immunohistochemical staining of slides

Normal horse serum blocking solution (Vector Laboratories) was used at a 1/40 dilution with 1x PBS to block the samples. 100 μL were added on each slide and samples were incubated therein for 20 minutes at room temperature. Subsequently samples were incubated overnight at 4°C with 100 μL of the primary antibody diluted in 1x PBS at specific ratios (Table D). The slides were then washed with 1x PBS three times and were incubated in 100 μL of the secondary antibody (diluted at a 1/500 ratio with 1x PBS) for 45 minutes in room temperature. A wash with 1x PBS was repeated three times and slides were incubated with 100 μL streptavidin-conjugated horseradish peroxidase reagent (Streptavidin-HRP Novocastra, Leica Biosystems) for 30 minutes in room temperature. Slides were washed anew with 1x PBS and a few drops of aminoethyl carbazole (AEC) solution (Dako Agilent) were added on the moist sections on the slides. The slides were incubated with the AEC solution for 3-20 minutes and were further submerged into 1x PBS

when the staining reaction was visible under the microscope. Samples were washed with 1x PBS and were counterstained by incubation in haematoxylin for 1.5 minutes. Subsequently the slides were washed with fresh H_2O and 1x PBS and were mounted with the use of Aquatex mounting medium (Merck Millipore). Mounted slides were dried overnight.

Table D: Antibodies used for immunohistochemistry and immunofluorescence

Primary antibody against	**Origin**	**IHC (/IF) Dilution**	**Manufacturer**	**Antigen retrieval buffer**
Cleaved CASPASE-3	rabbit	1:400 (for IF)	Cell Signaling	-
CTD110.6	mouse	1:1,000	Cell Signaling	pH=6
E-Cadherin	mouse	1:800	BD Transduction Laboratories	pH=6
SR-BI	mouse	1:500/1:250 (for IF)	BD Transduction Laboratories	pH=6 / pH=9
STAT5	mouse	1:400	BD Transduction Laboratories	pH=6
VEGFA	goat	1:200	Santa Cruz Biotechnology	pH=6
Secondary antibody	**Origin**	**Dilution**	**Manufacturer**	
Dylight 488 anti-rabbit	sheep	1:400	Abcam	
Dylight 550 anti-mouse	donkey	1:400	Abcam	
anti-mouse	goat	1:500	Vector Laboratories	
anti-goat	rabbit	1:500	Vector Laboratories	

3.7.4 Periodic acid - schiff (PAS) staining

1) Sections were deparaffinized and rehydrated as described at 3.7.2

2) Reaction with periodic acid

Slides were submerged and incubated in periodic acid solution 1% (Carl Roth) for 5 minutes. Subsequently they were washed with tap H_2O for 3 minutes and rinsed in distilled H_2O.

3) Staining with Schiff's reagent

Samples were submerged and incubated in Schiff's reagent solution (Carl Roth) for 15 minutes. Slides were then washed with tap H_2O for 3 minutes and rinsed in distilled H_2O.

4) Haematoxylin counterstaining

Slides were incubated in filtered haematoxylin (Carl Roth) for 2 minutes. Subsequently slides were washed with H_2O for 3 minutes.

5) Dehydration of sections

Slides were submerged in each 50% -, 70% - and 96% ethanol for 2 minutes and subsequently in 100% isopropanol for 5 minutes. The slides were further incubated in xylene twice for 5 minutes.

6) Mounting of stained slides

The slides were mounted as described at 3.7.2.

For evaluation a Zeiss microscope was used.

3.8 Microscopic Analysis

3.8.1 For immunohistochemical/H&E/PAS stainings

Slides were analyzed with the Zeiss Axiophot light microscope and images were captured with the AxioCam ERC55 camera (Zeiss).

3.8.2 For immunofluorescence stainings

Immunofluorescence images were taken with a Leica TCS SP8 microscope.

3.9 Quantitative PCR (qPCR)

3.9.1 mRNA isolation

1) Cell lysis and homogenisation

Four replicates of the collagen I gels used for the vertical three-dimensional gel invasion assay were collected. The gels were incubated and resuspended in 300 µL RNA Lysis Buffer (peqGOLD Total RNA Kit, VWR Peqlab) for 30 minutes.

2) DNA removal and RNA binding

The lysate was transferred to a DNA removing column (peqGOLD Total RNA Kit, VWR Peqlab), which was inserted into a 2 mL collection tube (peqGOLD Total RNA Kit, VWR Peqlab). The DNA removing column was centrifuged in a microcentrifuge (Microcentrifuge 5415 R, Eppendorf) at 13,400 rpm for 1 minute at room temperature and the flow-through was transferred into a 1.5 mL micro-centrifuge tube containing an equal volume of 70% ethanol. The sample was transferred after proper vortexting into a PerfectBind RNA column (peqGOLD Total RNA Kit, VWR Peqlab) placed in a 2 mL collection tube and was centrifuged at 12,200 rpm for 1 minute.

3) RNA column wash

The PerfectBind RNA column was washed with 500 µL of RNA Wash Buffer I (peqGOLD Total RNA Kit, VWR Peqlab) in a fresh 2 mL collection tube by centrifugation at 12,200 rpm for 15 seconds. The flow-through was discarded and 600 µL of Wash Buffer II (peqGOLD Total RNA Kit, VWR Peqlab) were added into the PerfectBind RNA column. The column was subsequently centrifuged at 12,200 rpm for 15 seconds and the washing step with Wash Buffer II was repeated.

4) RNA elution and quantification

After removal of the flow-through, the PerfectBind RNA column was centrifuged at 12,200 rpm for 2 minutes to dry and was subsequently inserted into a 1.5 mL micro-centrifuge tube. 10 µL of sterile RNase-free water (peqGOLD Total RNA Kit, VWR Peqlab) were added on the PerfectBind RNA column and after 2 minutes of incubation the column was centrifuged at 8,650 rpm for 1 minute. The elution step was repeated with additional 10 µL of sterile RNase-free water and the

eluted mRNA concentration was quantified with the NanoDrop Spectrophotometer ND-1000 (Thermo Scientific). Eluted mRNA samples were stored at -80°C after quantification.

3.9.2 cDNA synthesis

1) Sample preparation for cDNA synthesis

The respective volume of each mRNA sample containing 375 ng mRNA was mixed together with RNase-free H_2O (GoScript™ Reverse Transcription System, Promega) and with 0.5 µL of random primers (GoScript™ Reverse Transcription System, Promega) to a final volume of 10 µL in order to produce 375 ng of cDNA.

Samples were centrifuged briefly and were incubated at 70°C for 5 minutes followed by further incubation on ice for 5 minutes.

A reverse transcription reaction mix was prepared for all samples with following substances (Table E), which were mixed and vortexed briefly:

Table E: Volumes of substances used for the reverse transcription master mix per sample

1)	5.5 µL of nuclease-free water
2)	4 µL of GoScript™ 5x Reaction Buffer
3)	3 µL of $MgCl_2$
4)	1 µL of PCR nucleotide mix
5)	6.5 µL of Recombinant RNasin® Ribonuclease Inhibitor
6)	1 µL GoScript™ Reverse Transcriptase

All substances used for the reaction mix, which are mentioned in Table E were included in the GoScript™ Reverse Transcription System Kit (Promega).

2) Reverse transcription to cDNA

Each sample was mixed with 10 µL of the master mix and was incubated in the heat block (Thriller, VWR Peqlab) for 1.5 hours at program number 2 (annealing at 25°C for 5 minutes, reverse transcription at 42°C for one hour, inactivation of reverse transcriptase at 70°C for 15 min, cooling down of the heat block at 4°C).

The transcribed cDNA samples were kept on ice and were diluted to a 75 ng/µL concentration with nuclease-free water for further analysis with the qPCR method. All cDNA samples were stored at -80°C.

3.9.3 qPCR reaction

1) qPCR master mix preparation

A reaction mix was prepared on ice for each gene analyzed and following substances were mixed together (Table F):

Table F: Volumes of substances used for the qPCR master mix per replicate

1)	4 µL of GoTaq® qPCR Master Mix, 2X (Promega)
2)	0.5 µL of Forward Primer of gene of interest (10 µM)
3)	0.5 µL of Reverse Primer of gene of interest (10 µM)
4)	2 µL of nuclease-free water (GoTaq® qPCR Master Mix Kit, Promega)

2) qPCR plate loading

Each cDNA sample was analyzed in duplicates and the mRNA expression of the genes of interest (Table G) was normalized to the housekeeping gene expression of β-actin.

Table G: Primers used in the qPCR Master Mix

Primer name/ Gene of interest	**5' -> 3' sequence forward**	**5' -> 3' sequence reverse**
β-ACTIN	CTATCCAGGCTGTGCTATCCCTGT	CCTTAATGTCACGCACGATTTCC
SR-BI (SCARBI)	GTACGTCCTCCTGGCGCTGG	GCAGCACAGAGCCCTTGGGA
SNAIL2 (SNAI2)	CAGACCCGCTGGCAAGATGC	ATTGGGTAGCTGGGCGTGGAA
COL12A1	CGCCGCTACCTCTCCCTGTTG	AGACACTCCATCCCTTCTGCCTCA
CTGF	CAAGGGCCTCTTCTGTGACT	ACGTGCACTGGTACTTGCAG

For each cDNA sample and replicate, 7 µL of the reaction mix were pipetted to each well of the 96-well PCR plate (Multiplate® PCR Plates™, Bio-Rad) containing 3 µL of the respective cDNA sample (Figure 17).

The qPCR plate was subsequently sealed with Microseal 'B' Adhesive Sealing Films (Bio-Rad) and centrifuged at 1,000 rpm for 1 minute. The qPCR plate was analyzed using the StepOnePlus™ Real-Time PCR System (Thermo Scientific) in the following template:

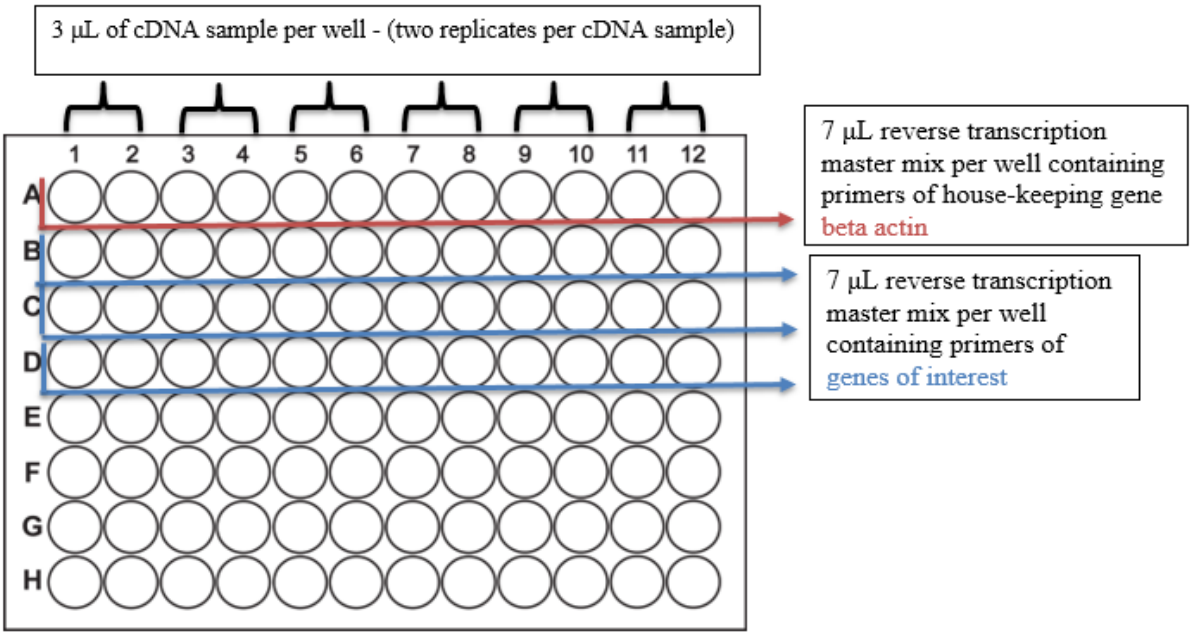

Figure 17: qPCR 96-well plate experimental setup.
Each sample was loaded in two wells in order to produce two technical replicates and each row of the 96-well plate was used for a single gene of interest.

3) qPCR data analysis

The StepOne™ Software v2.3 (Thermo Scientific) was used for data analysis.

4. Results

4.1 Spheroid formation with melanoma cell lines

Six different melanoma cell lines were used for spheroid formation. Spheroids were formed in 96-well round bottom plates (3.3.1.1) and in hanging drops (3.3.1.2). Each cell line formed spheroids of optimal size and shape with the help of one of these two methods (Figure 18). Spheroids illustrated in Figure 18 a., b., d. and e. were obtained by the 96-well round bottom plate method while spheroids on Figure 18 c. and 4 f. were derived using the hanging drop method. Spheroids aggregated from the same number of cells (2,500 cells/sphere). The three metastatic cell lines 1205Lu, MCM1DLN and 451Lu (Figure 18 a., b. and c.) were of similar size after 48 hours of incubation, however 1205Lu and MCM1DLN spheroids displayed a less compact and irregular surface (Figure 18 a., b.). This was due to the fact that a part of the seeded cells did not aggregate to the central part of the spheroid and formed a non-aggregated region around a central compact core (Figure 18 b.). Spheroids derived from non-metastatic cells as well as from the metastatic cell line WM3854 were of smaller size than spheroids originating from the metastatic cell lines 1205Lu, MCM1DLN and 451Lu (Figure 18 a.- c.). In addition, spheroids obtained from two non-metastatic cell lines MCM1G and WM793b consistently displayed a more compact structure and regular surface than their isogenic metastatic counterparts, MCM1DLN and 1205Lu, respectively (Figure 18 e. and b. compared to Figure 18 d. and a.).

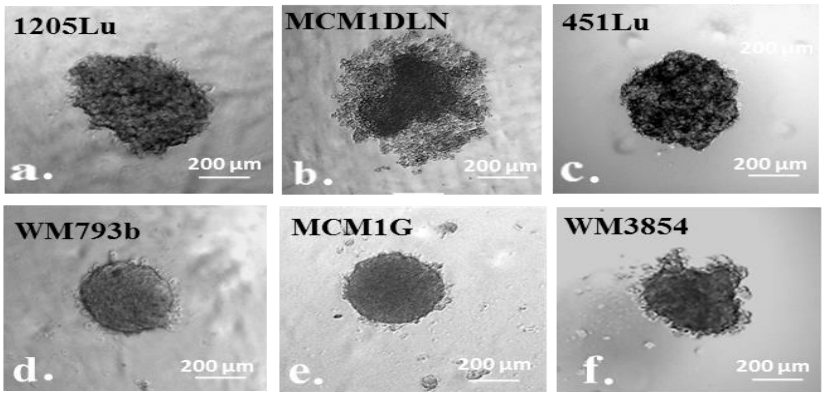

Figure 18: Representative images of spheroids of three different metastatic and two non-metastatic melanoma cell lines (4x magnification). Morphology of formed spheroids consisting of 2,500 cells of: a.) the 1205Lu cell line. b.) the MCM1DLN cell line. c.) the 451Lu cell line. d.) the WM793b cell line. e.) the MCM1G cell line. f.) the WM3854 cell line. Spheroid formation time was 48-72 hours. Scale bars represent 200 µm.

4.2 siRNA mediated SR-BI knock-down in melanoma cell lines

Several melanoma cell lines of metastatic and non-metastatic origin were transfected with siRNA targeting *SR-BI* to investigate the effect of its absence on the physiologic processes and on the metastatic potential of these cells in further assays. In order to validate the efficiency of the siRNA mediated *SR-BI* gene knock-down the melanoma cell lines were immunohistochemically stained for the presence of the SR-BI protein 72 hours post transfection.

4.2.1 Evaluation of SR-BI knock-down efficiency in melanoma cell lines used for further assays

The metastatic cell lines MCM1DLN and 1205Lu express high levels of SR-BI. After transfection with *SR-BI* siRNA a vast reduction in SR-BI protein expression was observed by immunohistochemical staining anti-SR-BI (Figure 19, top panels) compared to control cells (transfected with non-targeting siRNA). The metastatic cell line WM3854 transfected with *SR-BI* siRNA showed only a slightly reduced SR-BI staining compared to the non-targeting control (Figure 19, middle panel). Immunohistochemically stained cells of the non-metastatic cell line WM793b showed hardly any SR-BI expression with merely counterstained cell nuclei for both conditions (transfection with non-targeting siRNA and *SR-BI* targeting siRNA, Figure 19 bottom panel). The metastatic cell line 451Lu was not included in the immunohistochemical analysis due to technical issues, but the siRNA mediated SR-BI knock-down efficiency in this cell line was proved later in further assays (4.5.1 and 4.6). Taken together, this analysis demonstrated that 1205Lu and MCM1DLN cells express high levels of SR-BI which was efficiently reduced upon siRNA mediated knockdown, whereas WM793b cells were low or absent of SR-BI protein expression. Surprisingly, WM3854 cells, high in SR-BI levels, were not able to reduce SR-BI expression.

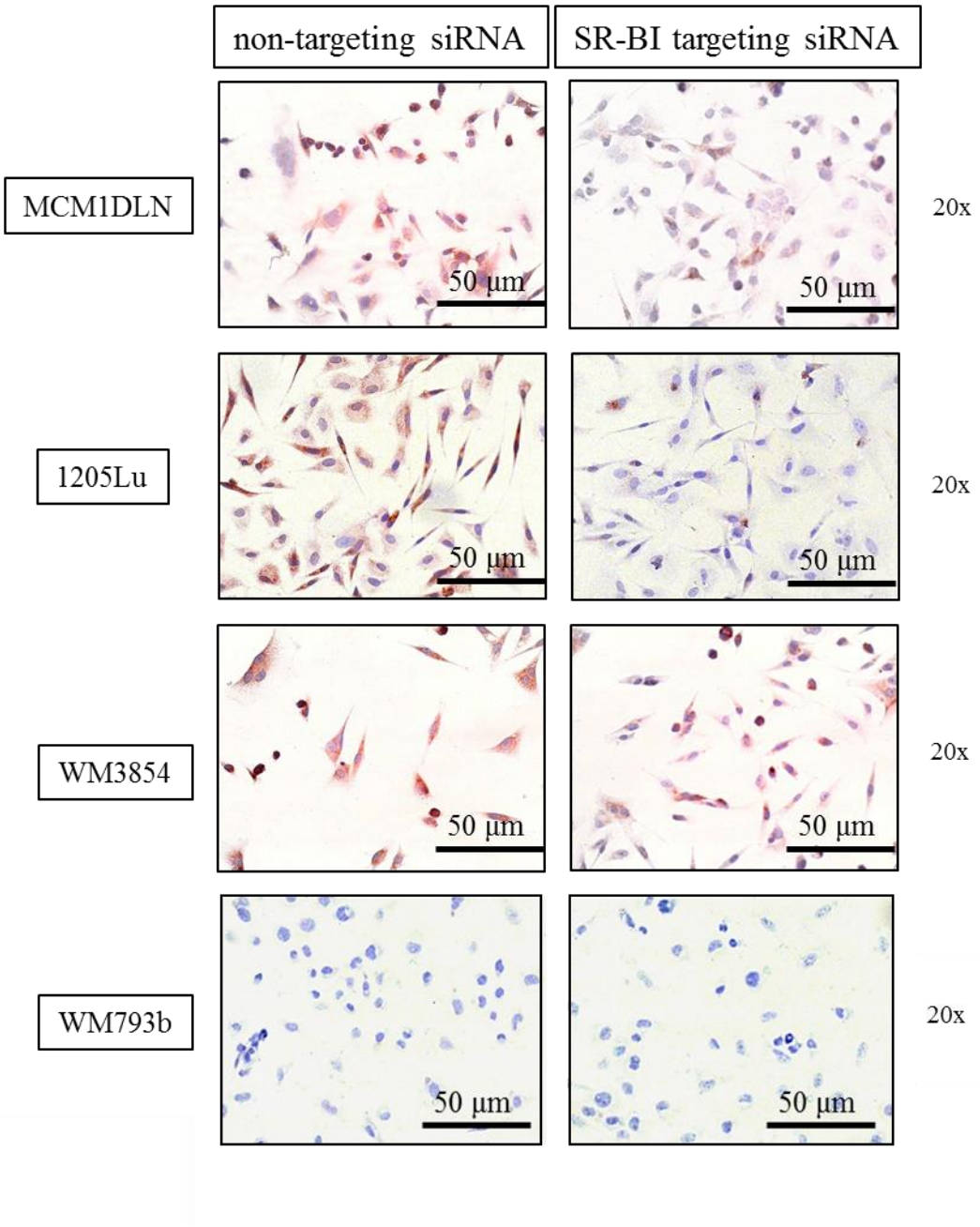

Figure 19: Evaluation of siRNA mediated SR-BI knock-down efficiency in cell lines used for the spheroid invasion assay. Cell lines were immunohistochemically stained for SR-BI protein analysis (AEC method, red signal). Nuclei are counterstained with hematoxylin (blue). Scale bars represent 50 µm.. N.A., not available.

4.2.2 Spheroid formation of metastatic melanoma cell lines with SR-BI knock-down

Next the phenotypic changes induced by the lack of SR-BI protein on spheroid formation in three metastatic cell lines were assessed. For this purpose, cells were transfected with *SR-BI* targeting siRNA and after 24 hours of transfection spheroid formation was induced. 48 hours after initiation the spheroids were microscopically examined in terms of size and form (Figure 20).

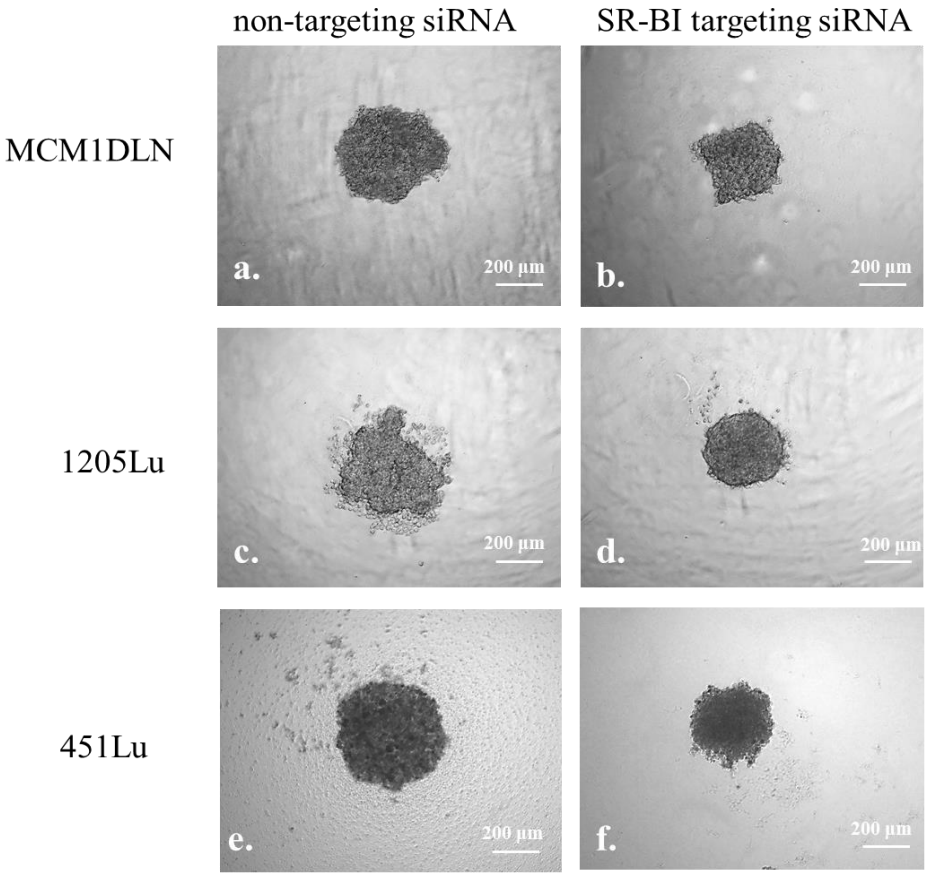

Figure 20: Effect of siRNA mediated SR-BI knock-down on spheroid formation in three different metastatic melanoma lines (4x magnification). Morphology of formed spheroids consisting of 2,500 cells of: a.) the MCM1DLN cell line transfected with non-targeting siRNA. b.) MCM1DLN cells exhibiting SR-BI knock-down. c.) 1205Lu cells transfected with non-targeting siRNA. d.) 1205Lu cells exhibiting SR-BI knock-down. e.) the 451Lu cell line transfected with non-targeting siRNA. f.) 451Lu cells exhibiting SR-BI knock-down. Spheroid formation time was 48 hours except for the spheroids of the cell line 451Lu, which were formed with the hanging drop method after 120 hours. Scale bars represent 200 µm.

Spheroids of cells with SR-BI knock-down demonstrated reduced size (Figure 21) and a more compact appearance (Figure 20 b., d., f.). The reduction in diameter was most prominent in 1205Lu spheroids; here the diameter of SR-BI knocked-down spheroids was almost 2-fold decreased compared to control spheroids of the same cell line. MCM1DLN and 451Lu spheroids also displayed a significant reduction in spheroid size (Figure 21). The effect of siRNA mediated SR-BI knock-down on the morphology of the spheroids was more evident in the 451Lu and 1205Lu spheroids as the spheroids derived from cells of these cell lines with SR-BI knock-down displayed a more regular shape as well as a higher degree of cohesiveness than control spheroids (Figure 20 d. and f.).

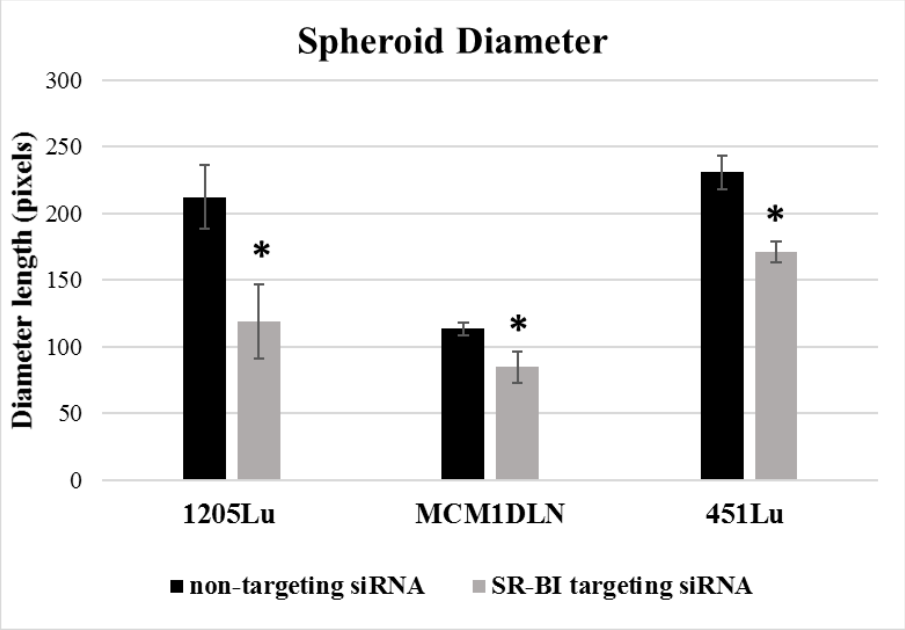

Figure 21: Spheroid size quantification of the metastatic cell lines 1205Lu, MCM1DLN, 451Lu with and without SR-BI knock-down. ***Bars represent mean size values of spheroids formed with 2.500 cells of the respective cell line transfected either with non-targeting siRNA or with SR-BI targeting siRNA (4x magnification). Error bars represent the standard deviation of the measurement. (n = 4). Significant differences between values of spheroids without SR-BI knock-down and of spheroids with SR-BI knock-down are marked with an asterisk. P-values are listed in the Appendix Table 7.4.***

4.3 Viability of melanoma cell spheroids after pharmacological treatment or siRNA mediated SR-BI knock-down

Specific pharmacologic inhibitors were used to validate SR-BI function in addition to the ablation of the receptor by siRNA. Substances that inhibit cholesterol synthesis and uptake were used to mimic the effect of the SR-BI knock-down. Thus, spheroids formed with metastatic and non-metastatic melanoma cell lines were treated with BLT-1, a SR-BI mediated lipid transport inhibitor and lovastatin, an inhibitor of cholesterol synthesis. The effect of the combination of BLT-1 and lovastatin treatment on the spheroids was compared to the SR-BI knock-down phenotype.

Frequently, the treated spheroids displayed massive cell death phenotypes accompanied by disintegration of spheroid structures. Thus, the spheroid size under these conditions could not be evaluated properly.

Therefore, the effect of the pharmacological treatment as well as of the SR-BI knock-down on spheroid cell viability was examined with the CellTiter-Glo® 3D Cell Viability Assay in order to evaluate the toxicity of these substances or of the SR-BI ablation in each cell model. The assay principle relies on the measurement of ATP levels released from lysed spheroids generating a luminescent readout that correspond to viability. 2-DG, a glycolysis and ATP production blocker was used as a negative control for cell viability.

Viability of all MCM1DLN spheroid treatments was significantly reduced compared to controls treated with DMSO. Combinations of BLT-1 (1, 3 and 9 μM) and lovastatin (5 and 10 μM) showed the highest impact on spheroid viability, which displayed a decrease by up to 13-fold compared to the control. Spheroids treated with BLT-1 or lovastatin alone also showed significantly reduced viability (>2-fold decrease) at all concentrations. Single lovastatin treatment, however, induced a slightly higher decrease in spheroid viability (5- to 6-fold) compared to single BLT-1 treatment, which decreased viability by 3- to 4-fold. Interestingly, spheroids generated by *SR-BI* siRNA transfected cells showed only a 1.5-fold viability decrease compared to the control spheroids, however non-targeting siRNA spheroids behaved similar, indicating a viability reduction due to prior transfection.

2-DG treated spheroids, which were used as negative control also showed a rather mild 2-fold decrease in viability (Figure 22).

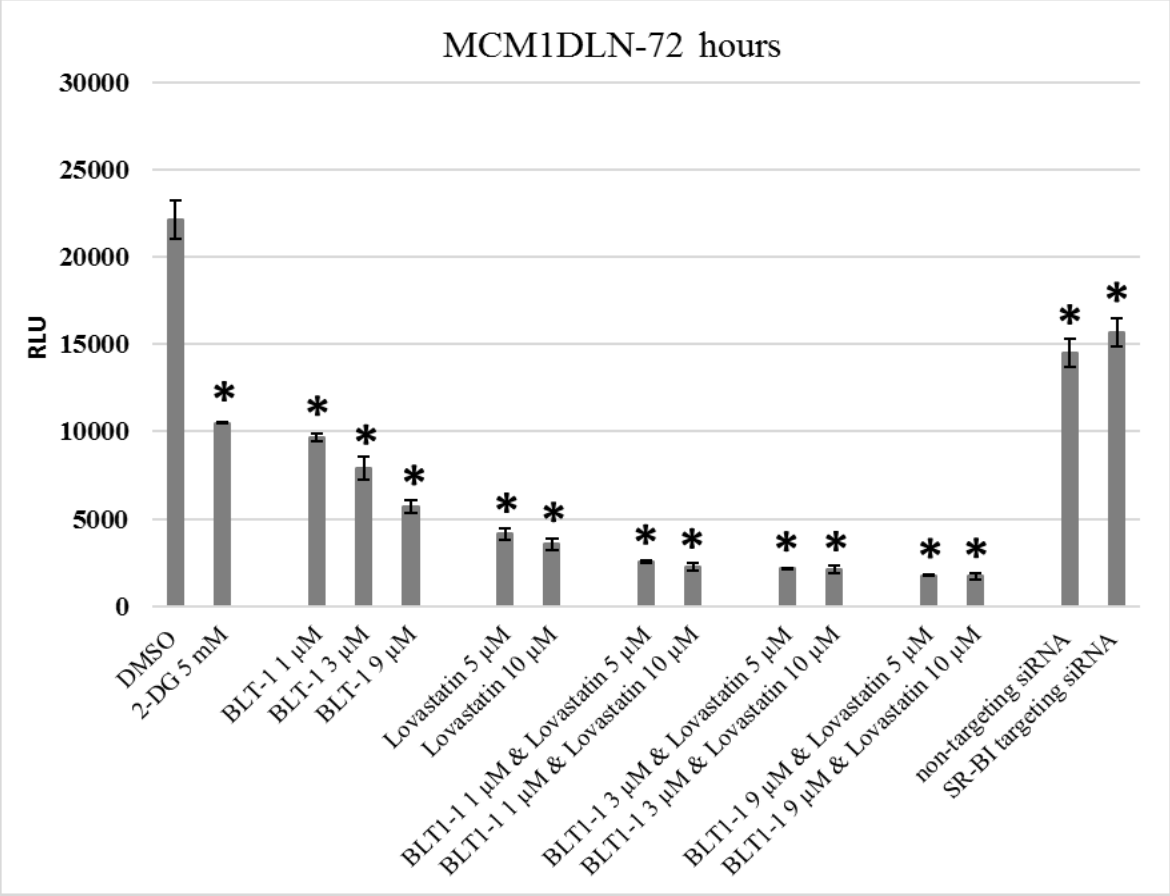

Figure 22: Viability evaluation of spheroids under different conditions formed with MCM1DLN cells assessed by the CellTiter-Glo® assay. 72 hours prior evaluation spheroids were treated with various pharmacological substances. Additionally, spheroids with and without SR-BI knock-down were also included in the assay. Bars represent mean values. Error bars represent standard deviation of the measurement (n = 3). Significant differences between pharmacologically/siRNA transfected spheroids and control spheroids (DMSO treated) are marked with an asterisk. RLU, relative light units. P-values are listed in the Appendix Table 7.4.

Combination treatment of 1205Lu spheroids with lovastatin and high BLT-1 concentrations (3 and 9 µM) induced a 10- to 25-fold decrease in viability. Spheroids treated with 1 µM of BLT-1 showed a higher decrease in viability when lovastatin was added, as the viability values thereupon

demonstrated a 2.5- to 4-fold decrease compared to DMSO controls. Single BLT-1 treatment induced a 2- to 40-fold decrease in viability with the lowest (1 μM) to the highest (9 μM) BLT-1 concentrations, respectively. In contrast, 1205Lu spheroids treated exclusively with lovastatin showed no significant decrease in viability demonstrating a relative resistance to the toxicity effect of this substance. Viability values of spheroids derived from *SR-BI* siRNA transfected cells showed no significant decrease compared to control spheroids. 2-DG treated spheroids, which were used as negative control showed a 2-fold decrease in viability (Figure 23).

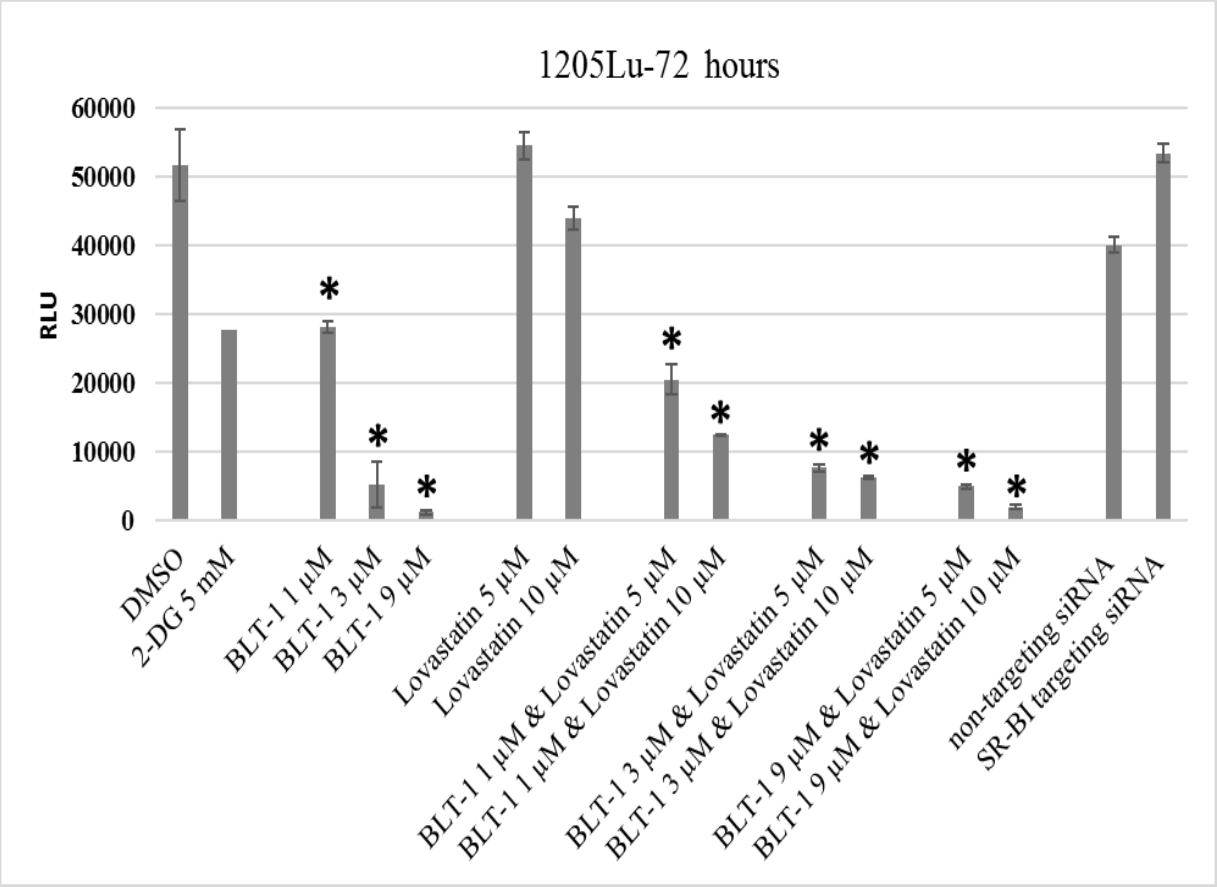

Figure 23: Viability evaluation of spheroids under different conditions formed with 1205Lu cells line assessed by the CellTiter-Glo® assay. 72 hours prior evaluation spheroids were treated with various pharmacological substances. Additionally, spheroids with and without SR-BI knock-down were also included in the assay. Bars represent mean values. Error bars represent standard deviation of the measurement (n = 3). Significant differences in viability values between pharmacologically/siRNA transfected spheroids and control spheroids (DMSO treated) are marked with an asterisk. RLU, relative light units. P-values are listed in the Appendix Table 7.4.

Pharmacological treatment induced a significant decrease in viability of WM3854 spheroids, especially when the substances BLT-1 and lovastatin were combined at their highest concentration. BLT-1 and lovastatin combination treatment of 9 and 10 µM, respectively, reduced the viability by 7.7-fold compared to control spheroids. Combination treatment of 1 µM BLT-1 and 5 µM lovastatin reduced the viability approximately only by 1.5-fold. Thus, it had nearly the same effect as the single treatment with 3 and 9 µM of BLT-1 or with 5 and 10 µM of single lovastatin treatment (= 1.5-fold decrease of viability). Transfection of spheroid cells with non-targeting and *SR-BI*-targeting siRNA induced only a 1.4- and 1.2-fold decrease in viability, respectively. 2-DG treated spheroids, which were used as negative control also showed merely an approximately 1.5-fold decrease in viability (Figure 24).

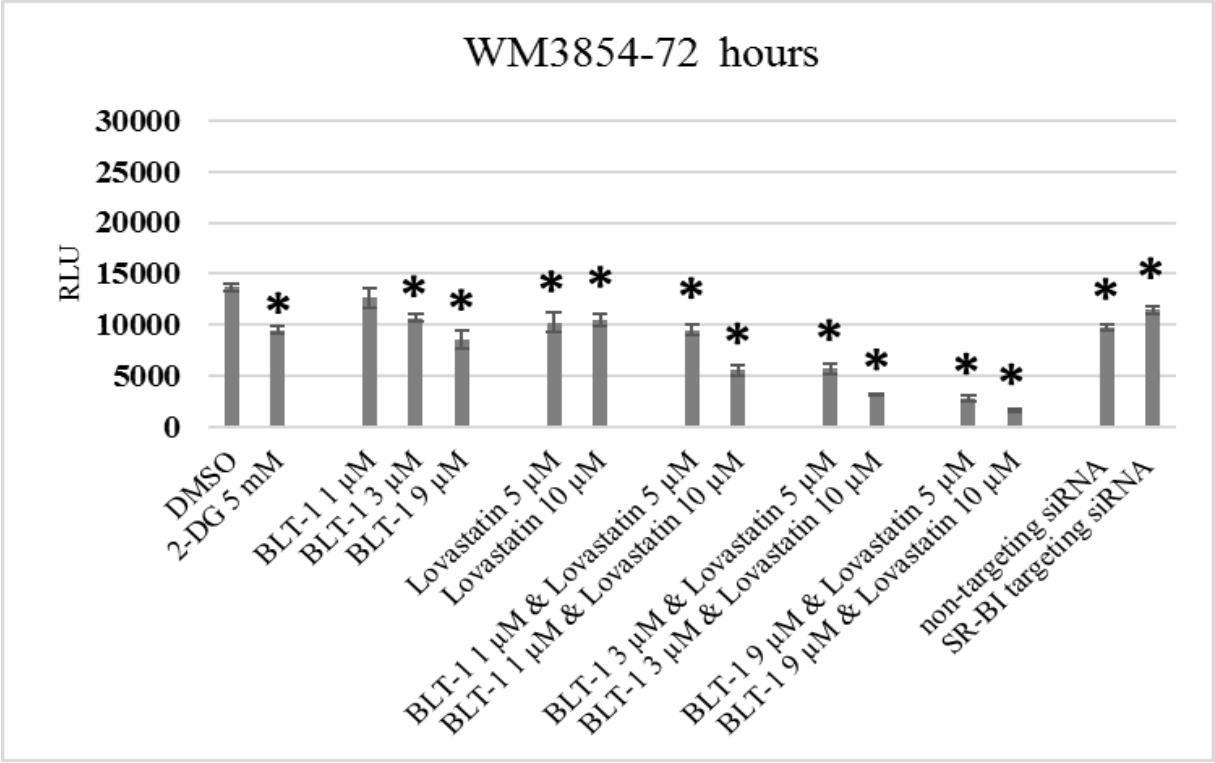

Figure 24: Viability evaluation of spheroids under different conditions formed with WM3854 cells assessed by the CellTiter-Glo® assay. 72 hours prior evaluation spheroids were treated with various pharmacological substances. Additionally, spheroids with and without SR-BI knock-down were also included in the assay. Bars represent mean values. Error bars represent standard deviation of the measurement (n = 3). Significant differences in viability values between pharmacologically/siRNA transfected spheroids and control spheroids (DMSO treated) are marked with an asterisk. RLU, relative light units. P-values are listed in the Appendix Table 7.4.

The non-metastatic cell line WM793b showed the highest decrease of viability also after combined treatment with BLT-1 and lovastatin. Treatment with these substances resulted to a 11-fold viability decrease when low concentrated (1 μM) BLT-1 was combined with 5 μM lovastatin whereas viability decreased by 37- fold upon combination treatment with 1 μM BLT-1 and 10 μM lovastatin.

Compared to control spheroids, combination treatment with high concentrated (9 μM) BLT-1 and 5 or 10 μM of lovastatin induced only a 20- to 25- fold decrease in viability, while surprisingly single treatment with 9 μM of BLT-1 induced an almost 80-fold reduction in viability. Single treatment with BLT-1 at its 1 μM and 3 μM concentration decreased spheroid viability only by 3.5- and 4.5-fold, respectively.

Treatment with lovastatin alone, however, only reduced spheroid viability by approximately 1.5- to 2- fold. siRNA transfected spheroids also showed a mild significant decrease in viability by a factor of 1.1- and 1.4- for non-targeting siRNA and *SR-BI* targeting siRNA, respectively. 2-DG treated spheroids showed an approximately 2.7-fold decrease in viability (Figure 25).

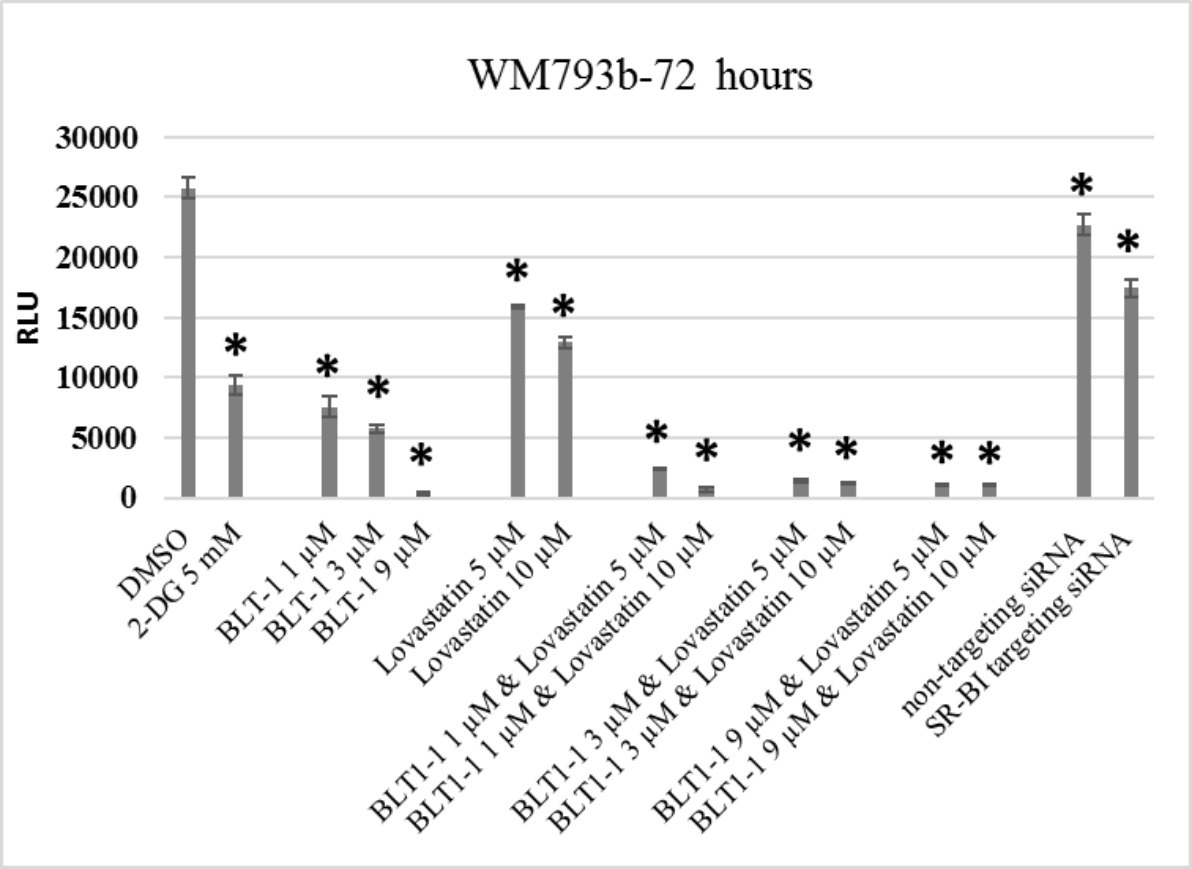

Figure 25: Viability evaluation of spheroids under different conditions formed with WM793b cells assessed by the CellTiter-Glo® assay. Spheroids were treated with various pharmacological substances 72 hours prior evaluation Additionally, spheroids with and without SR-BI knock-down were also included in the assay. Bars represent mean values. Error bars represent standard deviation of the measurement (n = 3). Significant differences in viability values between pharmacologically/siRNA transfected spheroids and control spheroids (DMSO treated) are marked with an asterisk. RLU, relative light units. P-values are listed in the Appendix Table 7.4.

4.4 Invasive capacity of three-dimensional culture systems

In a next step metastatic and non-metastatic melanoma cell lines were analyzed for invasive capabilities in various three-dimensional settings. Elucidation of the invasive capacity of melanoma cell lines in three-dimensional culture systems provided the advantage of a more physiological experimental setting closely representing the *in vivo* natural system.

4.4.1 Analysis of invasive capacity with the spheroid invasion assay

Spheroids of the metastatic melanoma cell lines MCM1DLN, 1205Lu, 451Lu and WM3854 as well as the non-metastatic cell line WM793b were analyzed for their invasive potential under different experimental conditions. After 24 hours of incubation in each experimental condition, the spheroids were embedded in collagen gels in which they were allowed to invade for another 24 hours at 37°C and 5% CO_2.

4.4.1.1 Invasive capacity of spheroids after pharmacological treatment or siRNA mediated SR-BI knock-down

Spheroids were treated with the pharmacological substances BLT-1 and lovastatin, which disturb the cells' physiological cholesterol uptake and synthesis mechanisms. Each substance was tested separately while a combination of 1 μM BLT-1 and 5 μM lovastatin was also included, as these were the lowest concentrations tested with the viability assay in 4.3. DMSO treatment was used as a control. Additionally, control/ *SR-BI* targeting siRNA spheroids were also analyzed for their invasive capacity in order to investigate the role of the SR-BI in spheroid invasiveness.

Figure 26 illustrates the experimental time points of MCM1DLN spheroid invasion into collagen gel matrices. Spheroid images were captured directly after seeding (0 hours) and 24 hours post embedding into collagen gels. MCM1DLN spheroids showed invasion into the collagen gel under all conditions, however differences in the extent of the invasive area between the different conditions were detected. (Figure 26). In order to highlight these differences in the invasive areas the microscopic images were magnified and only parts of the invasive spheroids are shown in Figure 26 c.

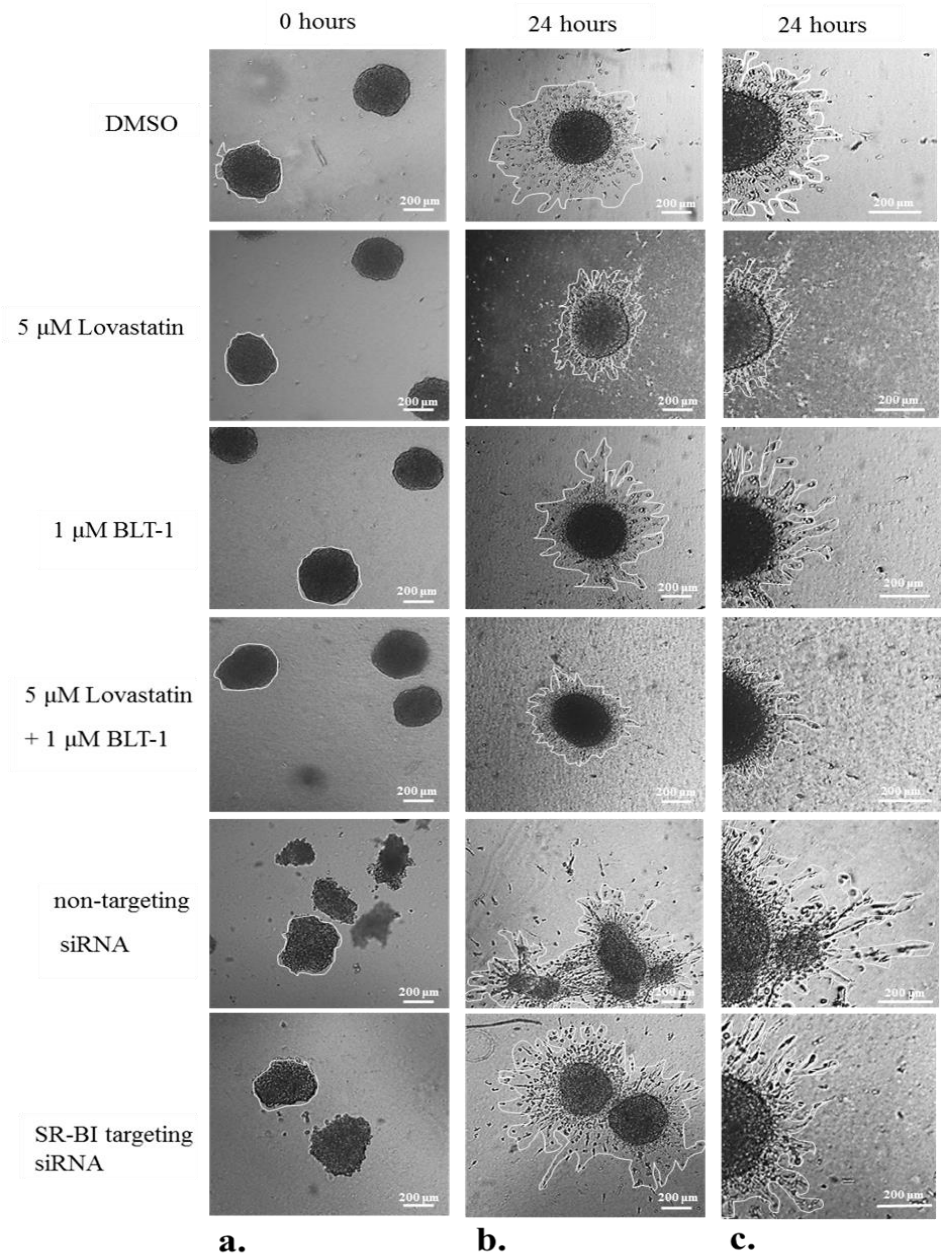

Figure 26: Spheroid invasion assay into collagen gels with the MCM1DLN cell line. Spheroids were pharmacologically treated with the left-listed substances for 6 hours prior to collagen embedding and were maintained in medium containing the respective substance after collagen polymerization. Spheroids formed with cells transfected with non-targeting and SR-BI targeting siRNA were included in the assay. Sprouting areas as well as the perimeter of initial spheroids are marked with white lines. a.) Representative images of initial spheroids captured after embedding and before invasion (0 hours) (10x magnification) b.) Images of spheroids captured at the end of the assay (24 hours) (10x magnification) c.) Close up view of the spheroid parts at the assays endpoint with focus on the invasive area. Scale bars represent 200 µm.

For quantitative analysis the invasive area of six spheroids for each condition was measured using the image analysis program ImageJ. Quantification displayed a significant reduction in invasive area of pharmacologically treated spheroids compared to control spheroids (Figure 27). Spheroids treated with lovastatin alone or in combination with BLT-1 displayed a 4.6- or a 3.3- fold decrease in invasive area, respectively, when compared to the invasive area of control spheroids. The invasive area of spheroids derived from cells transfected with either *SR-BI* targeting or non-targeting siRNA showed no significant reduction compared to the invasive area of control spheroids (Figure 27).

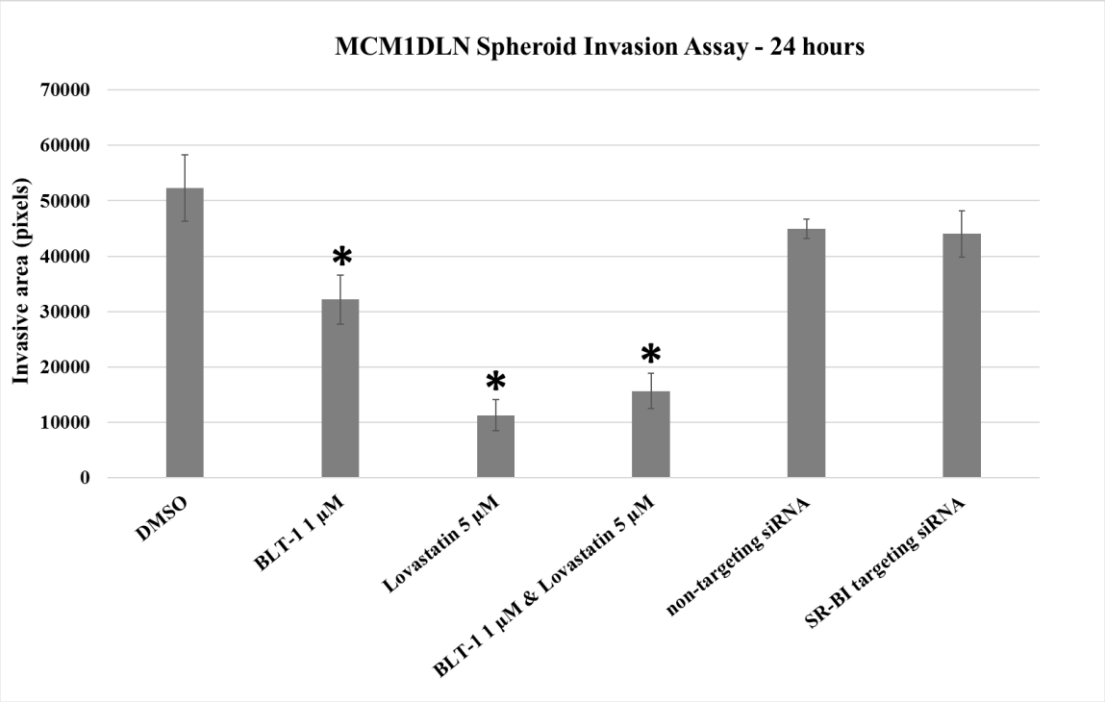

Figure 27: Quantified invasive area of MCM1DLN spheroids under pharmacological treatment or after SR-BI knock-down with siRNA (Figure 26). Bars represent mean values of the invasive area quantified in microscopic image after 24 hours. Error bars represent standard deviation of the measurement (n = 6). Significant differences in invasive area values between pharmacologically /siRNA treated spheroids and control spheroids (DMSO treated) are marked with an asterisk. P-values are listed in the Appendix Table 7.4.

Microscopic images shown in Figure 28 illustrate the experimental time points of 1205Lu spheroid invasion into collagen gel post embedding. Similar to Figure 26 spheroids on Figure 28 were treated prior to and post embedding with DMSO as a control, with a combination of 1 µM BLT-1

and 5 μM lovastatin (lowest concentration of both substances tested with the viability assay in Figure 22) and with BLT-1 and lovastatin alone. Initial spheroids were captured at 0 hours after embedding while invasive spheroids were captured 24 hours post embedding. The invasive area of 1205Lu spheroids highlighted with white lines (Figure 28) was generally reduced compared to that of the MCM1DLN cell line (Figure 26). Moreover, differences in invasive area between the various conditions were not that evident for this cell line (Figure 28).

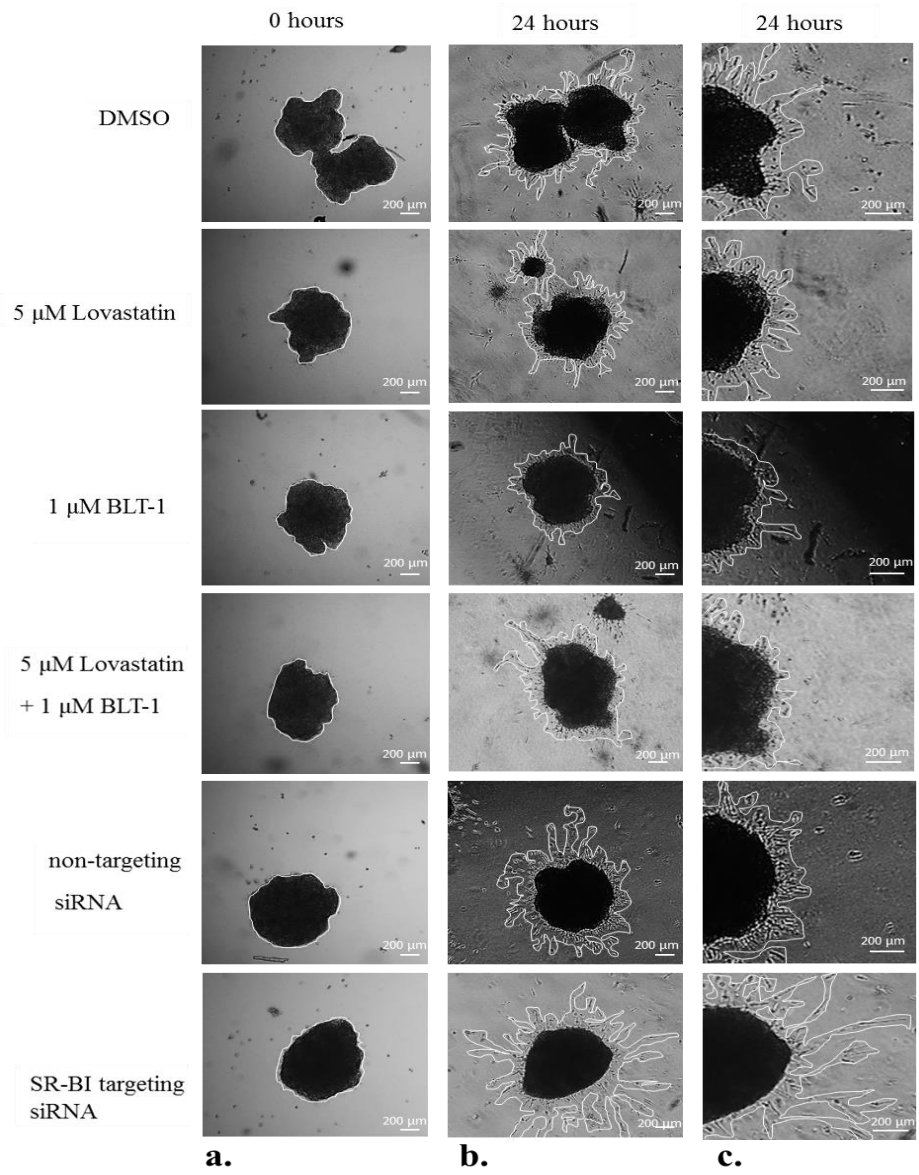

Figure 28: Spheroid invasion assay into collagen gels with the 1205Lu cell line. Spheroids were pharmacologically treated with the left-listed substances for 6 hours prior to collagen embedding and were maintained in medium containing the respective substance after collagen polymerization. Spheroids formed with cells transfected with non-targeting and SR-BI targeting siRNA were included in the assay. Sprouting areas as well as the perimeter of initial spheroids are marked with white lines. a.) Representative images of initial spheroids captured after embedding and before invasion (0 hours) (10x magnification) b.) Representative Images of spheroids captured at the end of the assay (24 hours) (10x magnification) c.) Magnified images of the spheroid parts at the assays endpoint with focus on the invasive area. Scale bars represent 200 µm.

Quantitative analysis of the invasive area of all six spheroids for each condition displayed no significant differences in invasive capacity between control spheroids and pharmacologically treated or siRNA transfected spheroids (Figure 29).

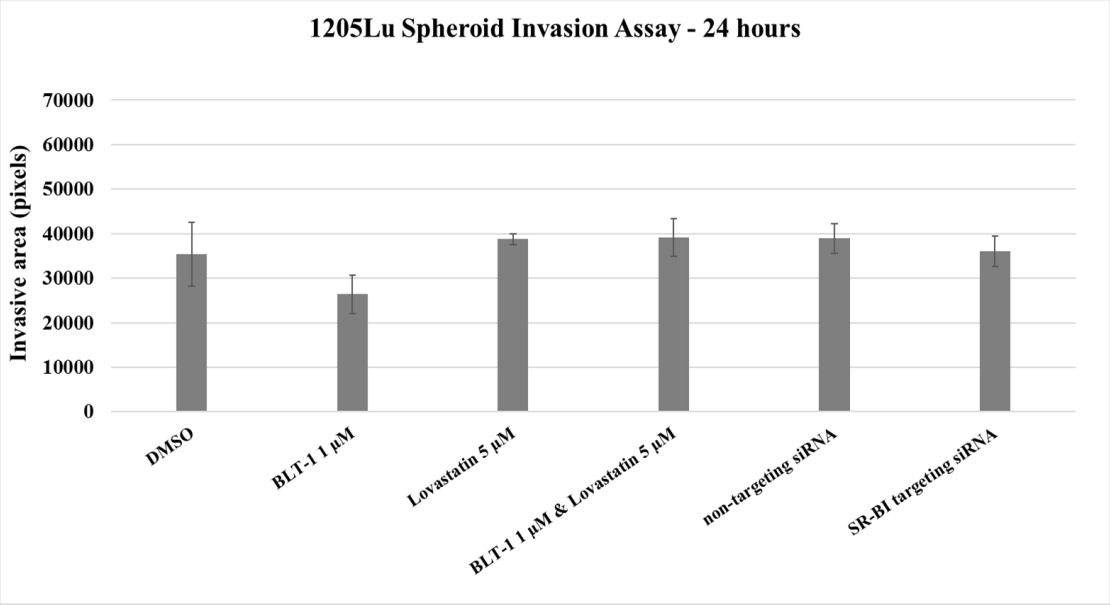

Figure 29: Quantified invasive area of 1205Lu spheroids under pharmacological or siRNA treatment (Figure 28). Bars represent mean values of the invasive area quantified in microscopic image after 24 hours. Error bars represent standard deviation of the measurement (n = 6). Significant differences in invasive area values between pharmacologically treated or siRNA mediated SR-BI knock-down spheroids and control spheroids (DMSO treated) are marked with an asterisk. P-values are listed in the Appendix Table 7.4.

Figure 30 and Figure 31 illustrate the time points of spheroid invasion of spheroids formed with the metastatic and the non-metastatic cell line WM3854 and WM793b, respectively. Since there was no invasive area visible at 24 hours post embedding (Figure 30 b. and Figure 31 b.) no quantification of the microscopic images was possible. Cell lines WM3854 and WM793b were hence further excluded from 3D invasion assays in this study.

Spheroids of the 451Lu cell line showed no invasion 24 hours post embedding (data not shown). This cell line was thus not used for further analysis with the spheroid collagen gel invasion assay under pharmacological treatment or with SR-BI knock-down of the spheroids.

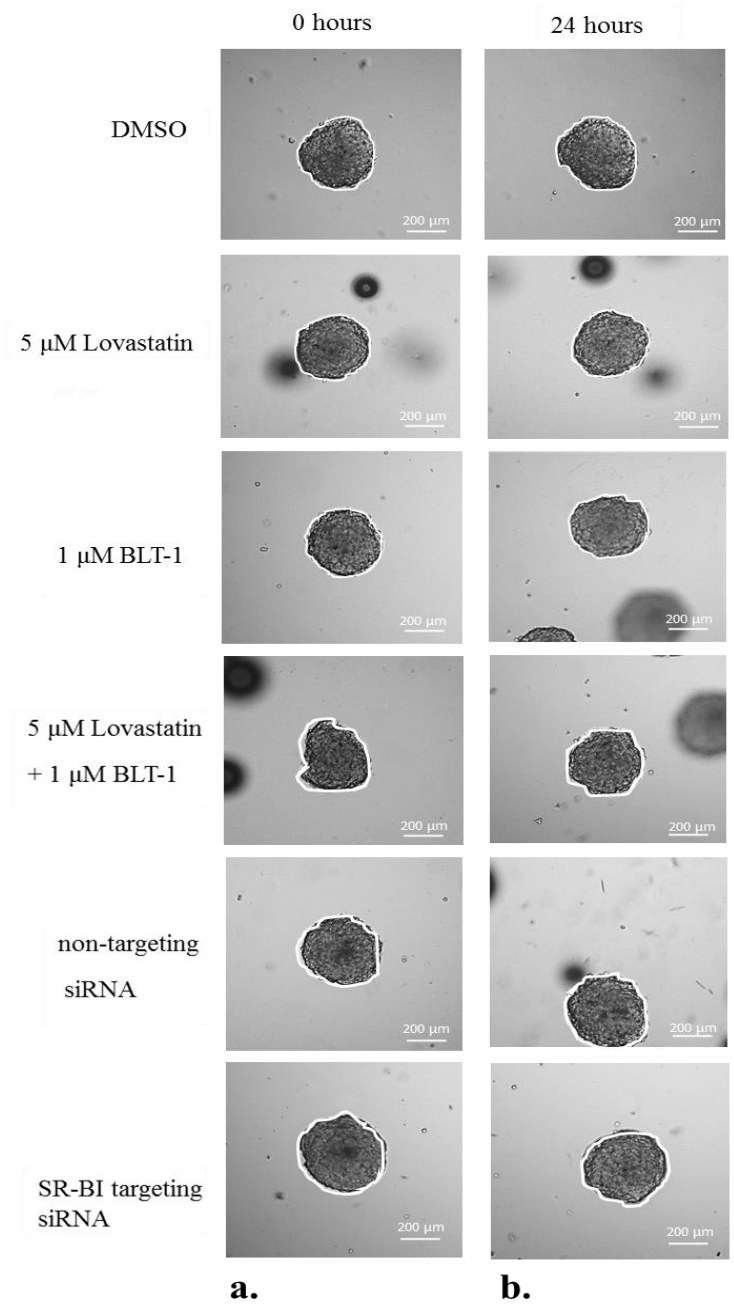

Figure 30: Lack of spheroid invasion into collagen gels with the WM3854 cell line. Spheroids were pharmacologically treated with the left-listed substances for 6 hours prior to collagen embedding and were maintained in medium containing the respective substance after collagen polymerization. Spheroids formed with cells transfected with non-targeting and SR-BI targeting siRNA were included in the assay. The perimeter and invasive area of spheroids are marked with white lines. a.) Images of initial spheroids captured after embedding and before invasion (0 hours, 10x magnification) b.) Images of spheroids captured at the end of the assay (24 hours, 10x magnification). Scale bars represent 200 µm.

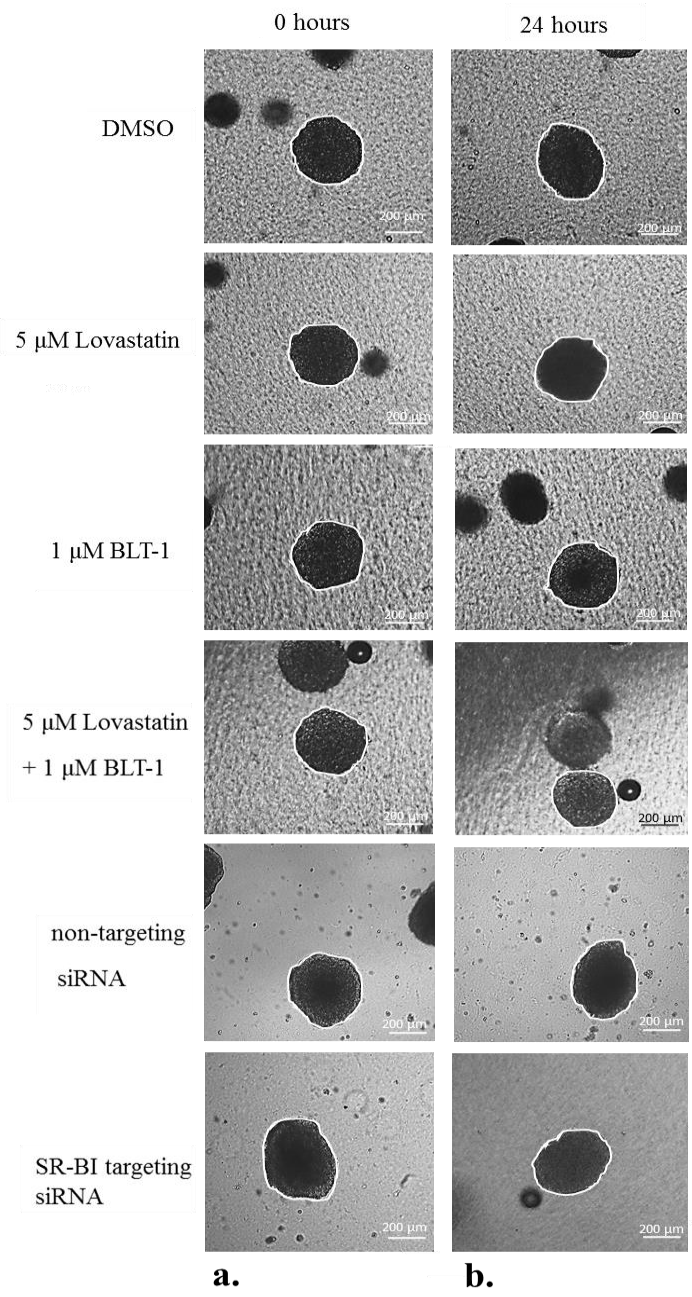

Figure 31: Lack of spheroid invasion into collagen gels with the WM793b cell line. Spheroids were pharmacologically treated with the left-listed substances for 6 hours prior to collagen embedding and were maintained in medium containing the respective substance after collagen polymerization. Spheroids formed with cells transfected with non-targeting and SR-BI targeting siRNA were included in the assay. The perimeter and invasive area of the spheroids are marked with white lines. a.) Representative images of initial spheroids captured after embedding and before invasion (0 hours, 10x magnification) b.) Representative images of spheroids captured at the end of the assay (24 hours, 10x magnification). Scale bars represent 200 µm.

4.4.1.2 Viability evaluation and SR-BI localization of BLT-1 and lovastatin treated spheroids by immunofluorescence analysis

MCM1DLN spheroids, which were analyzed with the spheroid invasion assay for their metastatic potential in collagen gel under different conditions (Figure 26) were further evaluated with immunofluorescence analysis. In order to analyze the viability of the different areas of control spheroids and of spheroids under combination treatment (BLT-1 and lovastatin), cleaved caspase-3 protein was used as an apoptosis marker. In addition, the SR-BI protein expression was also assessed in the spheroids in order to investigate a possible correlation between the HDL receptor and cell death. 4',6-diamidino-2-phenylindole (DAPI) was used as a nuclear staining (Figure 32).

Microscopic analysis revealed detachment of a small lateral area of the spheroid treated with the BLT-1/lovastatin combination (Figure 32 b.). Additionally, a slight increase of cleaved caspase-3 positive cells (yellow signal) is visible in the BLT-1 and lovastatin treated spheroid and especially within the detached area of this spheroid (Figure 32 b.) compared to control (Figure 32 a.). Cleaved caspase-3 positive cells are located predominantly towards the outer area of the control treated spheroid (Figure 32 a.) while cleaved caspase-3 positive cells can be seen distributed through the whole area under BLT-1/lovastatin treatment (Figure 32 b.). However, for a clear-cut interpretation of this finding, image analysis based quantification of different spheroid areas in multiple experiments are required.

The SR-BI signal (pink signal) also appeared with a higher intensity in the BLT-1 and lovastatin treated spheroid surface (Figure 32 b.) than in the control treated spheroids (Figure 32 a.) with SR-BI positive cells located mostly in the center of the treated spheroid.

The microscopic images of the merged channels (overlay) with the cleaved CASPASE-3, SR-BI and DAPI signals for both control and BLT-1/lovastatin treated spheroids did not show any evident co-localization or correlation of the cleaved caspase-3 signal (yellow) and the SR-BI signal (pink) (Figure 32).

Taken together, there might be changes in spatial distribution of apoptosis and SR-BI expression. However, this needs further quantitative evaluation in the future.

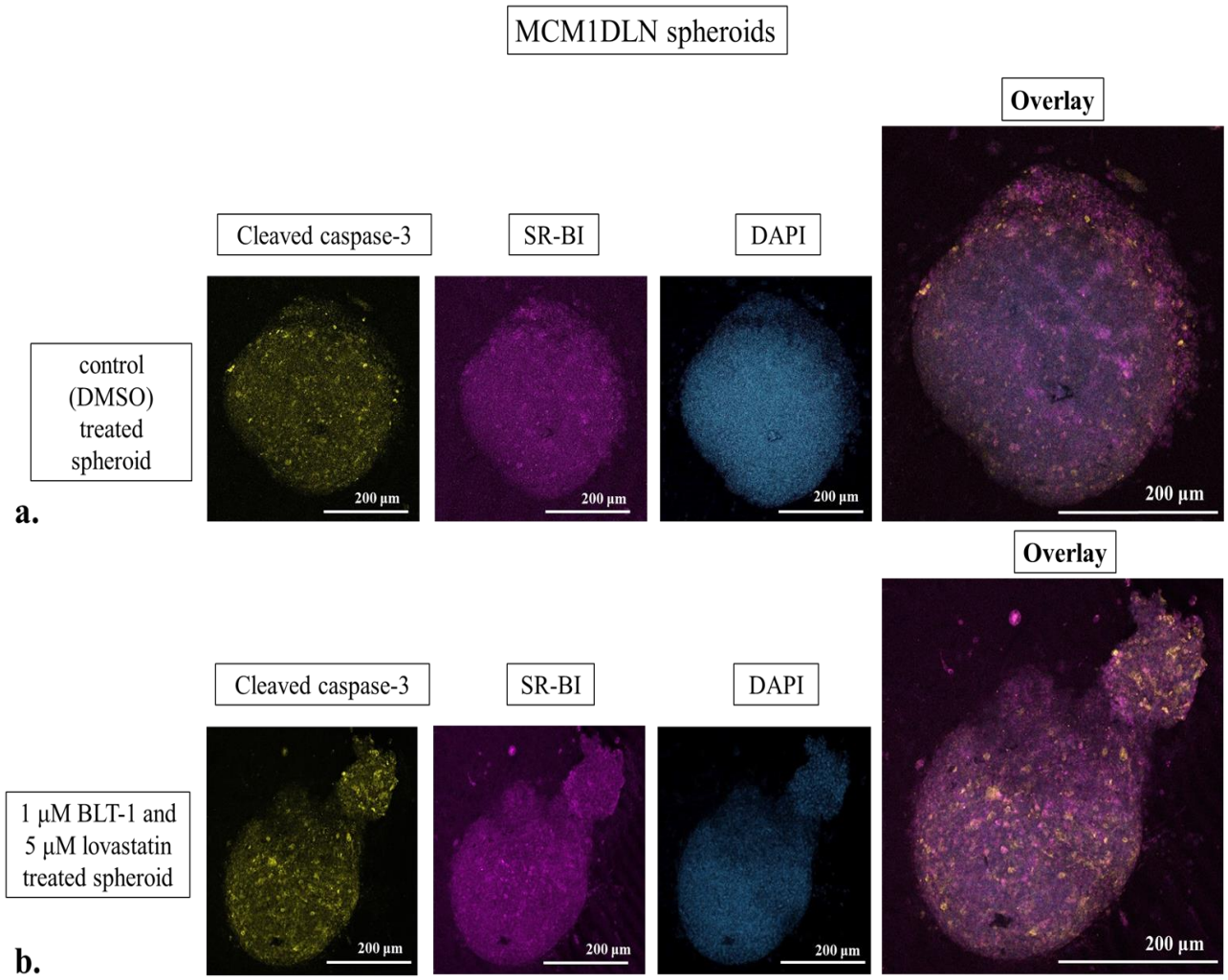

Figure 32: Immunofluorescence images of spheroids formed with MCM1DLN cells and treated with DMSO (control) or with the pharmacological substances BLT-1 and lovastatin. Spheroids were stained for the apoptosis marker cleaved caspase-3 (yellow), the receptor SR-BI (pink) and DAPI (blue). Images were captured with a confocal microscope at 20x magnification. Scale bars represent 200 µm. Merges of the three channels are shown in the right panel (overlay).

4.4.2 Invasiveness of metastatic melanoma cells with siRNA mediated SR-BI knock-down examined with an organotypic skin model assay

Further, the invasion potential of the three metastatic melanoma cell lines 1205Lu, MCM1DLN and 451Lu was also examined with an organotypic skin model assay in addition to the spheroid invasion assay. In this experimental setup cells were allowed to invade vertically into the collagen gel after forming three-dimensional layers. This model resembles cancer cells at the invasive front of a tumor. For functional analysis of SR-BI in melanoma, three cell lines were transfected either with non-targeting or with *SR-BI* targeting siRNA before seeding them on top of collagen gels. Subsequently, changes in the vertical invasion capacity of these metastatic melanoma cells were analyzed.

4.4.3.1 Vertical invasion capacity of melanoma cells with and without SR-BI knock-down in an organotypic skin model assay

Microscopic images of perpendicular sections derived from the organotypic assays performed with siRNA transfected 1205Lu cells are shown in in three different magnifications (10x, 20x, 40x). In the representative sections shown, there is a clear difference in the number of cells that fully invaded into the collagen gel between these two conditions. A higher number of 1205Lu cells with high endogenous expression of SR-BI (non-targeting siRNA transfection) were shown to invade the collagen gel compared to the SR-BI knock-down condition. In Figure 33 a few cells are shown to have entirely invaded the collagen gel under endogenous wild-type SR-BI expression (cells transfected with non-targeting siRNA) (left panel) while cells with SR-BI knock-down showed no invasion at all. (right panel). Three cells with SR-BI knock-down are potentially in the process of invading but clearly not detached from the tumor cell mass. (Figure 33).

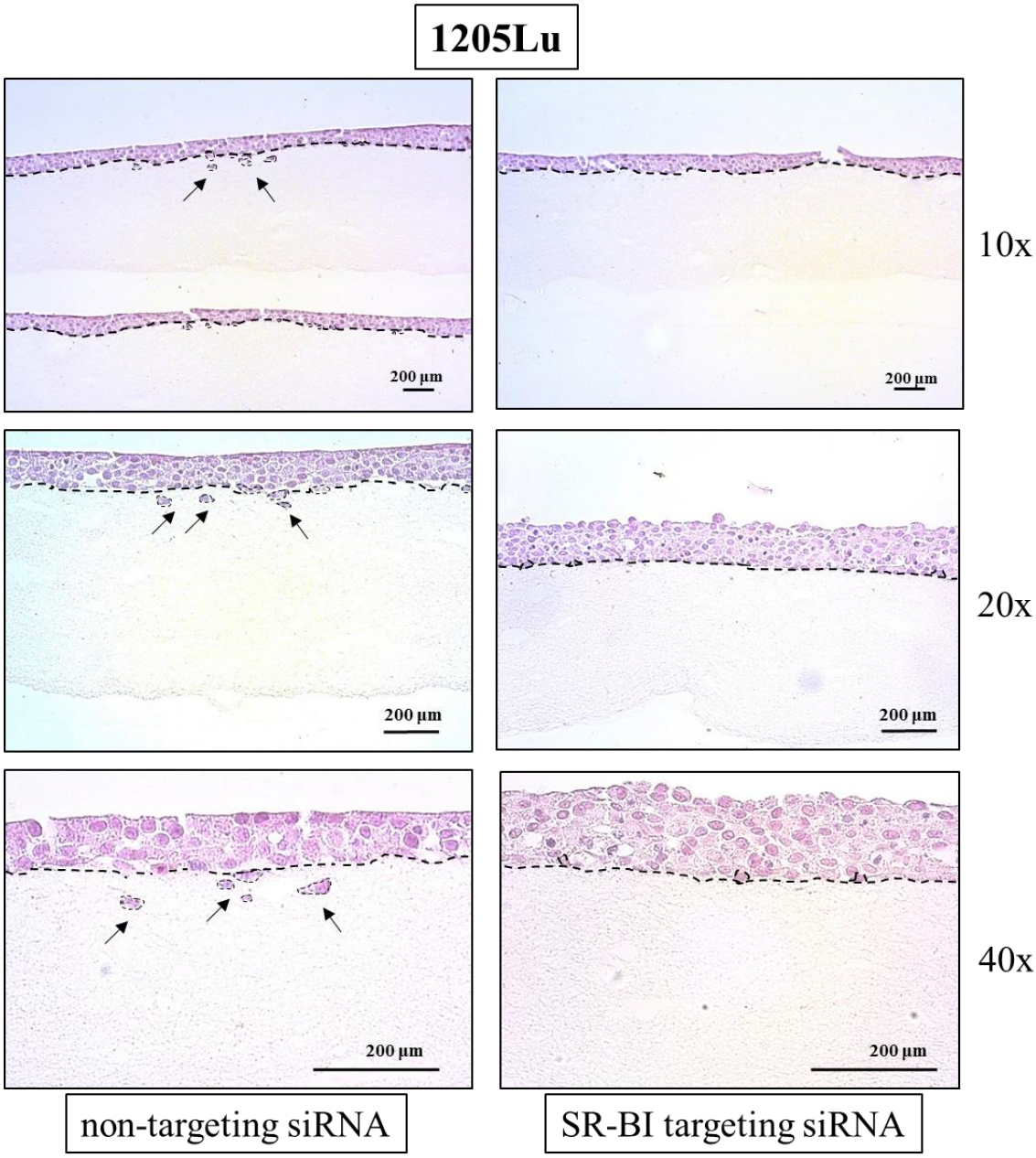

Figure 33: Representative images of H&E stained organotypic skin model assays demonstrating vertical invasion of the metastatic cell line 1205Lu. ***Cells were transfected with non-targeting control or SR-BI-targeting siRNA and were allowed to invade the collagen gel for 120 hours. An image for each of the three magnification scales (10x, 20x, 40x) is shown for each condition. Cells that invaded or are in the process of invading the collagen gel are marked with black dotted circles and arrows. A vertical black dotted line highlights the transition from the tumor cell layer to the collagen gel. Scale bars represent 200 µm.***

The MCM1DLN cell line generally demonstrated higher vertical invasion levels than the 1205Lu cells (Figure 34, compare to Figure 33). However, similar to the 1205Lu cells, the MCM1DLN control cells displayed elevated gel invasion when compared to cells with SR-BI knock-down (Figure 34). The microscopic images in Figure 34 (left panel) illustrate at least six cells or cell clusters of the MCM1DLN cells transfected with non-targeting siRNA that are completely detached from the cell layer and invading into the collagen gel. In contrast, only four cells or cell clusters being only partly detached from the cell layer were observed for the SR-BI knock-down condition in cells indicative for a reduced invasion potential (Figure 34, right panel).

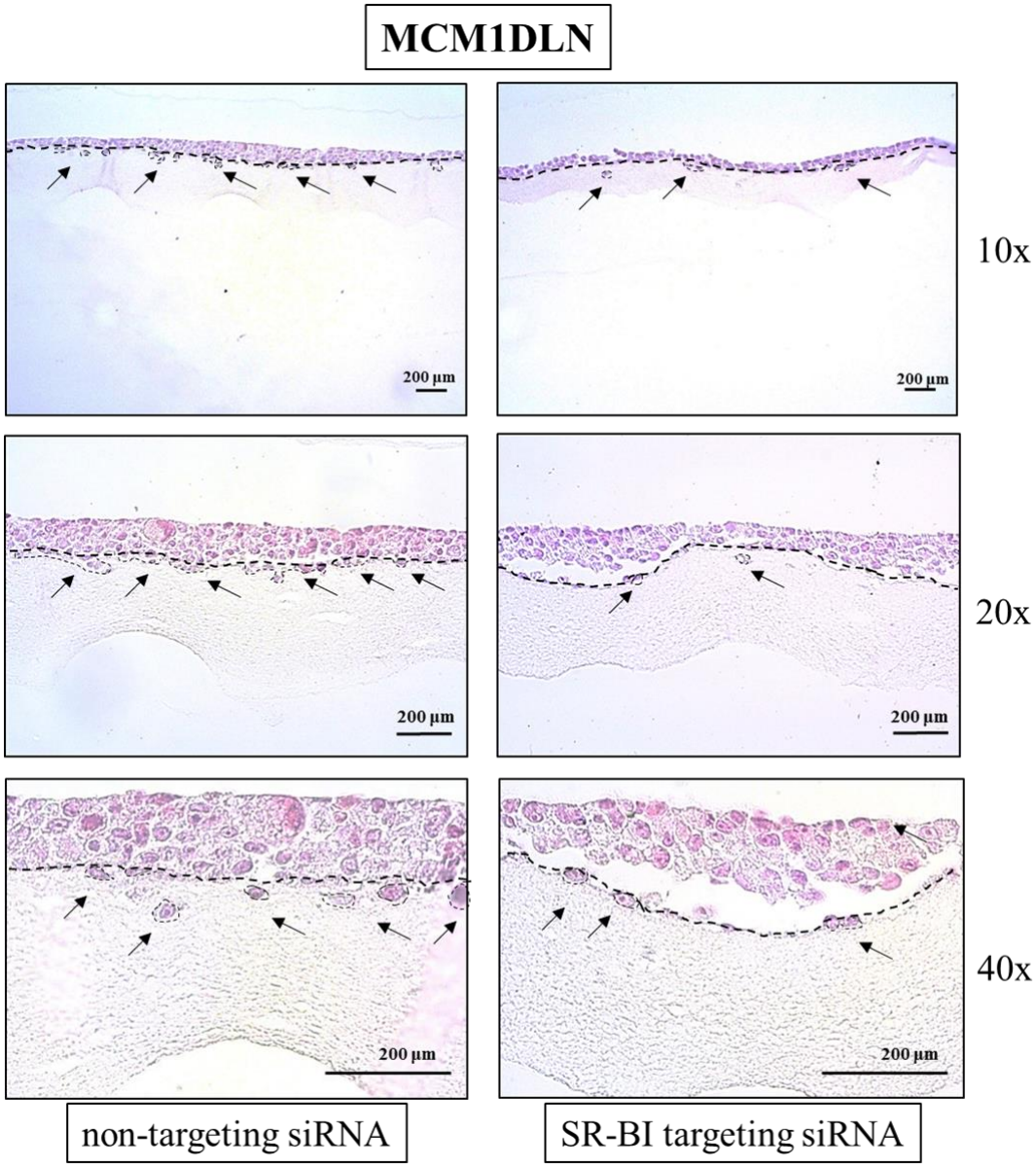

Figure 34: Representative images of H&E stained organotypic skin model assays demonstrating vertical invasion of the metastatic cell line MCM1DLN. Cells were transfected with non-targeting or SR-BI-targeting siRNA and were allowed to invade the collagen gel for 120 hours. An image for each of the three magnification scales (10x, 20x, 40x) is shown for each condition. Cells that invaded or are in the process of invading the collagen gel are marked with black dotted circles and arrows. A vertical black dotted line highlights the transition from cell layer to collagen gel. Scale bars represent 200 µm.

Due to complete absence of invasive capacity of the metastatic melanoma cell line 451Lu no microscopic images of the organotypic vertical invasion assay performed with this cell line is shown in this study.

In order to quantify the invasive rates of both metastatic cell lines tested under these two conditions (cells with SR-BI knock-down and cells without SR-BI knock-down) in the organotypic vertical invasion assay, microscopic images taken at different areas along the cell layers for each condition were quantified (n = 5). Quantification of the images was performed by evaluating the percentage of cells that had invaded or were in the process of invading the collagen gel relative to the cells present in the cell layer.

Figure 35 illustrates the mean invasion rates of both metastatic cell lines (1205Lu, MCM1DLN) which were evaluated with the organotypic vertical invasion assay and showed an invasive capacity under both conditions (non-targeting/*SR-BI* targeting siRNA transfection). The metastatic cell line 451Lu was not included in this figure since it showed a lack of invasive capacity under both conditions.

As already evident from the microscopic analysis above, the invasion rate of the 1205Lu cell line showed a significant 2-fold decrease when cells were transfected with *SR-BI* targeting siRNA compared to non-targeting siRNA transfected controls (Figure 35). The percentage of invasive 1205Lu control cells reached almost 10% whereas the invasive cell percentage for 1205Lu cells with SR-BI knock-down was approximately 5% (Figure 35). As already speculated above, quantitative assessment of MCM1DLN cell invasion revealed significantly higher invasion rates than these of the 1205Lu cells. The percentage of invasive MCM1DLN cells transfected with non-targeting siRNA reached almost 18% while only 7.5% of MCM1DLN cells with SR-BI knock-down displayed invasive capacity, which represents a significant 2.4-fold decrease of invasion compared to the controls (Figure 35).

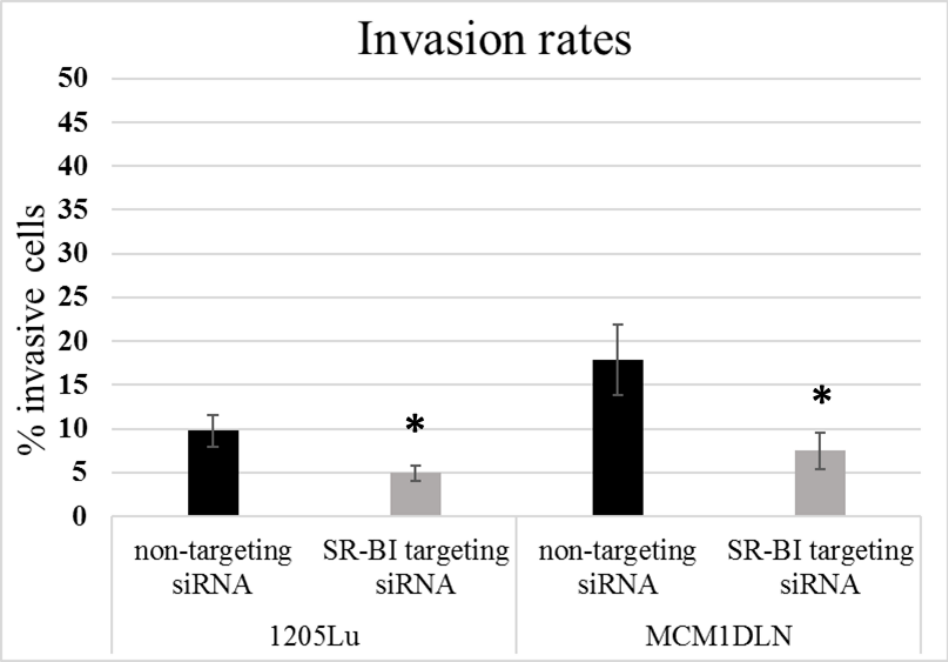

Figure 35: Quantification of the vertical invasion capacity of three metastatic cell lines under the effect of siRNA mediated SR-BI knock-down in the organotypic skin model assay. ***The metastatic cell lines 1205Lu and MCM1DLN with or without SR-BI knock-down were examined in terms of invasion. Several microscopic pictures (magnification 20x) were captured at different areas along the cell layer for each condition and cell line and invasive cells that have invaded or are in the process of invading the collagen gel after 120 hours were quantified for each image using ImageJ (example: Figure 20, Figure 21). Bars represent mean percentage values of invasive cells. Error bars represent standard deviation of the values (n = 5). Significant differences in invasive cells percentage values between two conditions (cells with SR-BI knock-down and cells without SR-BI knock-down) are marked with an asterisk. Values of the 451Lu cell line could not be included as this cell line demonstrated no vertical invasive capacity. P-values are listed in the Appendix Table 7.4.***

4.5 The effect of siRNA mediated SR-BI knock-down on cancer marker protein expression and on protein glycosylation – organotypic skin model assay

The effect of SR-BI on the malignancy of the metastatic melanoma cell lines 1205Lu, MCM1DLN and 451Lu was further investigated by tumor marker protein analysis and immunochistochemistry. Perpendicular sections of the above-mentioned cell lines used in the experimental setup of organotypic skin model assay were used for immunohistochemical staining for various proteins used as tumor markers as well as for staining of a protein glycosylation marker and polysaccharide production.

4.5.1 Evaluation of siRNA mediated SR-BI knock-down efficiency

Initially, the efficiency and maintenance of the siRNA mediated SR-BI knock-down in the above -mentioned metastatic cell lines in the organotypic skin model assay setup was evaluated by IHC. As demonstrated in Figure 36, SR-BI protein staining was significantly reduced in all three metastatic cell lines 1205Lu, MCM1DLN and 451LU (Figure 36 a., b., c.) upon SR-BI knock-down. The area showing positive staining on the microscopic images of different sections was quantified with the Image J program. Quantification of the stained area of the 1205Lu, MCM1DLN and 451Lu cell lines transfected with *SR-BI* targeting siRNA revealed a 6-, 12- and 5- fold decrease in SR-BI protein staining, respectively, when compared to the stained area of the same cell lines in the control condition. The cell line that demonstrated the highest endogenous SR-BI staining in control cells was the 1205Lu cell line (92% stained area) followed by the 451Lu and MCM1DLN cells (64% and 50% stained area, respectively) in the controls (Figure 36 d.). Thus, we concluded that efficient knock-down of SR-BI was still detectable after the long-term culture of the organotypic assays.

- SR-BI

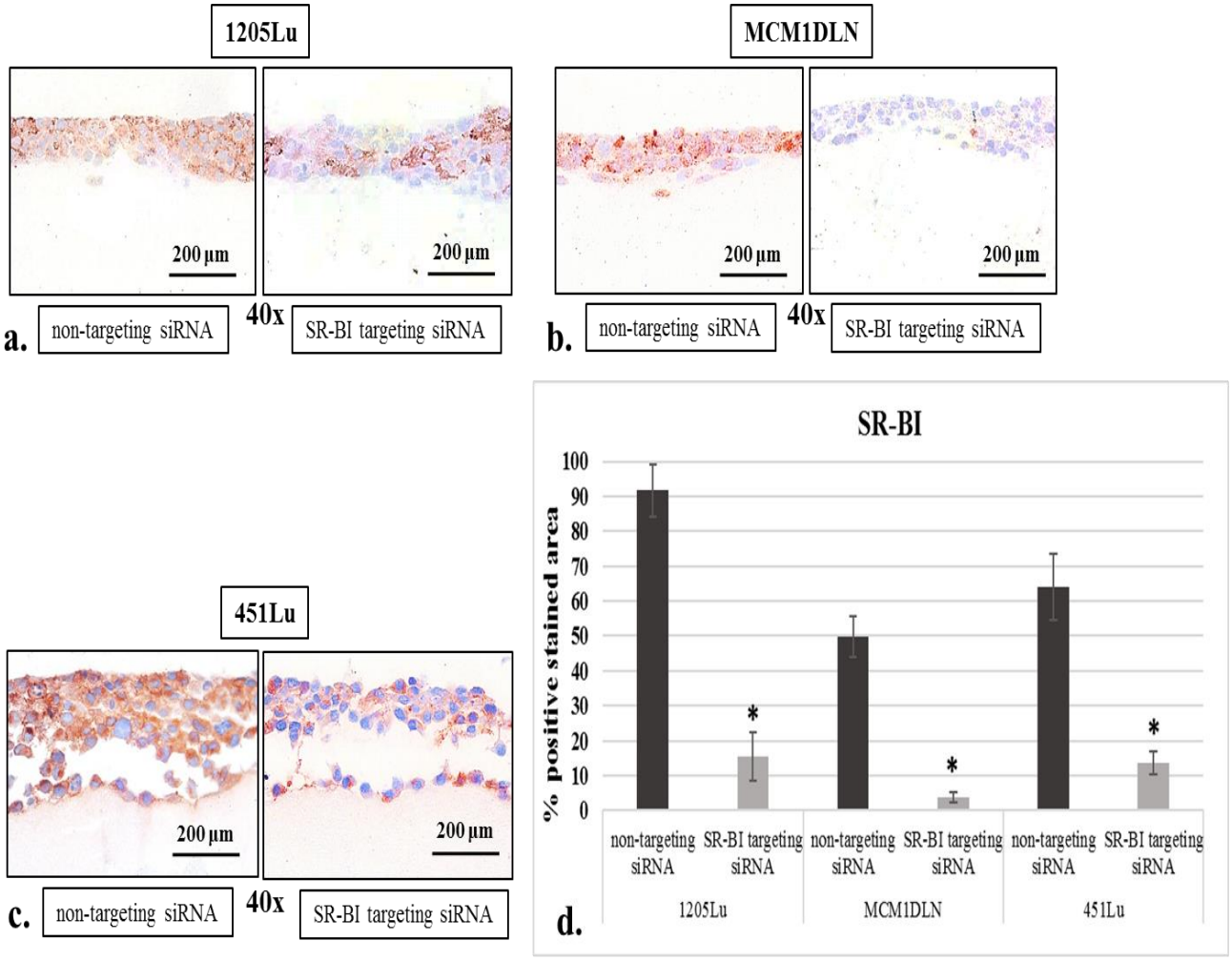

Figure 36: Validation of reduced SR-BI protein expression in three metastatic cell lines examined with the organotypic skin model assay after SR-BI targeting siRNA transfection. a) Microscopic images showing SR-BI protein expression in layers consisting of 1205Lu cells with or without siRNA mediated SR-BI knock-down. b) Microscopic images showing SR-BI protein expression in layers consisting of MCM1DLN cells with and without siRNA mediated SR-BI knock-down. c) Microscopic images showing SR-BI protein expression in layers consisting of 451Lu cells with and without siRNA mediated SR-BI knock-down. Protein expression was analyzed with the IHC method. Scale bars represent 200 µm. d) Quantified intensity of positive cells illustrating SR-BI protein expression in the organotypic skin model assay performed with metastatic cell lines 1205Lu, MCM1DLN, 451Lu with or without siRNA mediated SR-BI knock-down. Bars represent mean values of percentages of stained area versus total tumor cell area (20x magnification) as determined by ImageJ. Error bars represent standard deviation (n = 4). Significant differences in stained area percentage values between the two conditions (cells with SR-BI knock-down and cells without SR-BI knock-down) are marked with an asterisk. P-values are listed in the Appendix Table 7.4.

Subsequently, the effect of SR-BI knock-down on the expression of vascular endothelial growth factor A (*VEGFA*) was analyzed in the three cell lines of metastatic origin used in the organotypic skin model assay (Figure 37).

The VEGFA protein staining of the 1205Lu cells with SR-BI knock-down showed a very slight decrease with no significance compared to the 1205Lu control cells (Figure 37 a. and d.). However, in MCM1DLN cells, SR-BI knock-down resulted in a significant 2.3-fold reduction in the stained area compared to the control MCM1DLN cells (Figure 37 b. and d.). Due to low quality of the staining and detachment of the tumor cell layer in case of 451Lu SR-BI knock-down cells no representative VEGFA protein staining was technically achievable (Figure 37 c., right panel). Thus, the quantification of the stained percentage of these cells was also not possible resulting in a lack of statistically relevant data. In control cells, VEGFA protein staining showed the highest intensity in the 1205Lu cells (78% stained area) followed by the 451Lu and MCM1DLN control cells (24% and 15% stained area, respectively) (Figure 37 d.).

- VEGFA

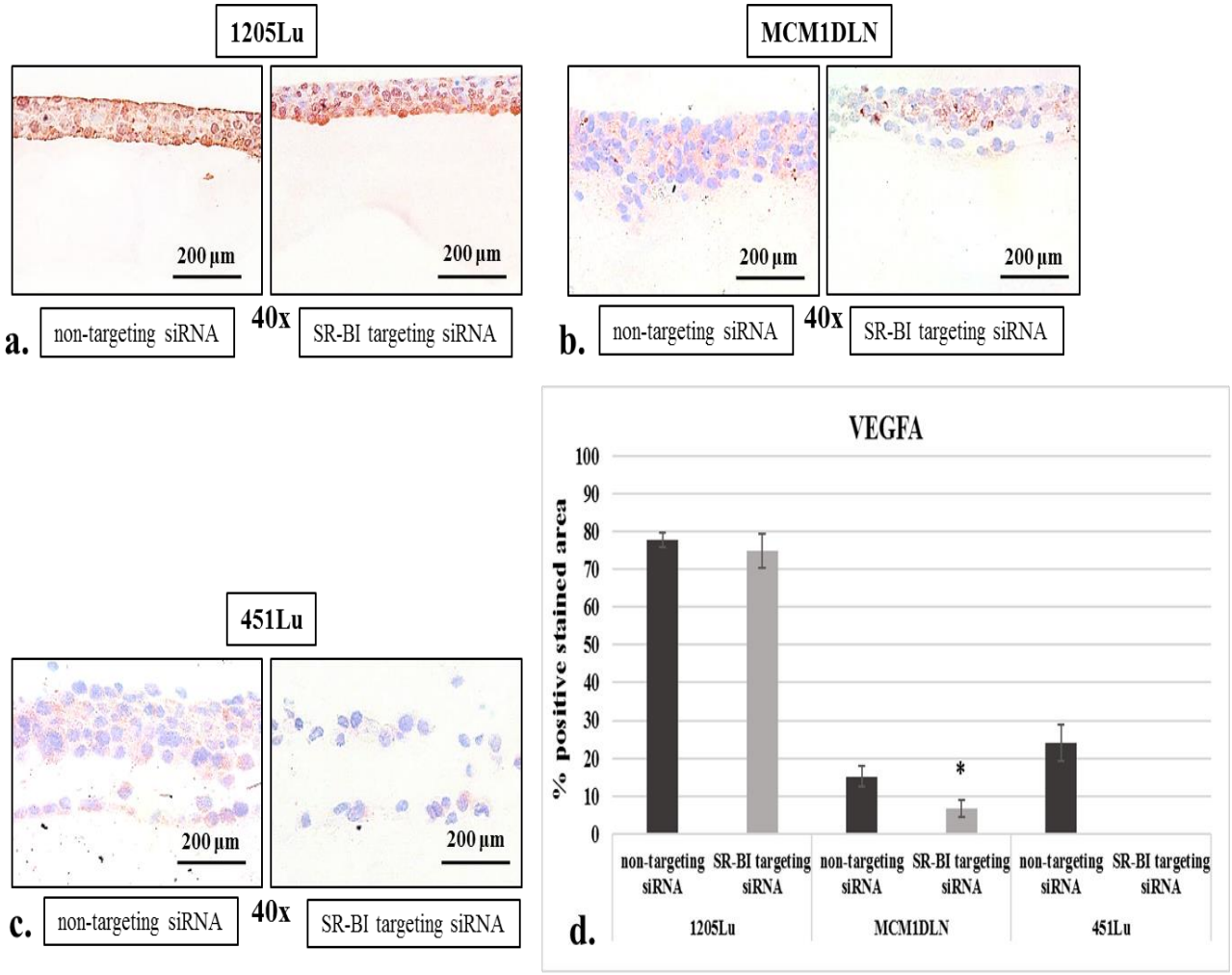

Figure 37: VEGFA protein expression levels in three metastatic cell lines with and without SR-BI knock-down examined with the organotypic skin model assay. a) Representative microscopic images showing VEGFA protein expression in layers consisting of 1205Lu cells with or without siRNA mediated SR-BI knock-down. b) Representative microscopic images showing VEGFA protein expression in layers consisting of MCM1DLN cells with and without siRNA mediated SR-BI knock-down. c) Microscopic images showing VEGFA protein expression in layers consisting of 451Lu cells with and without siRNA mediated SR-BI knock-down. Protein expression was analyzed with the IHC method. Scale bars represent 200 µm. d) Quantified intensity of positive cells illustrating VEGFA protein expression as assessed by ImageJ analysis in the organotypic skin model assay performed with metastatic cell lines 1205Lu, MCM1DLN, 451Lu with or without siRNA mediated SR-BI knock-down. Bars represent mean values of percentages of stained area versus total tumor cell area (20x magnification). Error bars represent standard deviation (n = 4). Significant differences in stained area percentage values between the two conditions (cells with SR-BI knock-down and cells without SR-BI knock-down) are marked with an asterisk. P-values are listed in the Appendix Table 7.4.

Next, the expression of the tumor marker protein STAT5 was immunohistochemically determined in the same samples of the organotypic skin model assay performed with three metastatic cell lines under the effect of SR-BI knock-down (Figure 38).

Surprisingly, *SR-BI* siRNA mediated knock-down in 1205Lu cells increased STAT5 positive area significantly by a factor of 1.4-fold compared to that of the control 1205Lu cells (Figure 38 a. and d.). However, the quantification of STAT5 positive area in MCM1DLN cells did not show any statistically significant difference between the two conditions (cells with SR-BI knock-down and cells without SR-BI knock-down, Figure 38 b. and d.). Sections of 451Lu SR-BI knock-down organotypic skin models used for STAT5 staining were of low quality. For that reason, the percentage of positive STAT5 area in 451Lu cells with SR-BI knock-down was omitted in the diagram (Figure 38 d.) and no comparison between cells with SR-BI knock-down and cells without SR-BI knock-down was possible (Figure 38 c. and d.). The percentage of STAT5 stained area was the highest in the 451Lu control cells (87% stained area) as well as in the 1205Lu cells with SR-BI knock-down (84% stained area). 1205Lu control cells and MCM1DLN cells (for both conditions) displayed approximately 60-68% positivity (Figure 38).

- STAT5

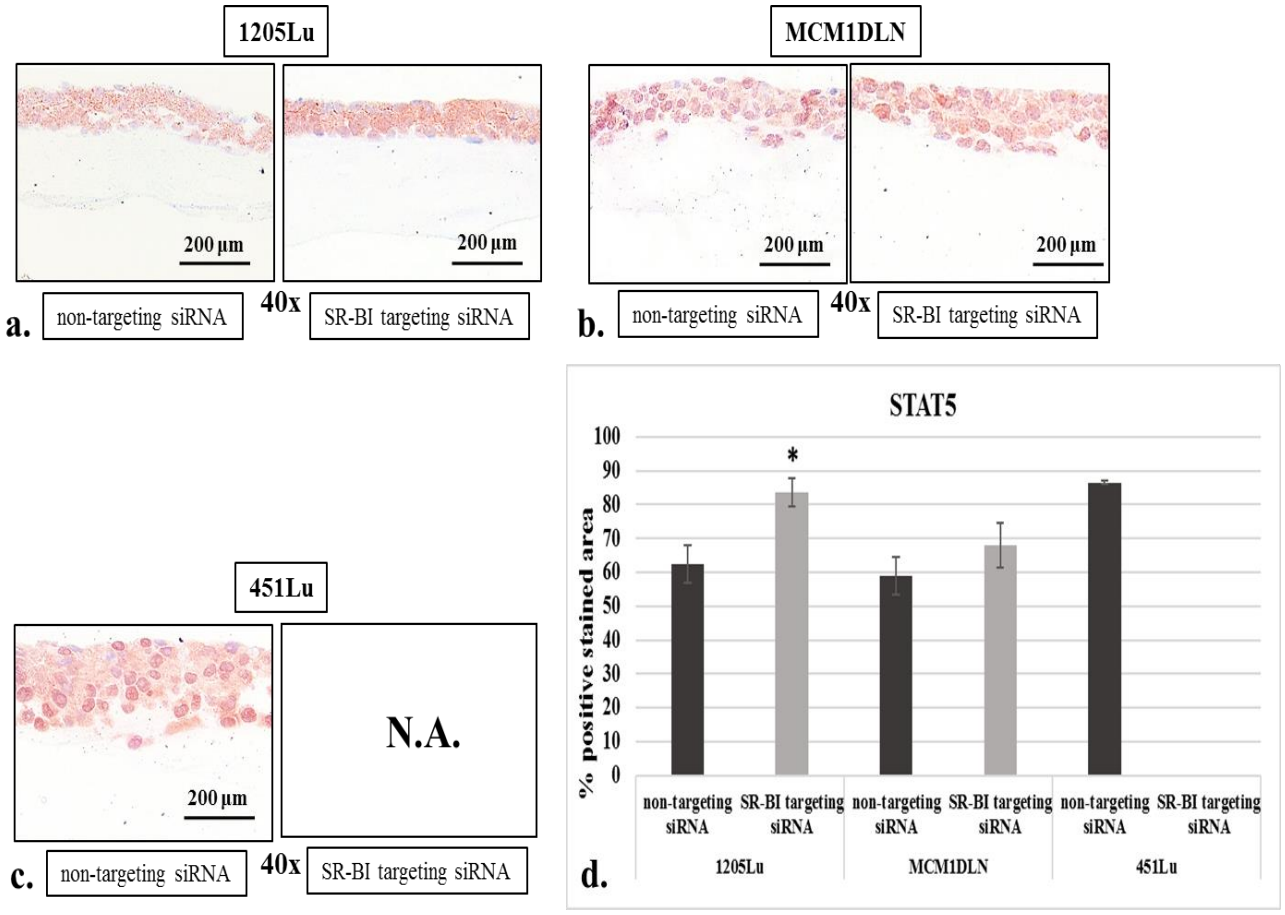

Figure 38: STAT5 protein expression levels in three metastatic cell lines with and without SR-BI knock-down examined with the organotypic skin model assay. a) Representative microscopic images showing STAT5 protein expression in layers consisting of 1205Lu cells with or without siRNA mediated SR-BI knock-down. b) Representative microscopic images showing STAT5 protein expression in layers consisting of MCM1DLN cells with and without siRNA mediated SR-BI knock-down. c) Microscopic images showing STAT5 protein expression in layers consisting of 451Lu cells with and without siRNA mediated SR-BI knock-down. Protein expression was analyzed with the IHC method. Scale bars represent 200 µm. N. A., not available due to low quality sections. d) Quantified intensity of positive cells illustrating STAT5 protein expression in the organotypic skin model assay performed with metastatic cell lines 1205Lu, MCM1DLN, 451Lu with or without siRNA mediated SR-BI knock-down measured by image analysis using ImageJ. Bars represent mean values of percentages of stained area versus total tumor cell area (20x magnification) as determined by ImageJ. Error bars represent the standard deviation (n = 4). Significant differences in stained area percentage values between the two conditions (cells with SR-BI knock-down and cells without SR-BI knock-down) are marked with an asterisk. P-values are listed in the Appendix Table 7.4.

Since STAT5 is translocated to the nucleus post its activation through phosphorylation [103] the cellular localization of STAT5 was also examined as an indication for STAT5 activation. 451Lu samples were excluded from this examination, due to low quality of samples with SR-BI knock-down cells. STAT5 protein in samples of 1205Lu cells under both conditions was predominantly detected in the cytoplasmic area of the cells (Figure 39 a.). MCM1DLN samples however demonstrated nuclear localization of the STAT5 protein mainly in the control samples, whereas nuclear localization of STAT5 was significantly decreased in MCM1DLN SR-BI knock-down cells (Figure 39 b.). Quantification of cells with positive nuclear STAT5 signal also demonstrated a 2-fold decrease of cells with nuclear STAT5 in MCM1DLN SR-BI knock-down samples (11.4%) compared to the respective control samples (24.1%, Figure 39 c.).

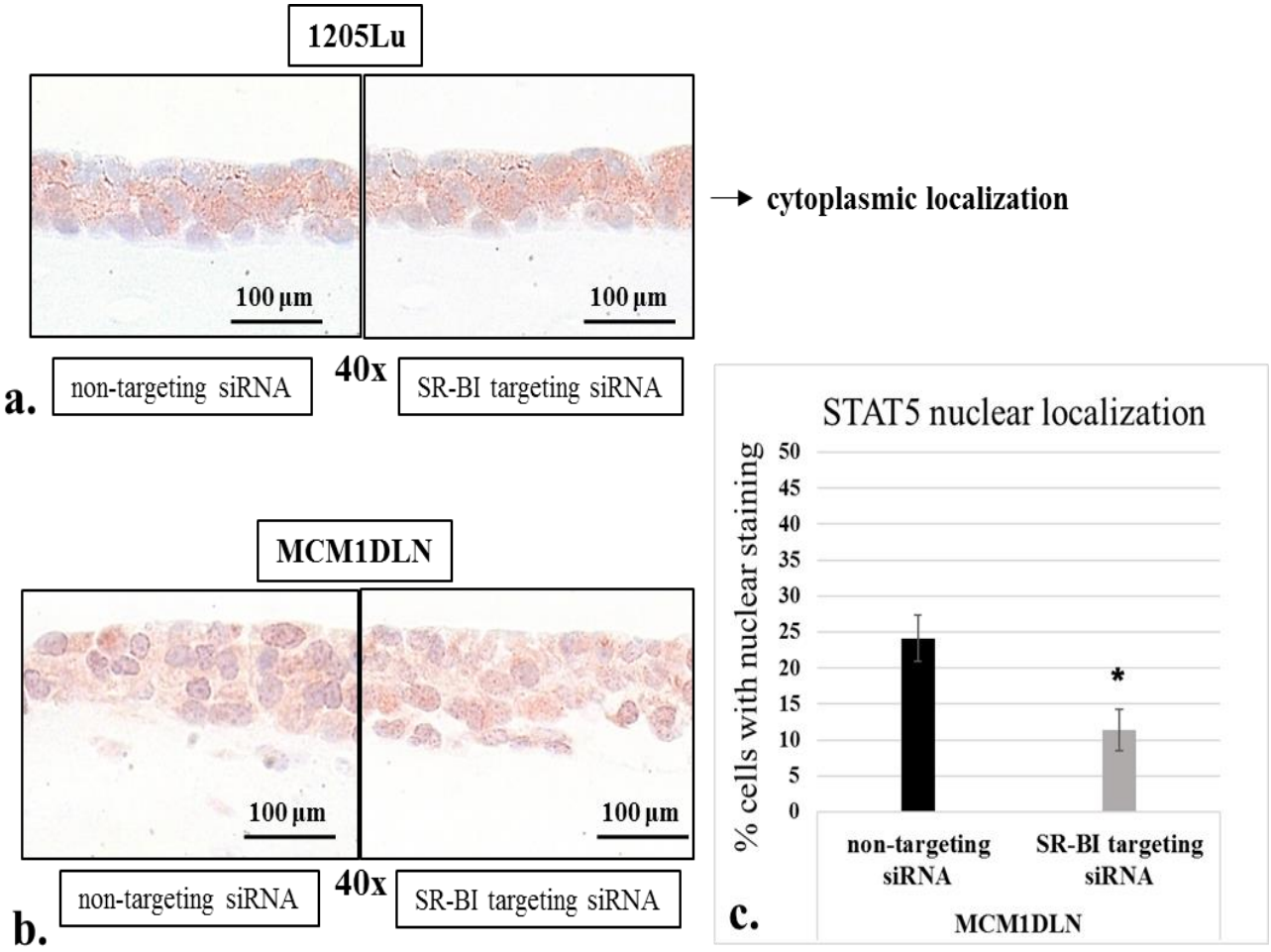

Figure 39: STAT5 cellular localization in the 1205Lu and MCM1DLN metastatic cell lines with and without SR-BI knock-down examined with the organotypic skin model assay. a) Magnified regions of representative microscopic images showing STAT5 protein localization in layers consisting of 1205Lu cells with or without siRNA mediated SR-BI knock-down. b) Magnified regions of representative microscopic images showing STAT5 protein localization in layers consisting of MCM1DLN cells with or without siRNA mediated SR-BI knock-down. c) Quantified intensity of positive cells illustrating STAT5 protein expression in the organotypic skin model assay performed with metastatic cell lines 1205Lu, MCM1DLN, 451Lu with or without siRNA mediated SR-BI knock-down measured by image analysis using ImageJ. Bars represent mean percentage values of cells with nuclear STAT5 signal (40x magnification). Error bars represent the standard deviation (n = 4). Significant differences in percentage values between the two conditions (cells with SR-BI knock-down and cells without SR-BI knock-down) are marked with an asterisk. P-values are listed in the Appendix Table 7.4.

Further, the levels of protein glycosylation and more specifically O-GlcNAcylation were quantified using a specific antibody, again determining the positive stained area on the microscopic IHC images (as for Figure 36,Figure 37 andFigure 38). Sections stained for O-GlcNAcylation (Figure 40) showed a clearly decreased positive stained area in the 1205Lu and MCM1DLN cells with SR-BI knock-down compared to the respective control cells. (Figure 40 a. and b.). Quantification revealed that the percentages of stained 1205Lu or MCM1DLN cells were significantly reduced by 1.2- and 2.5-fold in the knock-downs, respectively (Figure 40 d.). The percentages of positive stained area in the 451Lu cell layers did not show any significant difference between these two conditions. (Figure 40 c. and d.). The highest percentages of O-GlcNAcylation positive cells were observed in 451Lu cells for both conditions (65%-70%). 1205Lu cells showed a similarly high percentage of positive stained area (57%-68%). However, the cell line MCM1DLN demonstrated a relatively low positive stained area for both conditions (27% positive stained area for control cells and 11% positive stained area for cells with SR-BI knock-down, Figure 40 d.).

- Protein glycosylation/O-GlcNAc antibody (CTD110.6)

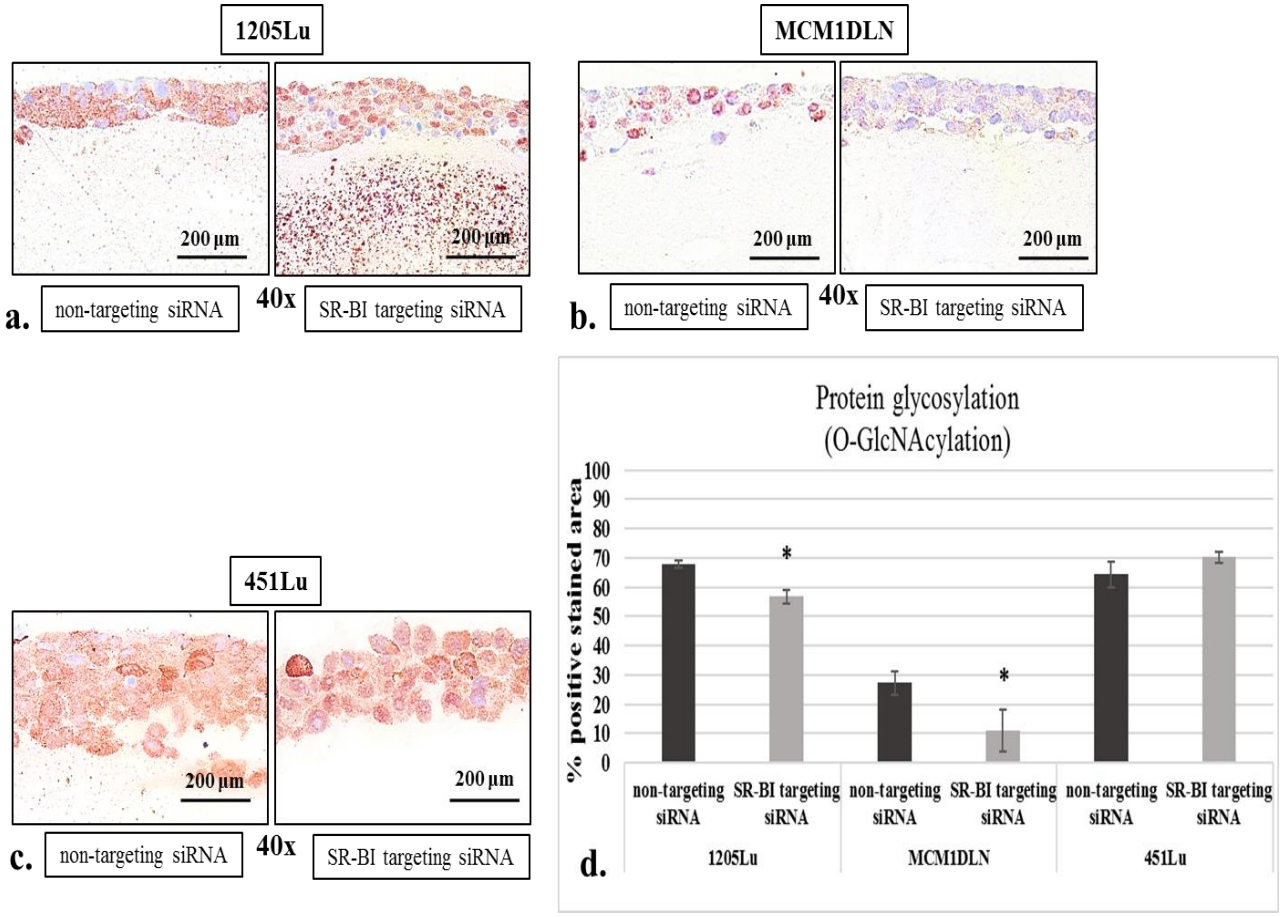

Figure 40: Protein glycosylation (O-GlcNAcylation) levels in three metastatic cell lines with and without SR-BI knock-down examined with the organotypic skin model assay. a) Representative microscopic images showing protein glycosylation (O-GlcNAc on proteins) in layers consisting of 1205Lu cells with or without siRNA mediated SR-BI knock-down. b) Representative microscopic images showing protein glycosylation (O-GlcNAc on proteins) in layers consisting of MCM1DLN cells with and without siRNA mediated SR-BI knock-down. c) Microscopic images showing protein glycosylation (O-GlcNAc on proteins) in layers consisting of 451Lu cells with and without siRNA mediated SR-BI knock-down. Protein glycosylation (O-GlcNAc on proteins) was analyzed with the IHC method. Scale bars represent 200 µm. d) Quantified intensity of positive cells illustrating protein glycosylation (O-GlcNAc on proteins) in the organotypic skin model assay performed with metastatic cell lines 1205Lu, MCM1DLN, 451Lu with or without siRNA mediated SR-BI knock-down. Bars represent mean values of percentages of stained area versus total tumor cell area (20x magnification) as determined by ImageJ. Error bars represent standard deviation (n = 4). Significant differences in stained area percentage values between the two conditions (cells with SR-BI knock-down and cells without SR-BI knock-down) are marked with an asterisk. P-values are listed in the Appendix Table 7.4.

In addition to protein glycosylation analysis, the cellular polysaccharide and carbohydrate levels were assessed in the same organotypic skin models. This assessment was carried out with the periodic acid - schiff base (PAS) staining method in order to investigate a possible correlation between protein glycosylation and polysaccharide levels.

Quantification of the different organotypic skin model assays revealed a significant increase in positive stained area in cells with SR-BI knock-down for all three cell lines. However, the difference in positively stained area between the two conditions was not clearly visible by eye on the microscopic images of the 1205Lu and MCM1DLN cell lines (Figure 41 a. and b.). Despite that fact, when quantified, 1205Lu and MCM1DLN cell layers with SR-BI knock-down demonstrated a 2- and 1.5-fold increase in the stained area, respectively. The percentage of stained area of the 451Lu cells with SR-BI knock-down (Figure 41 c.) also showed an increase by 1.6-fold compared to that of the 451Lu control cells (Figure 41).

Polysaccharide and carbohydrate levels appeared to be the highest in the 1205Lu and 451Lu cell lines with 17% and 20% positive stained area for the control cells as well as with 33.7% and 32% positive stained area for the cells with SR-BI knock-down, respectively. The MCM1DLN cell layer demonstrated only 9% - 13% positive stained area in cells without and with SR-BI knock-down, respectively (Figure 41 d.).

- Polysaccharide and carbohydrate levels

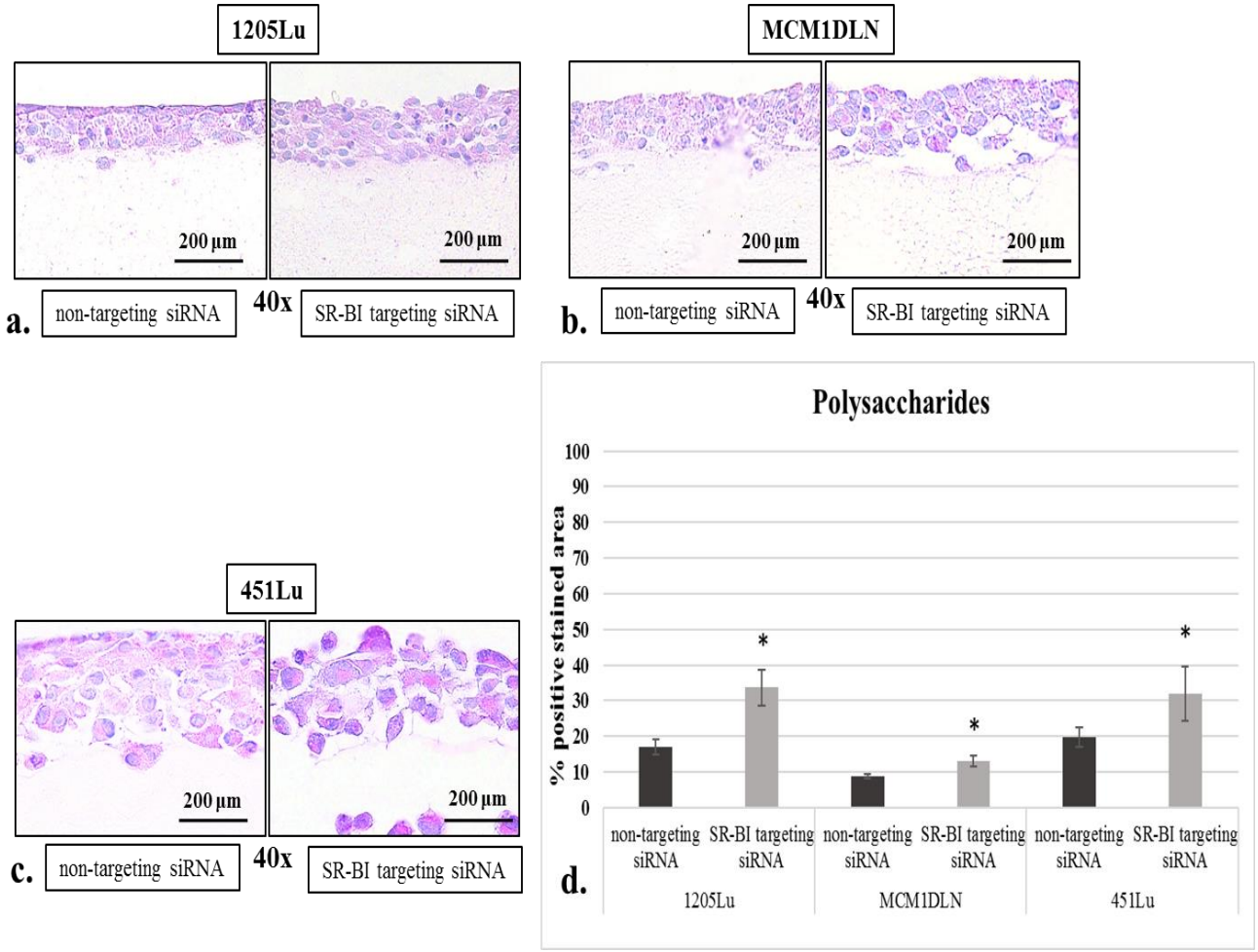

Figure 41: Determination of polysaccharide levels in three metastatic cell lines with and without SR-BI knock-down in the organotypic skin model assay by PAS staining. ***a) Microscopic images showing polysaccharide and carbohydrate levels in layers consisting of 1205Lu cells with or without siRNA mediated SR-BI knock-down. b) Microscopic images showing polysaccharide and carbohydrate levels in layers consisting of MCM1DLN cells with and without siRNA mediated SR-BI knock-down. c) Microscopic images showing polysaccharide and carbohydrate levels in layers consisting of 451Lu cells with and without siRNA mediated SR-BI knock-down. Polysaccharide and carbohydrate levels were analyzed with the PAS method. Scale bars represent 200 µm. d) Quantified intensity of positive cells illustrating polysaccharide (and carbohydrate) levels in the organotypic skin model assay performed with metastatic cell lines 1205Lu, MCM1DLN, 451Lu with or without siRNA mediated SR-BI knock-down. Bars represent mean values of percentages of stained area versus total tumor cell area (20x magnification) as determined by ImageJ. Error bars represent standard deviation (n = 4). Significant differences in stained area percentage values between the two conditions (cells with SR-BI knock-down and cells without SR-BI knock-down) are marked with an asterisk. P-values are listed in the Appendix Table 7.4.***

In order to examine a possible effect of the *SR-BI* gene ablation in the cellular adhesion of all three metastatic cell lines mentioned above and tested with the organotypic skin model assay, perpendicular sections were immunohistochemically stained for the E-Cadherin protein (Figure 42). However, E-Cadherin positivity was not seen at the cell surface and cell borders as expected but predominantly in the cell nucleus and cytoplasm.

Microscopic evaluation revealed that for all cell lines except for the 451Lu cells (Figure 42 c.) the SR-BI knock-down condition showed a clearly stronger staining (Figure 42 a. and b.). Quantification of the microscopic images revealed a significant 3.8- and 2-fold increase in percentages of stained area in 1205Lu and MCM1DLN SR-BI knock-down cell layers compared to that of control cell layers, respectively (Figure 42 d.).

The quality of the microscopic images of the 451Lu cell layers with SR-BI knock-down was low due to probably decreased cohesiveness of this sample on the glass slides (Figure 42 c., right panel). However, quantification of the available images of the 451Lu cell line was possible and revealed no significant difference in the positive stained area between the two conditions (cell layer with control/SR-BI knock-down cells, Figure 42 d.).

MCM1DLN cells displayed the largest stained area (38% and 76% positive stained area for control and SR-BI knock-down cell layers, respectively). 451Lu cell layers showed less stained area than the MCM1DLN cells (33% and 36% positive stained area for control and SR-BI knock-down cell layers, respectively). The layers of the 1205Lu cell line showed the lowest E-Cadherin staining with 8% and 32% stained area for control and SR-BI knock-down cell layers, respectively (Figure 42 d.).

- E-Cadherin

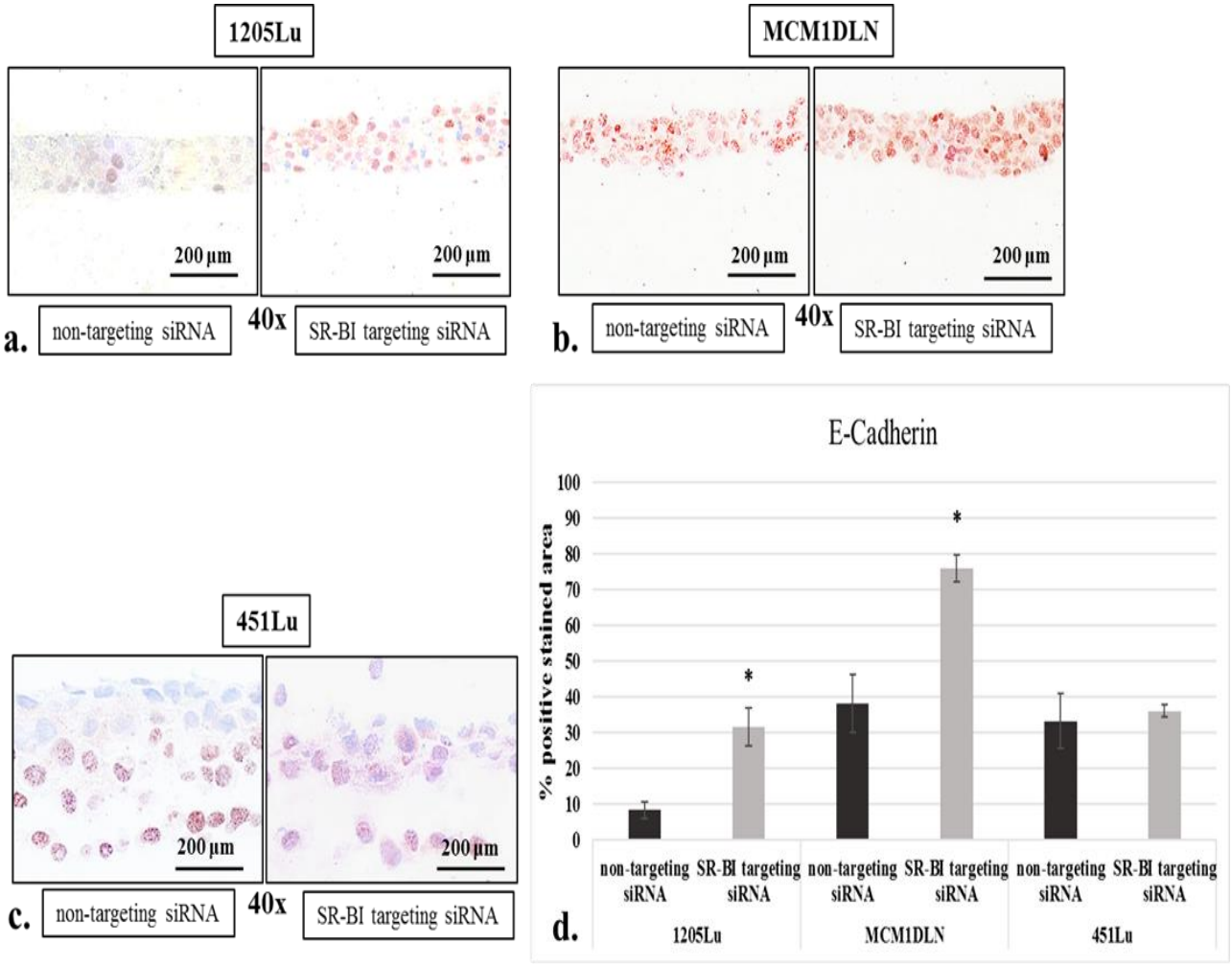

Figure 42: Assessment of E-Cadherin protein levels in three metastatic cell lines with and without SR-BI knock-down in the organotypic skin model assay. a) Representative microscopic images showing E-Cadherin protein expression in layers consisting of 1205Lu cells with or without siRNA mediated SR-BI knock-down. b) Representative microscopic images showing E-Cadherin protein expression in layers consisting of MCM1DLN cells with and without siRNA mediated SR-BI knock-down. c) Microscopic images showing E-Cadherin protein expression in layers consisting of 451Lu cells with and without siRNA mediated SR-BI knock-down. Protein expression was analyzed with the IHC method. Scale bars represent 200 µm. d) Quantified intensity of positive cells illustrating E-Cadherin protein expression in the organotypic skin model assay performed with metastatic cell lines 1205Lu, MCM1DLN, 451Lu with or without siRNA mediated SR-BI knock-down. Bars represent mean values of percentages of stained area versus total tumor cell area (20x magnification) as determined by ImageJ. Error bars represent standard deviation (n = 4). Significant differences in stained area percentage values between the two conditions (cells with SR-BI knock-down and cells without SR-BI knock-down) are marked with an asterisk. P-values are listed in the Appendix Table 7.4.

In parallel to every immonohistochemical staining mentioned above, perpendicular sections of all samples were also used as negative controls for evaluating the secondary antibody specificity. The experimental procedure of these samples was the same, however the primary antibody was not used in these samples for the immunohistochemical staining.

Representative microscopic images on Figure 43 illustrate the absence of positive red stained cells in the samples of all three metastatic cell lines used (1205Lu, MCM1DLN and 451Lu). The blue color of the cell nuclei staining (counterstaining) with hematoxylin is visible in all samples (Figure 43).

- Control stainings for antibody specificity

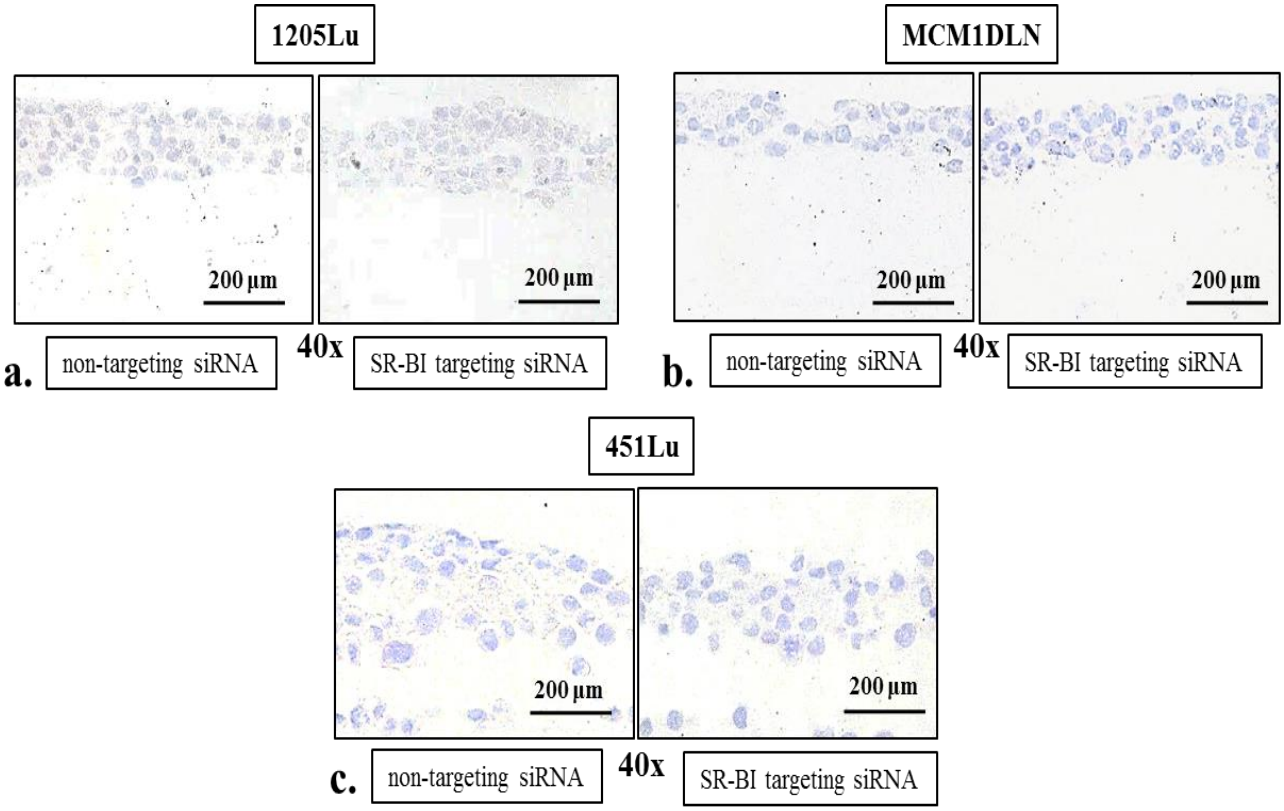

Figure 43: Determining the background for immunohistochemistry in the organotypic skin model assays using secondary antibody-only controls. a) Microscopic images illustrating the lack of IHC staining signal in layers consisting of 1205Lu cells with or without siRNA mediated SR-BI knock-down. b) Microscopic images illustrating the lack of IHC staining signal in layers consisting of MCM1DLN cells with or without siRNA mediated SR-BI knock-down. c) Microscopic images illustrating the lack of IHC staining signal in layers consisting of MCM1DLN cells with or without siRNA mediated SR-BI knock-down. Samples were analyzed with the IHC method without the use of the respective primary antibody for each protein expression analysis. Scale bars represent 200 µm.

4.6 The effect of siRNA mediated SR-BI knock-down on the mRNA expression of genes involved in transcriptional repression, cell adhesion and cell migration – organotypic skin model assay

Samples of 1205Lu, MCM1DLN and 451Lu cells derived from the organotypic skin models were additionally analyzed with the quantitative PCR method. The mRNA expression of several genes playing important roles in transcriptional repression, cell adhesion and cell migration was examined for changes upon SR-BI depletion and quantified for each cell line and for each condition. Initially, proper *SR-BI* mRNA depletion by siRNA was validated.

As illustrated in Figure 44, all samples from SR-BI knock-down cells showed a clear decrease in *SR-BI* mRNA expression compared to control cells. As expected, MCM1DLN cells with SR-BI knock-down displayed the highest decrease in *SR-BI* mRNA expression by 16.6-fold compared to MCM1DLN cells with endogenous *SR-BI* mRNA expression. 1205Lu cells transfected with *SR-BI* siRNA showed a 6-fold decreased expression of *SR-BI* mRNA compared to the control condition. Knock-down of SR-BI in the 451Lu cell line was not as effective as in the two above-mentioned cell lines, as cells transfected with *SR-BI* siRNA showed a mere 2.3-fold decrease in *SR-BI* mRNA expression compared to 451Lu control cells (Figure 44).

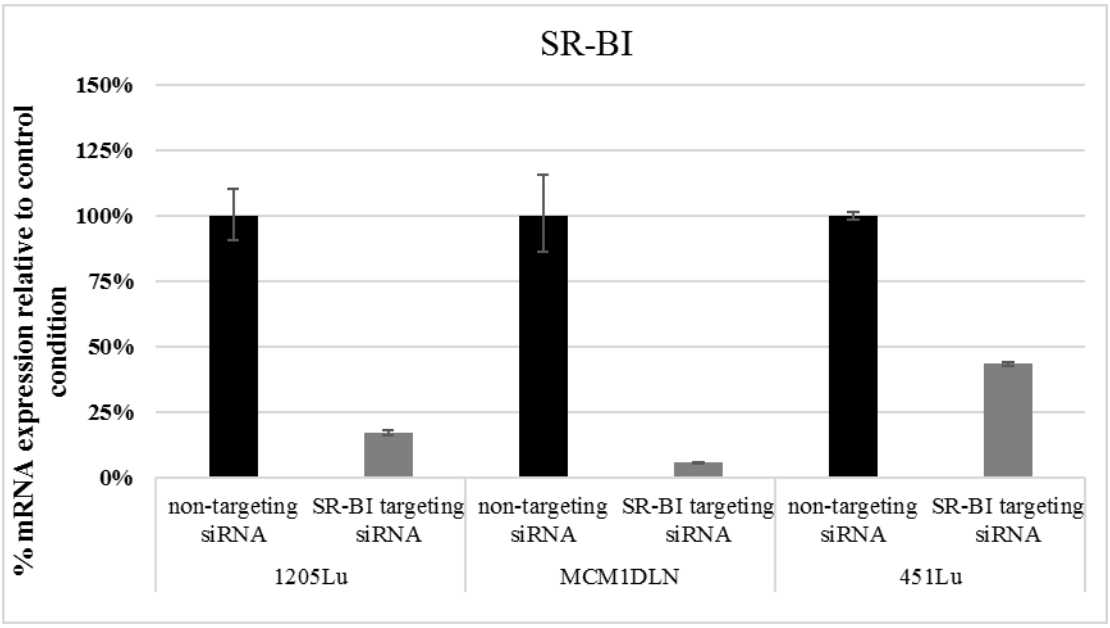

Figure 44: Validation of SR-BI mRNA expression in three metastatic cell lines examined by the organotypic skin model assay after SR-BI targeting siRNA transfection. mRNA levels were measured after examination of vertical invasion capacity of these cell lines for 120 hours. Bars represent relative values measured by the qPCR method and normalized to the housekeeping gene β-ACTIN. Error bars represent the range of the values as technical replicates (n=2) were used at each measurement.

Expression analysis of the repressor *SNAIL2* by quantitative PCR revealed an evident decrease in the mRNA levels of *SNAIL2* in the samples derived from SR-BI knock-down cells. MCM1DLN and 1205Lu cells with SR-BI knock-down demonstrated a 20- and 6.7-fold decrease in *SNAIL2* mRNA levels, respectively, compared to control cells of these cell lines. *SNAIL2* mRNA expression was reduced only by 2-fold in 451Lu SR-BI knock-down cells compared to control cells (Figure 45).

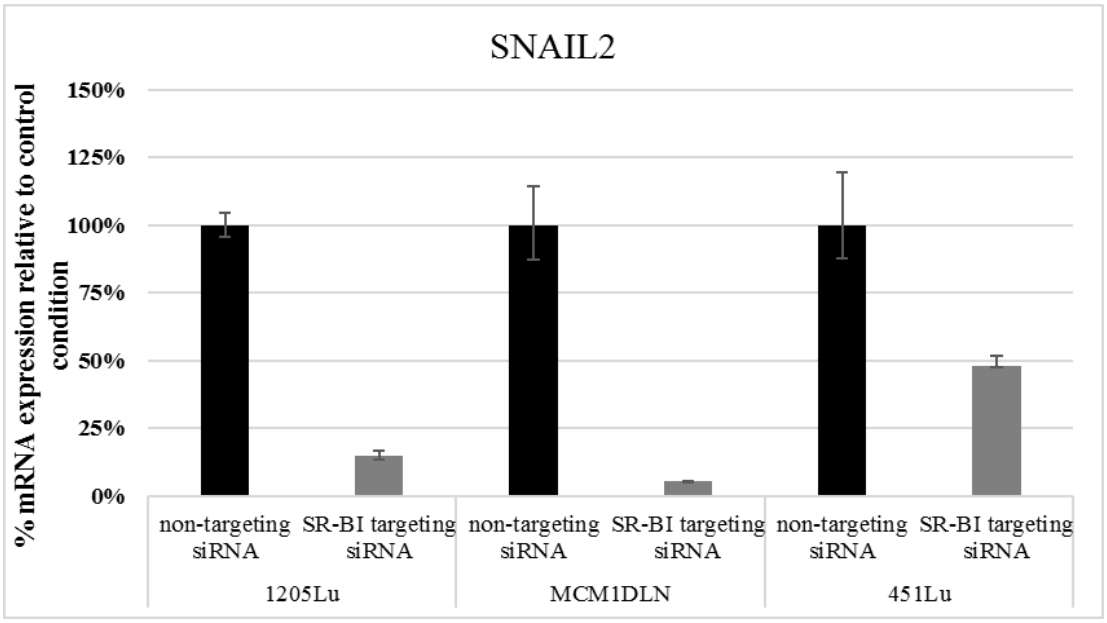

Figure 45: mRNA expression of SNAIL2 in three metastatic cell lines examined with the organotypic skin model assay after SR-BI targeting siRNA transfection. mRNA levels were measured after examination of vertical invasion capacity of these cell lines for 120 hours. Bars represent mean relative values measured by the qPCR method and normalized to the housekeeping gene β-ACTIN. Error bars represent the range of the values as technical replicates (n=2) were used at each measurement.

The extracellular matrix gene collagen 12 (*COL12A1*) which can contribute to cell adhesion showed an increase in mRNA abundance in MCM1DLN and 451Lu cells with SR-BI knock-down. Compared to the samples derived from control cells, the samples of SR-BI knock-down cells showed a 1.5- and 1.2-fold increase in *COL12A1* mRNA for the MCM1DLN and 451Lu cell line, respectively. Surprisingly, *COL12A1* mRNA levels showed a 2-fold decrease in expression in 1205Lu samples when SR-BI was knocked-down in these cells (Figure 46).

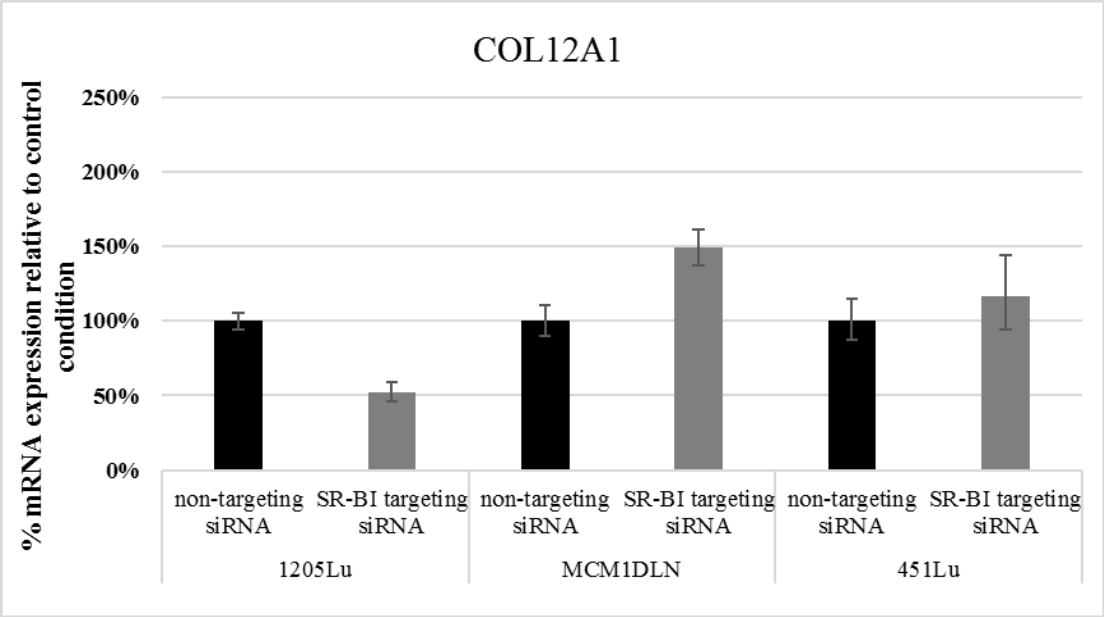

Figure 46: mRNA expression levels of COL12A1 in three metastatic cell lines in the organotypic skin model assay after SR-BI targeting siRNA transfection. mRNA levels were measured after examination of vertical invasion capacity of these cell lines for 120 hours. Bars represent relative values measured by the qPCR method and normalized to the housekeeping gene β-ACTIN. Error bars represent the range of the values as technical replicates (n=2) were used at each measurement.

The mRNA levels of the cell adhesion gene, connective tissue growth factor (*CTGF*) also demonstrated a clear increase in 1205Lu and MCM1DLN cells when SR-BI was depleted compared to the control cells. *CTGF* mRNA levels were increased by 1.5- and 2-fold in SR-BI knock-down 1205Lu and MCM1DLN cells, respectively. In contrast, 451Lu cells showed approximately the same levels of *CTGF* mRNA in cells of both conditions (endogenous SR-BI versus SR-BI knock-down). There was a mere 1.2-fold decrease of mRNA levels observed for the 451Lu cells with SR-BI knock-down compared to the control cells (endogenous SR-BI) (Figure 47).

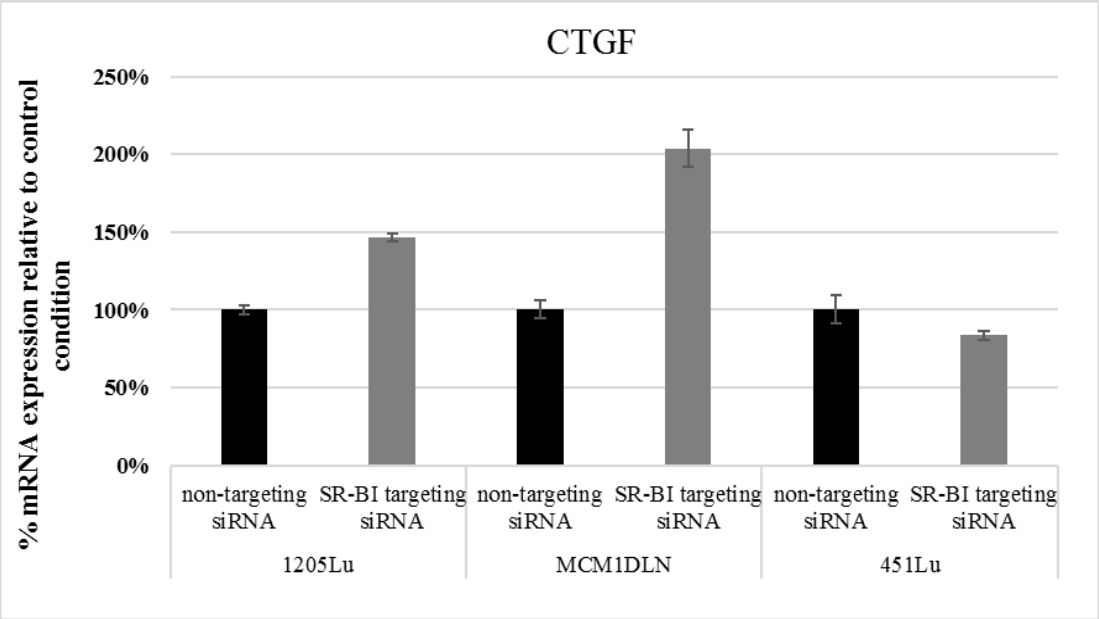

Figure 47: mRNA expression levels of CTGF in three metastatic cell lines in the organotypic skin model assay after SR-BI targeting siRNA transfection. mRNA levels were measured after examination of vertical invasion capacity of these cell lines for 120 hours. Bars represent relative values measured by the qPCR method and normalized to the housekeeping gene β-ACTIN. Error bars represent the range of the values as technical replicates (n=2) were used at each measurement.

The quantitative PCR analysis conducted with the above-mentioned samples was carried out in two technical replicates and four biological replicates were pooled together. For further validation as well as statistical analysis of the results and in order to analyze the mRNA expression of further genes involved in the malignant phenotype of the cells, a repetition of the exact experiment is necessary in future experiments.

Part of the results presented in this study are shown in:

Katharina Kinslechner, David Schörghofer, Birgit Schütz, **Maria Vallianou**, Bettina Wingelhofer, Wolfgang Mikulits, Clemens Röhrl, Markus Hengstschläger, Richard Moriggl, Herbert Stangl and Mario Mikula. Malignant Phenotypes in Metastatic Melanoma are Governed by SR-BI and its Association with Glycosylation and STAT5 Activation. Mol Cancer Res January 1 2018 (16) (1) 135-146; DOI: 10.1158/1541-7786.MCR-17-0292

5. Discussion

The major aim of this thesis was to analyze the possible correlation between expression of the SR-BI receptor and the metastatic properties as well as potential of melanoma cells. Since previous studies indicated a significant role of SR-BI expression in cancer progression and aggressiveness of breast [69] and prostate cancer [72], experiments were conducted to investigate the possible prevalence of this effect in melanoma. To better replicate the *in vivo* situation for this study, all experiments were performed as 3D melanoma spheroids or as organotypic skin models.

5.1 Spheroid formation

Initially, various methods were tested in order to form 3D spheroids of 2,500 cells. Metastatic and non-metastatic melanoma, partly constituting pairs of isogenic cell lines (1205Lu & WM793b as well as MCM1DLN & MCM1G) were used for this purpose. It was observed that all human melanoma cell lines mentioned in this study could successfully form compact spheroids. Metastatic melanoma lines display a slightly larger surface and less compact form (Figure 18). This could possibly be explained by the properties of metastatic cells as they tend to lose their cell-cell adhesion capacity through downregulation of E-cadherin [104]. Yet, the involvement of additional cell-cell adhesion molecules, which might be lost during metastatic conversion of melanoma cells, has to be also taken into consideration. However, this was not the objective of this master thesis and thus not studied in detail any further.

5.2 Spheroid formation of metastatic melanoma cell lines with SR-BI knock-down

As a next step, the SR-BI receptor gene was knocked-down with the use of *SR-BI* siRNA in four metastatic melanoma cell lines (MCM1DLN, 1205Lu, 451Lu and WM3854) and in one non-

metastatic melanoma cell line, WM793b. The analysis of the *SR-BI* gene knock-down effectiveness via immunohistochemistry showed the successful ablation of the *SR-BI* gene in the metastatic melanoma lines MCM1DLN and 1205Lu cells, while the *SR-BI* gene knock-down was only partly efficient for the metastatic cell line WM3854 (Figure 19). Regardless of the missing data about the efficiency of the *SR-BI* gene ablation in the 451Lu melanoma line, the metastatic cell lines 1205Lu, MCM1DLN and 451Lu were used for melanoma spheroid formation after knock-down of the *SR-BI* gene (Figure 20) and their size and morphology were compared to that of the control spheroids (Figure 21). The comparison demonstrated a significant reduction in spheroid size for all three cell lines (25-45% decrease in size) and a more compact appearance for the 1205Lu and 451Lu cell line. The decreased size of the spheroids could be explained by the reduced proliferation rate of cells with an ablated *SR-BI* gene, a finding that was reported by a previous study [68]. These results could also be an indication of the inverse correlation of SR-BI expression and the cell to cell adhesive capacity of melanoma cells. Data indicating the correlation of SR-BI and cell to cell adhesion have been already published [105] and report reduced invasiveness of melanoma cells upon SR-BI ablation in 3D cell culture models. Additionally, as mentioned in 5.1, spheroids of non-metastatic cell lines, similarly, also demonstrated a more compact form and smaller size compared to the spheroids of their isogenic metastatic cell line. Thus, we conclude that loss of SR-BI is either associated with decreased proliferation or increased cell adhesion properties or a combination of both, leading to reduced spheroid size. Of note, spheroids formed with 1205Lu, MCM1DLN and 451Lu cells with an ablated *SR-BI* gene thus show a tendency to simulate the phenotype of spheroids formed with non-metastatic melanoma cell lines.

5.3 Viability of melanoma cell spheroids after pharmacological treatment or siRNA mediated SR-BI knock-down

In order to validate the effects of inhibiting the selective lipid uptake with an additional method other than siRNA mediated SR-BI knock-down, melanoma cell lines were in parallel treated with

the pharmacologic cholesterol synthesis inhibitor lovastatin and/or with the lipid transport blocker BLT-1. As a first step, we tried to define the highest non-toxic concentrations of these substances on melanoma cells. Additionally, we examined the effect of siRNA transfection on melanoma cell viability. The viability of treated and siRNA transfected spheroids was evaluated by measuring ATP levels as an indicator for cellular viability.

All spheroids, except 1205Lu spheres, showed statistically significantly reduced ATP levels after SR-BI knock-down. However, ATP levels of the respective control siRNA transfected spheroids also decreased significantly by approximately the same degree. Thus, this loss of viability can be explained by the toxicity of the siRNA liposomal transfection [106] and not by the loss of SR-BI. Spheroids of the 1205Lu cell line showed no statistically significant decrease in ATP levels after siRNA transfection, thus indicating that these cells seem to be more robust against liposomal transfection. In contrast, all spheroids (except WM3854) treated with BLT-1, demonstrated a higher decrease in ATP levels/viability than the respective SR-BI knock-down spheroids or the non-targeting siRNA controls. It was therefore concluded that reduced ATP levels/viability rates post BLT-1 treatment were rather an off-target effect of the inhibitor, which might interfere with cellular mechanisms, crucial to cellular health. Indeed, there has been already reported that BLT-1 binding to SR-BI is irreversible and extended treatment with BLT-1 is highly toxic for the cells used in *in vitro* assays [107]. Another explanation for the difference of viability rates between BLT-1 treated cells and SR-BI knock-down cells could be a possible activation of compensation mechanisms in cells with SR-BI knock-down. This activation could counteract the effects of cholesterol uptake inhibition on the cells' viability. Yet, there is no further evidence to support this theory and further research is needed to clarify this observation.

It was generally observed that ATP levels of melanoma spheroids were greatly reduced 72 hours post combined treatment with lovastatin and BLT-1 for all cell lines. However, considering the above-discussed side effect of BLT-1, this observation might just indicate that combining the two substances is even more deleterious for the cells.

Due to the high viability decrease of MCM1DLN cells also with the single lovastatin treatment, it can be assumed that there is a possible sensitivity of the MCM1DLN spheroids to the single lovastatin treatment. The results about MCM1DLN's sensitivity to lovastatin treatment are

supported by the findings of another study suggesting lovastatin as a therapeutic agent against melanoma after demonstrating that lovastatin induced cytotoxicity and apoptosis in human and murine melanoma cells [108].

On the other hand, the 1205Lu and WM793b cell line demonstrated high sensitivity only to the BLT-1 single or combined treatment and not to the lovastatin single treatment (Figure 23, 25). This observation could be due to the BLT-1 off-target effects (as discussed above) or due to inhibition of lipid uptake via SR-BI in these cell lines. In a similar study it has been demonstrated that cell death of 1205Lu was induced only after cholesterol transport was inhibited [109] (similarly to lipid uptake inhibition by BLT-1) and not after treatment with statin. The results of this study [109] are further in accordance with the results of our study, as the single lovastatin treatment does not seem to affect the viability of the 1205Lu cells (Figure 23). The decrease in viability of its counterpart, WM393b, treated with lovastatin is also much weaker than with the BLT-1 treatment (Figure 25). Statins' inability to induce cell death through cholesterol synthesis inhibition was also reported in another study with the cell line WM35 [110]. In this paper is was, however, also mentioned that the exogenous addition of IL-6 to simvastatin-treated WM35 cells highly increased the apoptotic rates induced by the statin drug alone [110]. Thus, one explanation for the lack of sensitivity of only some melanoma cell lines to statin-induced cell death, could be the low IL-6 production/secretion by these cell lines and thereby its marginal or absent autocrine effect [110]. However, for further confirmation of this hypothesis in this experiment, the IL-6 concentration of the melanoma cell lines 1205Lu and WM793b should be determined.

Despite the observation that all cell lines used in this experiment showed a high decrease of cell viability, even with the single lovastatin or BLT-1 treatments, the metastatic cell line WM3854 surprisingly showed a larger decrease in ATP levels (>50%) after spheroid treatment with higher concentrated lovastatin and BLT-1 combinations (Figure 24). It could be thus concluded that WM3854 is rather resistant to the treatments compared to the rest of the melanoma cell lines used in this experiment.

Consequently, due to the toxicity effects of the above-mentioned inhibitors, it was decided that combination treatment of these substances could be used for further experiments merely in their lowest concentration tested (5 μM lovastatin and 1 μM BLT-1). However, a shorter incubation

time, which would not exceed the 24-hour timeframe had to be also used in order to avoid toxicity effects.

5.4 Invasive capacity of three-dimensional culture systems

5.4.1 Spheroid invasion assay after treatment or *SR-BI* gene ablation

5.4.1.1 Invasive capacity of spheroids after pharmacological treatment or siRNA mediated SR-BI knock-down

After determining the optimal BLT-1 and lovastatin concentrations for the 24-hour combination treatment of melanoma spheroids in 5.3, these inhibitors were evaluated for their impact on invasion of the above-mentioned melanoma cell lines. Thus, MCM1DLN, 1205Lu, WM3854 and WM793b spheroids seeded into collagen gels were subjected to BLT-1 and lovastatin single and combination treatment. In parallel, spheroids of the same melanoma cell lines with SR-BI knock-down as well as non-targeting control spheroids were subjected to the same collagen gel invasion assay. The results of the different conditions and treatments were subsequently compared.

The first results in Figure 26 and 27 demonstrated that, a significant decrease in invasiveness was shown only for BLT-1 and/or lovastatin treated MCM1DLN cell spheroids (38%-78% decrease of invasiveness) compared to the respective controls. This decrease could be probably explained by the toxicity of these substances (as shown in 5.3) resulting in cell death and consequently showing an indirect effect on cell invasion (as dead cells are not able to invade). Hence, a clear-cut influence of inhibitor treatment on MCM1DLN cells cannot be demonstrated. This assumption can be supported by the observation that MCM1DLN spheroids with an ablated *SR-BI* gene show only a slight (15%), non-significant reduction in invasion compared to control MCM1DLN spheroids. The latter fact is an indication that ablation of the *SR-BI* gene in this cell line shows no effect on invasiveness in the 3D spheroid cell culture model after 24 hours.

The 1205Lu spheroids showed only a slight (25%) non-significant decrease in invasiveness after

treatment with BLT-1, while the 1205Lu spheroids with an ablated *SR-BI* gene showed no difference in invasiveness compared to control 1205Lu spheroids (Figure 28, 29). Again, we concluded that loss of SR-BI expression displayed no effect on the invasiveness of 1205Lu cells in the 3D spheroid cell culture after 24 hours. Treatment of the 1205Lu spheroids with 1 μM BLT-1 and/or 5 μM lovastatin had no apparent effect on invasiveness after a 24 hour-treatment, unlike the MCM1DLN treated spheroids. This could be probably explained by the lower toxicity of the 24-hour treatment with these substances to the 1205Lu cell line, compared to the MCM1DLN spheroids.

Spheroids of the cell line 451Lu failed to invade into the collagen I gel and were thus considered unsuitable for further use in the spheroid invasion assay (data not shown). Yet, a similar study revealed that the melanoma cell line 451Lu exhibited invasive capacity when used in the matrigel invasion assay [111]. This finding suggests that the 451Lu cell line has the ability to invade a basal lamina-like matrix (as matrigel, which is rich in laminin and collagen IV [112]) but shows no invasive activity in a collagen I-composed matrix.

Similarly, WM3854 and WM793b spheroids also failed to demonstrate any invasive capacity in this culture system (Figure 30, 31) and were thus regarded as unsuitable for the spheroid invasion assay in collagen I. Our results are in agreement with an earlier study, where the inability of invasion of certain melanoma cell lines, such as WM793b, has already been reported [113].

To sum up, the results of the spheroid invasion assay indicated that the majority of melanoma cell lines used in this study could not be used because of their inability to invade as spheroids into collagen gels and that SR-BI knock-down had no effect on the invasive capacity of the 1205Lu and MCM1DLN spheroids. These results are contradictory to data from a similar study with renal cell carcinoma, where correlation of invasiveness and *SR-BI* gene ablation was examined with the transwell assay [114]. In that study, results demonstrated a clear decrease in invasiveness of renal carcinoma cells with SR-BI knock-down after 24 hours.

However, the lack of differences in melanoma spheroid invasiveness during the short time frame of 24 hours does not necessarily mean that there is no effect of SR-BI depletion on invasion of melanoma cells. The effects of *SR-BI* gene loss in melanoma invasiveness could be subtle and could thus appear late after knock-down. In our case, it is possible that recognizable differences in

invasion could be detectable only after a longer time period. Therefore, we concluded that results about the effect of *SR-BI* gene loss on invasiveness of metastatic melanoma cell lines should also be revised with the use of an additional invasion assay in a 3D setting, such as the organotypic skin model assay, which is characterized by a much longer experimental incubation time.

5.4.1.2 Immunofluorescence analysis of treated MCM1DLN spheroids used in the invasion assay

Treated and control MCM1DLN spheroids, which showed a significant difference in invasiveness (Figure 27) albeit due to the decrease in cell survival (as discussed in 5.4.1.1) were further analyzed with immunofluorescence in order to enable visual localization of apoptotic cells as well as of SR-BI protein expressing cells in the spheroids. The immunofluorescence analysis mainly revealed an increase in cleaved caspase-3 positive (apoptotic) cells in the central part and in the detached small area of the treated spheroid as well as a slight increase in SR-BI positive cells in the central area of the same spheroid (Figure 32 b.).

We also expected, that after treatment, apoptotic cells with a positive cleaved caspase-3 signal would increase and be rather localized in peripheral areas of the spheroid, which were directly affected by the treatment. The findings of the immunofluorescence analysis indicate an expected increase in apoptotic cells after treatment, yet in the core of the spheroids, which would rather be expected merely for control spheroids of larger size due to hypoxic conditions in the core of these spheroids [115]. An increase of apoptotic cells in the core area of glioblastoma spheroids has also been reported after treatment with the cytostatic drug temozolomide [116], however the reason for this observation is unclear. In our case of increased apoptosis in the center of treated spheroids, it could be that the level of cholesterol inside the spheroid is lower than at the outer rim. This might explain why inhibition of SR-BI and cholesterol synthesis has a higher impact on the cells inside the spheroids, since these cells suffer from a more severe cholesterol shortage than cells in the periphery. The treatment of the spheroids with BLT-1 and lovastatin, could thus lead to a more rapid increase in apoptotic cell death in the inner core of the spheroid.

Interestingly, higher SR-BI expression seems to be present in cells in the center of the treated spheroid. This might be a mechanism to counteract the shortage of cholesterol by upregulation of

the receptor especially under treatment, since the cells inside the spheroid could experience the shortage of cholesterol earlier than the outer cells (as discussed above). Another study performed with liver cell carcinoma also reported a strong association between cholesterol concentration and SR-BI localization, regulated by transcytosis [117]. However, no other report describing altered SR-BI expression in melanoma spheroids is available so far, thus further experiments are necessary to clarify this observation.

In summary, based on the results of this experiment (Figure 32), it could be assumed that upon treatment changes occur in the rate as well as in the spatial distribution of apoptosis, while alterations in localization of cells with high SR-BI expression also occur after treatment of the MCM1DLN spheroids with BLT-1 and lovastatin. However, in order to obtain more accurate conclusions, the repetition of this experiment as well as a more detailed quantitative evaluation of the results is required in the future.

5.4.2 Vertical invasive capacity of metastatic melanoma cell lines after SR-BI knock-down in an organotypic skin model assay

After evaluating the results of the collagen I spheroid invasion assay (5.4.1.1), it was decided to exclude treatment of melanoma cells with BLT-1 and lovastatin from further experiments, as the effects on invasiveness in some melanoma cell lines were presumably induced merely by the toxicity of this treatment (cell death) and not by inhibition of SR-BI mediated lipid uptake and cholesterol metabolism.

Since there was no evident effect of the *SR-BI* gene ablation on invasiveness of the 3D spheroids, it was decided to analyze the effect of the *SR-BI* gene knock-down on the vertical invasive capacity of melanoma cell lines. This assay best mimics the histological and tissue architecture of human skin and enables analysis of melanoma invasion for a long time frame (>24 hours up to weeks) [118]. Consequently, the metastatic cell lines MCM1DLN, 1205Lu and 451Lu were tested with the organotypic skin model assay in collagen I. It was, however, not possible to reach any conclusions about the 451Lu cells, as this cell line again demonstrated a lack of any invasive capacity in this experimental setup. Similar results were obtained from the spheroid invasion assay

in collagen I (described in 4.4.1) and were in accordance with results from a previous study [119]. Thus, based on the findings of this study and on previous results discussed in 5.4.1.1, the cell line 451Lu can be declared as unsuitable for use in invasion assays with collagen matrices.

In contrast, microscopic images (Figure 33, 34) as well as quantification of these images (Figure 35) clearly demonstrated a significant decrease of cell invasiveness into collagen I matrix for both MCM1DLN and 1205Lu cell lines upon *SR-BI* gene ablation. The difference between the control cells and SR-BI knock-down cells in invasion rates was more pronounced in the MCM1DLN melanoma cell line, that demonstrated a 58% decrease in the number of invasive cells. As the control MCM1DLN cells generally demonstrated higher invasion rates (18% invasive cells) than the 1205LU control cells (10% invasive cells), it was expected that the degree of attenuation of MCM1DLN cell invasion would be higher than that of the 1205Lu cell line. Yet, the 1205Lu cell line showed a highly reduced (approximately 50%) invasion capacity into the collagen gel after SR-BI ablation. We concluded, that in this 3D model system, which is considered a skin equivalent and therefore closely mimics the *in vivo* situation of melanoma cancer, SR-BI ablation reduces the invasive capacity of the metastatic melanoma lines MCM1DLN and 1205Lu. Based on this finding, as well as on previously-mentioned results about reduced size and more compact form of spheroids with SR-BI knock-down (5.2), we could also conclude that SR-BI depletion can contribute to mitigation of the invasive properties of metastatic melanoma cell lines. Similarly, reduced melanoma cell migration as well as a disrupted EMT phenotype upon SR-BI knock-down in melanoma cells was reported [105] and further support these conclusions .

5.5 The effect of siRNA mediated SR-BI knock-down on cancer marker protein expression and on protein glycosylation

As a further step, MCM1DLN, 1205Lu and 451Lu samples, tested with the organotypic skin model assay, were further used for analysis of important genes associated with cancer hallmarks. With the use of immunohistochemistry, the expression of some tumor growth and promotion regulators such as *VEGFA* [120], *STAT5* [121] as well as the cell-cell adhesion protein E-Cadherin were

analyzed. We aimed to investigate a possible correlation between *SR-BI* gene loss and altered expression of proteins crucial to cancer progression and metastasis in the above metastatic cell lines. In addition, as protein glycosylation has been recently linked to the EMT process [122] and cancer progression [123], the extend of glycosylated proteins was also analyzed in the samples. Since O-GlcNAcylation has been associated with development of chronic diseases such as cancer and is regarded as an essential post-translational modification (PTM) [124], we decided to specifically analyze this type of protein glycosylation. Hence, an antibody recognizing endogenous O-GlcNAc levels on proteins was used for IHC.

Initially, we confirmed that the *SR-BI* gene was ablated for the respective SR-BI knock-down conditions of cells used in the organotypic skin model assay. The results on Figure 36 illustrated a statistically significant decrease (>50%) of SR-BI protein expression in *SR-BI* targeting siRNA transfected cells compared to the control transfected cells. Thus, we concluded that the siRNA transfection was efficient for all cell lines. We could also conclude that the SR-BI protein was sufficiently depleted in the knock-down cells and its levels remained low until the end of the experiment.

The VEGFA protein showed, as expected, a significant decrease after SR-BI ablation in the MCM1DLN cells. This observation on Figure 37 is in accordance with published data about reduced VEGFA mRNA expression after SR-BI ablation in the same cell line [105]. This fact could thus imply that lack of the SR-BI receptor might indeed ameliorate melanoma tumor growth by reducing VEGFA, which supports tumor angiogenesis [125]. However, similar results were not observed in the 1205Lu cells, where there was no significant difference in VEGFA levels between the two conditions. Furthermore, due to technical complications, we were unable to draw conclusions about VEGFA expression regulation through SR-BI knock-down in 451Lu cells. Consequently, although there is some evidence on VEGFA reduction further analysis is needed to draw clear conclusions.

Intriguingly, expression of STAT5 is shown to increase with statistical significance in the metastatic 1205Lu cell line after *SR-BI* gene ablation (Figure 38). Our findings about STAT5 expression are however partly inconsistent with previous studies, as STAT5 expression has been reported to be positively associated with SR-BI expression in patient material [105]. We therefore

expected STAT5 levels to decrease, rather than to increase upon *SR-BI* gene ablation. Yet a similar increase with statistical significance was not observed in the metastatic MCM1DLN cells, where there was no significant difference in STAT5 levels post *SR-BI* gene ablation. Interestingly, similar data about the absence of an *in vitro* effect of SR-BI knock-down on STAT5 protein levels [105] support our results reported with the MCM1DLN cells. An explanation for this phenomenon could be that differences of STAT5 protein levels between conditions may only be detectable in long term [105]. A precise answer to the effect of SR-BI on STAT5 expression would be possible if phopsho-STAT5 levels or STAT5 transcriptional activity would be analyzed in the respective conditions. In addition, STAT5 needs to be localized to the nucleus to act as a transcription factor [103]. In that respect, it seems that SR-BI can influence nuclear STAT5 localization in the MCM1DLN cell line according to our data (see Figure 39 b. & c.). As illustrated on Figure 29 c., the percentage value of cells with ample nuclear STAT5 localization decreased by 50% upon SR-BI gene ablation. This observation implicates that nuclear localization of STAT5 and hence its activation is promoted by endogenous SR-BI expression. Findings, which have been published and report reduced DNA binding of STAT5 (indicating reduced levels of active STAT5) in SR-BI knock-down MCM1DLN cells [105] are thus also in accordance with the results of my study. However, the relationship between SR-BI and STAT5 expression needs to be further investigated with additional experimental assays and in more metastatic melanoma cell lines.

STAT5 signaling has been positively associated (inter alia) with the EMT process [126], which is accompanied by increased glycosylation and more specifically increased O-GlcNAcylation [122]. Therefore, the O-GlcNAcylation levels of our samples were also analyzed and interestingly demonstrated a significant decrease upon *SR-BI* gene ablation in all cells, except 451Lu (Figure 40). In the light of this decrease in SR-BI knock-down cells, our data could imply that SR-BI expression may promote O-GlcNAcylation and subsequently also contribute to the EMT process, as mentioned before. These results were in accordance to another report, showing reduced protein glycosylation upon *SR-BI* gene ablation of melanoma cells with the use of the WGA immunoprecipitation method [105]. In the same study, STAT5 glycosylation was also reported to decrease in SR-BI knock-down melanoma cells [105]. SR-BI ablation in metastatic melanoma cells thus seems to reduce glycosylation/O-GlcNAcylation levels subsequently contributing to decreased EMT and thereby to a less metastatic phenotype. However, additional experiments with

more metastatic cell lines are needed, to further confirm this theory, since glycosylation levels of 451Lu were not affected by *SR-BI* gene loss.

Protein glycosylation is a process, which involves polysaccharides, also known as glycans [127]. Therefore, the total level of polysaccharides and carbohydrates was also determined in our samples. We aimed to examine a possible effect of *SR-BI* gene loss on cellular polysaccharide and carbohydrate synthesis. Since glycosylation cell levels were reduced upon *SR-BI* gene loss, we also expected that polysaccharide levels might similarly decrease. Surprisingly however, it was shown that polysaccharide and carbohydrate levels were significantly elevated upon SR-BI ablation in all cell lines (Figure 41). This observation implies that alterations of O-GlcNAcylation levels are thus not associated with changes in polysaccharide synthesis.

Previous studies have shown, that polysaccharides are involved in immune responses and demonstrate anti-cancer properties in malignant cells [128]. It could thus be speculated that the total polysaccharide increase might be an indication for increased cellular polysaccharide synthesis triggered by SR-BI loss in order to support immune responses and anti-cancer activity in melanoma cells. However, since there is no previous data to support this highly speculative hypothesis, we decided to not further pursue polysaccharide-associated analysis.

As discussed above, glycosylation levels were significantly reduced in almost all SR-BI knock-downs, which could signify decreased EMT and a less metastatic phenotype. One essential change during the EMT process includes the depletion of E-Cadherin expression [129]. Hence, we also analyzed E-Cadherin expression. E-Cadherin was localized predominantly in the cell nucleus and cytoplasm rather than at the cell surface, where it is usually located performing its cell-cell adhesion function. However, aberrant cytoplasmic staining of E-Cadherin has been already reported in a previous study, where the same antibody (clone 36) was used [130]. Consequently, results of the E-Cadherin staining were regarded valid.

Analysis of E-Cadherin protein levels in our samples revealed a significant increase of the protein in all cell samples with SR-BI knock-down, except 451Lu (Figure 42). This finding may indicate that SR-BI expression represses E-Cadherin expression and potentially reduces cell-to-cell adhesion. It is yet unclear whether E-Cadherin is also located at the cell surface, since E-Cadherin membrane staining is possibly hidden by the nuclear/cytoplasmic staining. Our data thus suggests

that SR-BI expression might contribute to tumor invasiveness and metastasis by supporting the EMT process [105]. Further experimental evidence is however substantial to clarify E-Cadherin localization in these melanoma samples.

It should be furthermore mentioned that control stainings, examining antibody specificity, were also performed in addition to the above listed IHC stainings. Figure 43 demonstrates a representative example of a control staining. Each of the control stainings confirmed the specificity of the antibodies used in this study and verified the accuracy of each protein analysis.

In summary, the results of the IHC staining provided valuable insights about the effect of *SR-BI* gene ablation on proteins and on glycosylation associated with cancer progression. Our data imply that SR-BI expression in melanoma cells is associated with higher VEGFA expression while promoting the EMT process by increasing protein glycosylation and promoting E-Cadherin expression in melanoma cells. Further research in that aspect with more metastatic melanoma lines is yet needed to verify these findings.

5.6 The effect of siRNA mediated SR-BI knock-down on the mRNA expression of genes involved in transcriptional repression, cell adhesion and cell migration

After examining the protein levels of important cancer markers, we concluded that the SR-BI receptor may play an important role in EMT regulation. Hence, we decided to investigate the mRNA expression rates of an expanded set of genes involved in cell adhesion, migration and the EMT process.

Firstly, we validated the efficiency of the *SR-BI* gene ablation in our samples by demonstrating the substantial decrease of *SR-BI* mRNA levels in SR-BI knock-down cells (Figure 44). These results are similar to the results obtained from the same validation of SR-BI knock-down efficiency with IHC on Figure 36. *SR-BI* mRNA levels in all SR-BI knock-down samples are decreased by over 50% in both analyses (compare Figure 36 and 44). The cell lines MCM1DLN and 1205Lu show the greatest *SR-BI* mRNA and protein decrease after *SR-BI* siRNA transfection, which was approximately 80% and 90%, respectively.

Next, we analyzed important genes involved in the EMT process such as the oncogenic repressor of transcription *SNAIL2* [131] as well as the fibril-associated collagen gene *COL12A1* [132], which is contributing to cell adhesion [132, 133]. It has been previously reported that proteins of the Snail family induce cell migration and invasiveness by repressing epithelial markers and promoting mesenchymal markers [134]. Indeed, this analysis demonstrated that after *SR-BI* gene loss, *SNAIL2* mRNA levels were greatly reduced (≥50%) in all cell lines, and especially in 1205Lu and MCM1DLN cells (Figure 45). These results thus indicate that *SR-BI* gene ablation induces a prominent downmodulation of SNAIL2 expression, which is highly likely to impede EMT in our cell systems. This finding further supports the theory that SR-BI expression possibly contributes to the invasive potential of melanoma by supporting the EMT process.

On the other hand, the *COL12A1* gene expression showed a modest increase upon *SR-BI* gene ablation only in the MCM1DLN cells (Figure 46). Surprisingly, *COL12A1* mRNA appeared to decrease slightly rather than to increase in the 1205Lu SR-BI knock-down cells. In the 451Lu knock-down cells there was only a minor increase of *COL12A1* mRNA upon SR-BI knock-down (Figure 46). However, this increase cannot be considered significant as the increased levels are within the value range of the 451Lu control cells. As mentioned above, COL12A1 supports cell adhesion [132, 133], while previous studies demonstrated its decreased expression in subtypes of colorectal cancer [132]. Consequently, the indication of increased COL12A1 expression in MCM1DLN cells with an ablated *SR-BI* gene, suggests enhanced cell adhesion between cells lacking SR-BI and thus a possibly decreased invasive potential. Yet, due to lack of similar results in 1205Lu and 451Lu cell lines, more research is needed to elucidate if there is an association between COL12A1 and SR-BI expression in melanoma.

Furthermore, we analyzed the mRNA levels of another gene, which codes for the matricellular protein connective tissue growth factor (*CTGF*) and is also involved in ECM synthesis [135]. CTGF is reported to support skin cell adhesion, by acting as an adhesive substance for cells while connecting further ECM proteins [136]. A previous study has presented evidence for the role of *CTGF* as a mediator of collagen synthesis in fibroblasts [137]. Analysis of *CTGF* mRNA levels in our samples showed a clear increase upon SR-BI expression loss in the 1205Lu and an even more evident increase in the MCM1DLN cell line (Figure 47). In contrast to these findings, 451Lu SR-BI knock-down cells showed a mild decrease of *CTGF* mRNA (Figure 47). Thus, it can be stated

that SR-BI expression might inhibit cell adhesion and ECM synthesis by *CTCF* repression in some melanoma cell lines. Consequently, loss of ECM adhesion might act as a promoter of cell dissemination since these cells are rendered more motile by the decreased attachment to the matrix. More research in the future can lead to clear conclusions about the effect of SR-BI expression on melanoma invasion through *CTGF* regulation.

Overall, the above-discussed results provided first indications on the effect of SR-BI function on the EMT process and cell adhesion. According to these results it can be assumed that the EMT process is induced by SR-BI expression, which could trigger increased SNAIL2 expression. Results regarding the cell adhesion molecules COL12A1 and CTGF were not as clear, since they were not consistent in all cell lines. Consequently, more assays with more melanoma cell lines as well as a repetition of the mRNA analysis with an increased number of technical and biological replicates have to be conducted in order to give a clear statement about the effect of SR-BI expression on these proteins.

5.7 Conclusion

In conclusion, this study provides evidence about the tumor-promoting role of SR-BI in melanoma progression, as it is shown to promote cell migration, invasion and thus the metastatic potential of melanoma cell lines. Initially, it was shown that knock-down of SR-BI had no effect on the viability of cells constituting melanoma spheroids, while it significantly decreased the overall size and increased the compact form of metastatic melanoma spheroids. We therefore assume that SR-BI expression contributes to decreased cell-cell adhesion properties and, consequently, to the form of metastatic melanoma spheroids. Furthermore, pharmacological treatment with the substances BLT-1 and lovastatin, inhibiting lipid transport and cholesterol synthesis, led merely to a decrease in viability rather than to loss of invasiveness of melanoma spheroids. However, cells with endogenous SR-BI expression demonstrated significantly increased vertical invasion capacity in the organotypic skin model assay. This finding indicated that invasiveness of melanoma cells is promoted by the SR-BI receptor. Results also demonstrated an association of SR-BI expression with elevated VEGFA expression, while it was shown that SR-BI expression might promote the

5. DISCUSSION

EMT process by inducing protein glycosylation, SNAIL2 expression and by downregulating the E-Cadherin adhesion protein (Figure 48). Expression analysis of further cell adhesion- and ECM synthesis-associated genes like *COL12A1* and *CTGF* yielded further results supporting the indication that SR-BI expression induces loss of cell-adhesion and migration (Figure 48). However, further research is needed to link SR-BI activity and the migratory and/or invasive properties of human melanoma cells in order to confirm the potential function of the SR-BI receptor as a prognostic biomarker or a promising therapeutic target.

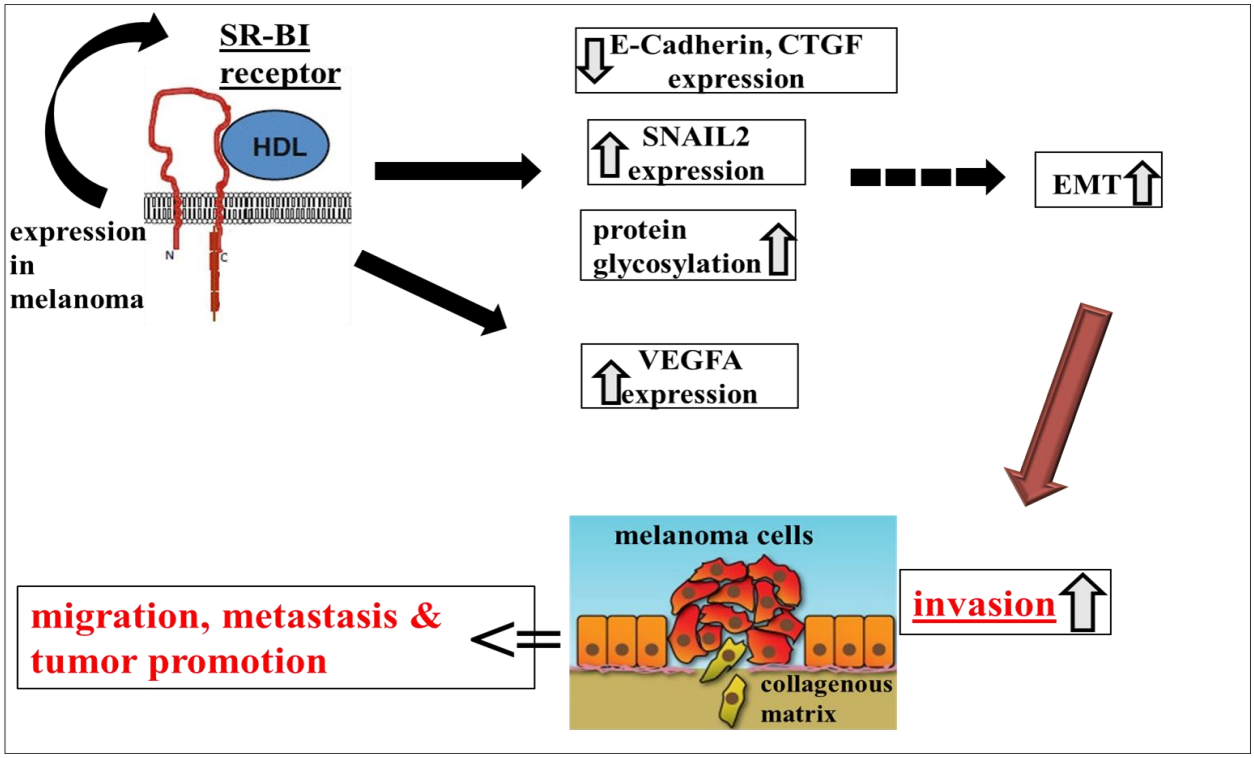

Figure 48: Schematic summary of the results of this study suggesting the tumor-promoting role of SR-BI expression in melanoma. SR-BI expression in melanoma was associated with increased invasion accompanied by increased VEGFA, SNAIL2 and protein glycosylation levels, while E-Cadherin and CTGF expression was reduced. Consequently, it was concluded that SR-BI promotes the EMT process and thereby the invasive capacity of the melanoma cells thus supporting metastasis.

6. References

1. Hallberg, O. and O. Johansson, *Malignant melanoma of the skin - not a sunshine story!* Med Sci Monit, 2004. **10**(7): p. CR336-40.
2. Pflugfelder, A., et al., *Malignant melanoma S3-guideline "diagnosis, therapy and follow-up of melanoma".* J Dtsch Dermatol Ges, 2013. **11 Suppl 6**: p. 1-116, 1-126.
3. Seite, S., et al., *Public primary and secondary skin cancer prevention, perceptions and knowledge: an international cross-sectional survey.* J Eur Acad Dermatol Venereol, 2017. **31**(5): p. 815-820.
4. Gavin, A., et al., *Trends in skin cancer knowledge, sun protection practices and behaviours in the Northern Ireland population.* Eur J Public Health, 2012. **22**(3): p. 408-12.
5. D'Orazio, J., et al., *UV radiation and the skin.* Int J Mol Sci, 2013. **14**(6): p. 12222-48.
6. Shain, A.H. and B.C. Bastian, *From melanocytes to melanomas.* Nat Rev Cancer, 2016. **16**(6): p. 345-58.
7. D'Orazio, J.A., et al., *Melanoma — Epidemiology, Genetics and Risk Factors*, in *Recent Advances in the Biology, Therapy and Management of Melanoma*, L.M. Davids, Editor. 2013, InTech: Rijeka. p. Ch. 01.
8. Johnson, T. *Non-invasive test offers quick skin cancer diagnosis. New imaging technique can detect skin cancers without invasive biopsy*. 2017 13 February 2017; Available from: https://www.nibib.nih.gov/news-events/newsroom/non-invasive-test-offers-quick-skin-cancer-diagnosis.
9. Cichorek, M., et al., *Skin melanocytes: biology and development.* Postepy Dermatol Alergol, 2013. **30**(1): p. 30-41.
10. Glatz, K., et al., *Frequent Mitotic Activity in Banal Melanocytic Nevi Uncovered by Immunohistochemical Analysis.* The American Journal of Dermatopathology, 2010. **32**(7): p. 643-649.
11. Tronnier, M., et al., *One single erythemagenic UV irradiation is more effective in increasing the proliferative activity of melanocytes in melanocytic naevi compared with fractionally applied high doses.* British Journal of Dermatology, 2006. **137**(4): p. 534-539.
12. Chan May, P., M. Chan Maren, and R. Tahan Steven, *Melanocytic nevi in pregnancy: histologic features and Ki-67 proliferation index.* Journal of Cutaneous Pathology, 2010. **37**(8): p. 843-851.
13. Richert, S., et al., *Widespread eruptive dermal and atypical melanocytic nevi in association with chronic myelocytic leukemia: case report and review of the literature.* Journal of the American Academy of Dermatology, 1996. **35**(2): p. 326-329.
14. Bosserhoff, A., *Melanoma Development. Molecular Biology, Genetics and Clinical Application*. 2011: Springer International Publishing, Cham, Switzerland. 1544.
15. Seuradge, J.W., E. *Melanoma*. 2012-2016 [cited 2012-2016; Available from: http://www.pathophys.org/melanoma/.
16. Takata, M., H. Murata, and T. Saida, *Molecular pathogenesis of malignant melanoma: a different perspective from the studies of melanocytic nevus and acral melanoma.* Pigment Cell Melanoma Res, 2010. **23**(1): p. 64-71.
17. Dermatologists, S. *Skin cancer. Melanoma*. Available from: http://www.skindermatologists.com/melanoma.html.
18. Curtin, J.A., et al., *Distinct sets of genetic alterations in melanoma.* N Engl J Med, 2005. **353**(20): p. 2135-47.
19. Viros, A., et al., *Improving Melanoma Classification by Integrating Genetic and Morphologic Features.* PLOS Medicine, 2008. **5**(6): p. e120.
20. Long, G.V., et al., *Prognostic and Clinicopathologic Associations of Oncogenic BRAF in Metastatic Melanoma.* Journal of Clinical Oncology, 2011. **29**(10): p. 1239-1246.

6. REFERENCES

21. Maldonado, J.L., et al., *Determinants of BRAF Mutations in Primary Melanomas.* JNCI: Journal of the National Cancer Institute, 2003. **95**(24): p. 1878-1890.
22. Shitara, D., et al., *Nevus-Associated MelanomasClinicopathologic Features.* American Journal of Clinical Pathology, 2014. **142**(4): p. 485-491.
23. Massi, G. and P.E. LeBoit, *Melanoma Arising in a Pre-Existent Nevus*, in *Histological Diagnosis of Nevi and Melanoma*, G. Massi and P.E. LeBoit, Editors. 2014, Springer Berlin Heidelberg: Berlin, Heidelberg. p. 619-632.
24. Shitara, D., et al., *Nevus-associated melanomas: clinicopathologic features.* Am J Clin Pathol, 2014. **142**(4): p. 485-91.
25. Shain, A.H., et al., *The Genetic Evolution of Melanoma from Precursor Lesions.* N Engl J Med, 2015. **373**(20): p. 1926-36.
26. De Lartigue, J. *Probing the Melanoma Genome Reveals New Targets and Challenges*. 2016 [cited 2016 June 17]; Available from: http://www.onclive.com/publications/oncology-live/2016/vol-17-no-12/probing-the-melanoma-genome-reveals-new-targets-and-challenges.
27. Menzies, A.M., et al., *Distinguishing clinicopathologic features of patients with V600E and V600K BRAF-mutant metastatic melanoma.* Clin Cancer Res, 2012. **18**(12): p. 3242-9.
28. Weinstock, M.A. and A.J. Sober, *The risk of progression of lentigo maligna to lentigo maligna melanoma.* Br J Dermatol, 1987. **116**(3): p. 303-10.
29. Candido, S., et al., *Analysis of the B-RafV600E mutation in cutaneous melanoma patients with occupational sun exposure.* Oncol Rep, 2014. **31**(3): p. 1079-82.
30. Krakhmal, N.V., et al., *Cancer Invasion: Patterns and Mechanisms.* Acta Naturae, 2015. **7**(2): p. 17-28.
31. Balch, C.M., et al., *Final version of 2009 AJCC melanoma staging and classification.* J Clin Oncol, 2009. **27**(36): p. 6199-206.
32. Stretch, J.R., et al., *Expression of mutant p53 in melanoma.* Cancer Res, 1991. **51**(21): p. 5976-9.
33. Birck, A., et al., *Mutation and allelic loss of the PTEN/MMAC1 gene in primary and metastatic melanoma biopsies.* J Invest Dermatol, 2000. **114**(2): p. 277-80.
34. Sanborn, J.Z., et al., *Phylogenetic analyses of melanoma reveal complex patterns of metastatic dissemination.* Proc Natl Acad Sci U S A, 2015. **112**(35): p. 10995-1000.
35. Reid, A.L., et al., *Markers of circulating tumour cells in the peripheral blood of patients with melanoma correlate with disease recurrence and progression.* Br J Dermatol, 2013. **168**(1): p. 85-92.
36. Valastyan, S. and R.A. Weinberg, *Tumor metastasis: molecular insights and evolving paradigms.* Cell, 2011. **147**(2): p. 275-92.
37. Tietze, L., et al., *Benign metastasizing leiomyoma: a cytogenetically balanced but clonal disease.* Hum Pathol, 2000. **31**(1): p. 126-8.
38. Dutton-Regester, K., et al., *Melanomas of unknown primary have a mutation profile consistent with cutaneous sun-exposed melanoma.* Pigment Cell Melanoma Res, 2013. **26**(6): p. 852-60.
39. Anbari, K.K., et al., *Melanoma of unknown primary site: presentation, treatment, and prognosis--a single institution study. University of Pennsylvania Pigmented Lesion Study Group.* Cancer, 1997. **79**(9): p. 1816-21.
40. Damsky, W.E., et al., *beta-catenin signaling controls metastasis in Braf-activated Pten-deficient melanomas.* Cancer Cell, 2011. **20**(6): p. 741-54.
41. Wagle, N., et al., *Dissecting therapeutic resistance to RAF inhibition in melanoma by tumor genomic profiling.* J Clin Oncol, 2011. **29**(22): p. 3085-96.
42. Kim, J.E., et al., *Heterogeneity of expression of epithelial–mesenchymal transition markers in melanocytes and melanoma cell lines.* Frontiers in Genetics, 2013. **4**: p. 97.
43. Murtas, D., et al., *Role of epithelial–mesenchymal transition involved molecules in the progression of cutaneous melanoma.* Histochemistry and Cell Biology, 2017. **148**(6): p. 639-649.
44. Li, F.Z., et al., *Phenotype Switching in Melanoma: Implications for Progression and Therapy.* Frontiers in Oncology, 2015. **5**: p. 31.

45. Luo, X., et al., *Emerging roles of lipid metabolism in cancer metastasis.* Mol Cancer, 2017. **16**(1): p. 76.
46. Lucenay, K.S., et al., *Cyclin E Associates with the Lipogenic Enzyme ATP-Citrate Lyase to Enable Malignant Growth of Breast Cancer Cells.* Cancer Res, 2016. **76**(8): p. 2406-18.
47. Su, Y.-W., et al., *Association between Phosphorylated AMP-Activated Protein Kinase and Acetyl-CoA Carboxylase Expression and Outcome in Patients with Squamous Cell Carcinoma of the Head and Neck.* PLoS ONE, 2014. **9**(4): p. e96183.
48. Hao, Q., et al., *Expression and roles of fatty acid synthase in hepatocellular carcinoma.* Oncol Rep, 2014. **32**(6): p. 2471-6.
49. Wang, H., et al., *The role of stearoyl-coenzyme A desaturase 1 in clear cell renal cell carcinoma.* Tumour Biol, 2016. **37**(1): p. 479-89.
50. Brohée, L., et al., *Lipin-1 regulates cancer cell phenotype and is a potential target to potentiate rapamycin treatment.* Oncotarget, 2015. **6**(13): p. 11264-11280.
51. Gómez de Cedrón, M. and A. Ramírez de Molina, *Microtargeting cancer metabolism: opening new therapeutic windows based on lipid metabolism.* Journal of Lipid Research, 2016. **57**(2): p. 193-206.
52. Lupu, R. and J.A. Menendez, *Pharmacological inhibitors of Fatty Acid Synthase (FASN)--catalyzed endogenous fatty acid biogenesis: a new family of anti-cancer agents?* Curr Pharm Biotechnol, 2006. **7**(6): p. 483-93.
53. Janardhan, S., P. Srivani, and G.N. Sastry, *Choline kinase: an important target for cancer.* Curr Med Chem, 2006. **13**(10): p. 1169-86.
54. Gorin, A., L. Gabitova, and I. Astsaturov, *Regulation of cholesterol biosynthesis and cancer signaling.* Curr Opin Pharmacol, 2012. **12**(6): p. 710-6.
55. Huang, C. and C. Freter, *Lipid Metabolism, Apoptosis and Cancer Therapy.* International Journal of Molecular Sciences, 2015. **16**(1): p. 924-949.
56. Ray, U. and S.S. Roy, *Aberrant lipid metabolism in cancer cells – the role of oncolipid-activated signaling.* The FEBS Journal, 2018. **285**(3): p. 432-443.
57. Simons, K. and E. Ikonen, *How Cells Handle Cholesterol.* Science, 2000. **290**(5497): p. 1721.
58. Cruz, P.M., et al., *The role of cholesterol metabolism and cholesterol transport in carcinogenesis: a review of scientific findings, relevant to future cancer therapeutics.* Front Pharmacol, 2013. **4**: p. 119.
59. Murai, T., *The role of lipid rafts in cancer cell adhesion and migration.* Int J Cell Biol, 2012. **2012**: p. 763283.
60. Zhuang, L., et al., *Cholesterol targeting alters lipid raft composition and cell survival in prostate cancer cells and xenografts.* Journal of Clinical Investigation, 2005. **115**(4): p. 959-968.
61. Clendening, J.W. and L.Z. Penn, *Targeting tumor cell metabolism with statins.* Oncogene, 2012. **31**(48): p. 4967-78.
62. Rao, S., et al., *Lovastatin mediated G1 arrest in normal and tumor breast cells is through inhibition of CDK2 activity and redistribution of p21 and p27, independent of p53.* Oncogene, 1998. **17**: p. 2393.
63. Mo, H. and C.E. Elson, *Studies of the isoprenoid-mediated inhibition of mevalonate synthesis applied to cancer chemotherapy and chemoprevention.* Exp Biol Med (Maywood), 2004. **229**(7): p. 567-85.
64. Silvente-Poirot, S. and M. Poirot, *Cholesterol metabolism and cancer: the good, the bad and the ugly.* Current Opinion in Pharmacology, 2012. **12**(6): p. 673-676.
65. Muntoni, S., et al., *Serum lipoproteins and cancer.* Nutrition, Metabolism and Cardiovascular Diseases. **19**(3): p. 218-225.
66. Uda, S., et al., *A lipoprotein source of cholesteryl esters is essential for proliferation of CEM-CCRF lymphoblastic cell line.* Tumor Biology, 2012. **33**(2): p. 443-453.
67. Llaverias, G., et al., *Role of Cholesterol in the Development and Progression of Breast Cancer.* The American Journal of Pathology, 2011. **178**(1): p. 402-412.

6. REFERENCES

68. Mooberry, L.K., et al., *Targeting the SR-B1 Receptor as a Gateway for Cancer Therapy and Imaging.* Front Pharmacol, 2016. **7**: p. 466.
69. Yuan, B., et al., *High scavenger receptor class B type I expression is related to tumor aggressiveness and poor prognosis in breast cancer.* Tumor Biology, 2016. **37**(3): p. 3581-3588.
70. Cao, W.M., et al., *A mutant high-density lipoprotein receptor inhibits proliferation of human breast cancer cells.* Cancer Res, 2004. **64**(4): p. 1515-21.
71. Danilo, C., et al., *Scavenger receptor class B type I regulates cellular cholesterol metabolism and cell signaling associated with breast cancer development.* Breast Cancer Res, 2013. **15**(5): p. R87.
72. Schorghofer, D., et al., *The HDL receptor SR-BI is associated with human prostate cancer progression and plays a possible role in establishing androgen independence.* Reprod Biol Endocrinol, 2015. **13**: p. 88.
73. Rajora, M.A. and G. Zheng, *Targeting SR-BI for Cancer Diagnostics, Imaging and Therapy.* Front Pharmacol, 2016. **7**: p. 326.
74. Rhainds, D. and L. Brissette, *The role of scavenger receptor class B type I (SR-BI) in lipid trafficking: Defining the rules for lipid traders.* The International Journal of Biochemistry & Cell Biology, 2004. **36**(1): p. 39-77.
75. Rigotti, A., H.E. Miettinen, and M. Krieger, *The Role of the High-Density Lipoprotein Receptor SR-BI in the Lipid Metabolism of Endocrine and Other Tissues.* Endocrine Reviews, 2003. **24**(3): p. 357-387.
76. Shen, W.-J., S. Azhar, and F.B. Kraemer, *SR-B1: A Unique Multifunctional Receptor for Cholesterol Influx and Efflux.* Annual Review of Physiology, 2017.
77. Varban, M.L., et al., *Targeted mutation reveals a central role for SR-BI in hepatic selective uptake of high density lipoprotein cholesterol.* Proceedings of the National Academy of Sciences of the United States of America, 1998. **95**(8): p. 4619-4624.
78. Reboul, E., et al., *Scavenger receptor class B type I (SR-BI) is involved in vitamin E transport across the enterocyte.* The Journal of Biological Chemistry, 2006. **281**(8): p. 4739-4745.
79. Barth, H., et al., *Scavenger Receptor Class B Is Required for Hepatitis C Virus Uptake and Cross-Presentation by Human Dendritic Cells.* Journal of Virology, 2008. **82**(7): p. 3466-3479.
80. Kleveland, E.J., et al., *Characterization of scavenger receptor class B, type I in Atlantic salmon (Salmo salar L.).* Lipids, 2006. **41**(11): p. 1017-1027.
81. Bian, Y., et al., *An enzyme assisted RP-RPLC approach for in-depth analysis of human liver phosphoproteome.* Journal of Proteomics, 2014. **96**: p. 253-262.
82. Hu, J., et al., *Differential Roles of Cysteine Residues in Cellular Trafficking, Dimerization, and Function of the HDL Receptor, SR-BI.* Biochemistry, 2011. **50**(50): p. 10860-10875.
83. Yu, M., et al., *Exoplasmic cysteine Cys384 of the HDL receptor SR-BI is critical for its sensitivity to a small-molecule inhibitor and normal lipid transport activity.* Proceedings of the National Academy of Sciences of the United States of America, 2011. **108**(30): p. 12243-12248.
84. Hoekstra, M., *SR-BI as target in atherosclerosis and cardiovascular disease - A comprehensive appraisal of the cellular functions of SR-BI in physiology and disease.* Atherosclerosis, 2017. **258**: p. 153-161.
85. Kim, J.B., *Three-dimensional tissue culture models in cancer biology.* Seminars in Cancer Biology, 2005. **15**(5): p. 365-377.
86. Bernhardt, G., et al., *Standardized kinetic microassay to quantify differential chemosensitivity on the basis of proliferative activity.* J Cancer Res Clin Oncol, 1992. **118**(1): p. 35-43.
87. Pouliot N, P.H., Burrows A, *Investigating Metastasis Using In Vitro Platforms*, in *Metastatic Cancer: Clinical and Biological Perspectives*, R. Jandial, Editor. 2000-2013, Madame Curie Bioscience Database [Internet]: Austin (TX): Landes Bioscience.
88. Vörsmann, H., et al., *Development of a human three-dimensional organotypic skin-melanoma spheroid model for in vitro drug testing.* Cell Death & Disease, 2013. **4**(7): p. e719.

6. REFERENCES

89. *Massive programmed cell death in intestinal epithelial cells induced by three-dimensional growth conditions: suppression by mutant c-H-ras oncogene expression.* The Journal of Cell Biology, 1995. **131**(6): p. 1587-1598.
90. Hirschhaeuser, F., et al., *Multicellular tumor spheroids: An underestimated tool is catching up again.* Journal of Biotechnology, 2010. **148**(1): p. 3-15.
91. Liu, H., et al., *Polarity and proliferation are controlled by distinct signaling pathways downstream of PI3-kinase in breast epithelial tumor cells.* The Journal of Cell Biology, 2004. **164**(4): p. 603-612.
92. Weaver, V.M., et al., *Reversion of the Malignant Phenotype of Human Breast Cells in Three-Dimensional Culture and In Vivo by Integrin Blocking Antibodies.* The Journal of Cell Biology, 1997. **137**(1): p. 231-245.
93. Friedl, P., Y. Hegerfeldt, and M. Tusch, *Collective cell migration in morphogenesis and cancer.* Int J Dev Biol, 2004. **48**(5-6): p. 441-9.
94. Amatangelo, M.D., et al., *Stroma-Derived Three-Dimensional Matrices Are Necessary and Sufficient to Promote Desmoplastic Differentiation of Normal Fibroblasts.* The American Journal of Pathology, 2005. **167**(2): p. 475-488.
95. Doillon, C.J., Gagnon, E., Paradis, R., and Koutsilieris, M., *Three-dimensional culture system as a model for studying cancer cell invasion capacity and anticancer drug sensitivity.* Anticancer Research, 2004. **24**: p. 2169–2177.
96. McMillin, D.W., J.M. Negri, and C.S. Mitsiades, *The role of tumour-stromal interactions in modifying drug response: challenges and opportunities.* Nat Rev Drug Discov, 2013. **12**(3): p. 217-28.
97. Hanahan, D. and Robert A. Weinberg, *Hallmarks of Cancer: The Next Generation.* Cell. **144**(5): p. 646-674.
98. Koutsilieris, M., et al., *Three-dimensional type I collagen gel system for the study of osteoblastic metastases produced by metastatic prostate cancer.* J Bone Miner Res, 1994. **9**(11): p. 1823-32.
99. Friedrich, J., et al., *Spheroid-based drug screen: considerations and practical approach.* Nature Protocols, 2009. **4**: p. 309.
100. Swoboda, A., et al., *MET expression in melanoma correlates with a lymphangiogenic phenotype.* Hum Mol Genet, 2012. **21**(15): p. 3387-96.
101. Amsbio. *Lipidure®-COAT Plates. Effective Tool for Spheroid Culture*. 2013 [cited 2013; Available from: http://www.amsbio.com/Lipidure-Coat.aspx.
102. Timpson, P., et al., *Organotypic collagen I assay: a malleable platform to assess cell behaviour in a 3-dimensional context.* J Vis Exp, 2011(56): p. e3089.
103. Krämer, O.H. and R. Moriggl, *Acetylation and sumoylation control STAT5 activation antagonistically.* JAK-STAT, 2012. **1**(3): p. 203-207.
104. Martin TA, Y.L., Sanders AJ, Lane J, Jiang WG, *Cancer Invasion and Metastasis: Molecular and Cellular Perspective*, in *Metastatic Cancer: Clinical and Biological Perspectives*, R. Jandial, Editor. 2000-2013, Madame Curie Bioscience Database [Internet]: Austin (TX): Landes Bioscience.
105. Kinslechner, K., et al., *Malignant Phenotypes in Metastatic Melanoma are Governed by SR-BI and its Association with Glycosylation and STAT5 Activation.* Mol Cancer Res, 2017.
106. Ruan, R., et al., *Topical and Targeted Delivery of siRNAs to Melanoma Cells Using a Fusion Peptide Carrier.* Scientific Reports, 2016. **6**: p. 29159.
107. Faloon PW, D.C., Youngsaye W, et al. . *A Small Molecule Inhibitor of Scavenger Receptor BI-mediated Lipid Uptake—Probe 1. 2011 Dec 15* 2010 [Updated 2014 Sep 18] [cited 2018; Available from: Available from: https://www.ncbi.nlm.nih.gov/books/NBK133420/
108. Shellman, Y.G., et al., *Lovastatin-induced apoptosis in human melanoma cell lines.* Melanoma Res, 2005. **15**(2): p. 83-9.

6. REFERENCES

109. Kuzu, O.F., et al., *Leelamine mediates cancer cell death through inhibition of intracellular cholesterol transport.* Molecular cancer therapeutics, 2014. **13**(7): p. 1690-1703.
110. Minichsdorfer, C., et al., *Tocilizumab unmasks a stage-dependent interleukin-6 component in statin-induced apoptosis of metastatic melanoma cells.* Melanoma Research, 2015. **25**(4): p. 284-294.
111. Meier, F., et al., *The adhesion molecule L1 (CD171) promotes melanoma progression.* Int J Cancer, 2006. **119**(3): p. 549-55.
112. Sodek, K.L., T.J. Brown, and M.J. Ringuette, *Collagen I but not Matrigel matrices provide an MMP-dependent barrier to ovarian cancer cell penetration.* BMC Cancer, 2008. **8**: p. 223-223.
113. Zucker, S.N., et al., *A dominant negative Cx43 mutant differentially affects tumorigenic and invasive properties in human metastatic melanoma cells.* Journal of Cellular Physiology, 2013. **228**(4): p. 853-859.
114. Xu, G.-h., et al., *Up-regulation of SR-BI promotes progression and serves as a prognostic biomarker in clear cell renal cell carcinoma.* BMC Cancer, 2018. **18**: p. 88.
115. Chambers, K.F., et al., *3D Cultures of Prostate Cancer Cells Cultured in a Novel High-Throughput Culture Platform Are More Resistant to Chemotherapeutics Compared to Cells Cultured in Monolayer.* PLOS ONE, 2014. **9**(11): p. e111029.
116. Günther, W., et al., *Temozolomide induces apoptosis and senescence in glioma cells cultured as multicellular spheroids.* British Journal of Cancer, 2003. **88**(3): p. 463-469.
117. Fruhwürth, S., et al., *Differential basolateral–apical distribution of scavenger receptor, class B, type I in cultured cells and the liver.* Histochemistry and Cell Biology, 2014. **142**(6): p. 645-655.
118. Chioni, A.-M. and R. Grose, *Organotypic modelling as a means of investigating epithelial-stromal interactions during tumourigenesis.* Fibrogenesis & Tissue Repair, 2008. **1**(1): p. 8.
119. Sinnberg, T., et al., *β-Catenin Signaling Increases during Melanoma Progression and Promotes Tumor Cell Survival and Chemoresistance.* PLOS ONE, 2011. **6**(8): p. e23429.
120. Claesson-Welsh, L. and M. Welsh, *VEGFA and tumour angiogenesis.* J Intern Med, 2013. **273**(2): p. 114-27.
121. Rani, A. and J.J. Murphy, *STAT5 in Cancer and Immunity.* Journal of Interferon & Cytokine Research, 2015. **36**(4): p. 226-237.
122. Carvalho-cruz, P., et al., *Cellular glycosylation senses metabolic changes and modulates cell plasticity during epithelial to mesenchymal transition.* Developmental Dynamics, 2017. **247**(3): p. 481-491.
123. Stowell, S.R., T. Ju, and R.D. Cummings, *Protein Glycosylation in Cancer.* Annual review of pathology, 2015. **10**: p. 473-510.
124. Ma, J. and G.W. Hart, *O-GlcNAc profiling: from proteins to proteomes.* Clinical proteomics, 2014. **11**(1): p. 8-8.
125. Claesson-Welsh, L. and M. Welsh, *VEGFA and tumour angiogenesis.* Journal of Internal Medicine, 2012. **273**(2): p. 114-127.
126. Koppikar, P., et al., *Constitutive Activation of STAT5 Contributes to Tumor Growth, Epithelial-Mesenchymal Transition, and Resistance to EGFR Targeting.* Clinical cancer research : an official journal of the American Association for Cancer Research, 2008. **14**(23): p. 7682-7690.
127. Krasnova, L. and C.-H. Wong, *Understanding the Chemistry and Biology of Glycosylation with Glycan Synthesis.* Annual Review of Biochemistry, 2016. **85**(1): p. 599-630.
128. Xu H, X.X., *Polysaccharide, a Potential Anti-Cancer Drug with High Efficacy and Safety.* Adv Oncol Res Treat 2016. **1**(2): p. 2: 110.
129. Jia, W., et al., *Epithelial-mesenchymal Transition (EMT) Markers in Human Pituitary Adenomas Indicate a Clinical Course.* Anticancer Research, 2015. **35**(5): p. 2635-2643.
130. Chetty, R. and S. Serra, *Membrane loss and aberrant nuclear localization of E-cadherin are consistent features of solid pseudopapillary tumour of the pancreas. An immunohistochemical study using two antibodies recognizing different domains of the E-cadherin molecule.* Histopathology, 2008. **52**(3): p. 325-330.

6. REFERENCES

131. Taneyhill, L.A., E.G. Coles, and M. Bronner-Fraser, *Snail2 directly represses cadherin6B during epithelial-to-mesenchymal transitions of the neural crest.* Development (Cambridge, England), 2007. **134**(8): p. 1481-1490.
132. Samatov, T.R., et al., *miRNA-mediated expression switch of cell adhesion genes driven by microcirculation in chip.* BioChip Journal, 2017. **11**(4): p. 262-269.
133. Sung, C.O., et al., *Genomic profiling combined with gene expression profiling in primary central nervous system lymphoma.* Blood, 2011. **117**(4): p. 1291.
134. Wang, Y., et al., *The Role of Snail in EMT and Tumorigenesis.* Current cancer drug targets, 2013. **13**(9): p. 963-972.
135. Quan, T., et al., *Reduced Expression of Connective Tissue Growth Factor (CTGF/CCN2) Mediates Collagen Loss in Chronologically Aged Human Skin.* Journal of Investigative Dermatology, 2010. **130**(2): p. 415-424.
136. Arnott, J.A., et al., *The Role of Connective Tissue Growth Factor (CTGF/CCN2) in Skeletogenesis.* Critical Reviews in Eukaryotic Gene Expression, 2011. **21**(1): p. 43-69.
137. Duncan, M.R., et al., *Connective tissue growth factor mediates transforming growth factor beta-induced collagen synthesis: down-regulation by cAMP.* FASEB J, 1999. **13**(13): p. 1774-86.

I have tried to contact all copyright owners of external figures used in this work and obtained the right to use the respective figures in this work. However, in case of a copyright infringement, please notify me at maria.vallianou@meduniwien.ac.at**.**

7. Appendix

7.1 List of Abbreviations

2D	two-dimensional
2-DG	2-deoxyglucose
3D	three-dimensional
ACC	acetyl-CoA carboxylase
ACLY	ATP citrate lyase
AEC	aminoethyl carbazole
ALM	acral lentiginous melanoma
ATCC	American Type Cell Culture Collection
ATP	adenosine triphosphate
BLT-1	blocker of lipid transport 1
BRAF	v-Raf murine sarcoma viral oncogene homolog B1
BSA	bovine serum albumin
CDKN2A	cyclin-dependent kinase inhibitor 2A
CE	cholesteryl ester
COL12A1	extracellular matrix gene collagen 12 alpha-1 chain
CSD	chronic sun-damage
CTD110.6	O-GlcNAc antibody
CTGF	connective tissue growth factor
DAPI	4',6-diamidino-2-phenylindole
DMSO	dimethyl sulfoxide
DNA	deoxyribonucleic acid
ECM	extracellular matrix
EDTA	ethylenediaminetetra-acetic acid
EGF	epidermal growth factor
EMT	epithelial-mesenchymal transition
FASN	fatty acid synthase
FCS	fetal calf serum
H&E	hematoxylin and eosin
HDL	high-density lipoproteins
HMG-CoA	enzyme 3-methyl-glutaryl-coenzyme A
IARC	International Agency for Research on Cancer
IF	Immunofluorescence
IHC	Immunohistochemistry

IL-6	interleukin-6
KIT	c-kit
LCAT	lecithin-cholesterol acyltransferase enzyme
LDL	low density lipoproteins
LMM	lentigo maligna melanoma
MAPK	mitogen-activated protein kinase
MIM	melanoma isolation media
MUP	melanomas of unknown primary
NF1	neurofibromin 1
NM	nodular melanoma
NRAS	neuroblastoma RAS
PAP	phosphatidate phosphatase
PAS	Periodic acid - schiff
PBS	phosphate buffered saline
PTM	post-translational modification
qPCR	quantitative polymerase chain reaction
Ras	rat sarcoma
RNA	ribonucleic acid
SCD	stearoyl-CoA desaturase
shRNA	small hairpin RNA
siRNA	small interfering RNA
SR-BI	scavenger receptor class B type I
SSM	superficial spreading melanoma
STAT5	signal transducer and activator of transcription 5
SWI/SNF	mating-type switching/sucrose non-fermentable
TERT	telomerase reverse transcriptase
TP53	tumor protein p53
UV	ultraviolet radiation
VEGFA	vascular endothelial growth factor A
WGA	wheat-germ agglutinin
WHO	World Health Organization
WNT	int/wingless

7.2 List of Figures

7. APPENDIX

7.3 List of Tables

7.4 List of p-values

List of p-values of all figures

Figure 21

control	*vs sample*	p-value
1205Lu spheroids w non-targeting siRNA	1205Lu spheroids w SR-BI targeting siRNA	0.0193
MCM1DLN spheroids w non-targeting siRNA	MCM1DLN spheroids w SR-BI targeting siRNA	0.0236
451Lu spheroids w non-targeting siRNA	451Lu spheroids w SR-BI targeting siRNA	< 0.0001

Figure 22

control	*vs sample:*	p-value
MCM1DLN spheroids treated with:	MCM1DLN spheroids treated with:	
DMSO	2-DG 5 mM	0.0001
DMSO	BLT-1 1 µM	0.0011
DMSO	BLT-1 3 µM	0.0010
DMSO	BLT-1 9 µM	< 0.0001
DMSO	Lovastatin 5 µM	< 0.0001
DMSO	Lovastatin 10 µM	< 0.0001
DMSO	BLT-1 1 µM & Lovastatin 5 µM	< 0.0001
DMSO	BLT-1 1 µM & Lovastatin 10 µM	< 0.0001
DMSO	BLT-1 3 µM & Lovastatin 5 µM	< 0.0001
DMSO	BLT-1 3 µM & Lovastatin 10 µM	< 0.0001
DMSO	BLT-1 9 µM & Lovastatin 5 µM	< 0.0001
DMSO	BLT-1 9 µM & Lovastatin 10 µM	< 0.0001
DMSO	spheroids w non-targeting siRNA	0.0014
DMSO	spheroids w SRBI targeting siRNA	0.0027

Figure 23

control	*vs sample:*	p-value
1205Lu spheroids treated with:	1205Lu spheroids treated with:	
DMSO	2-DG 5 mM	n.a.
DMSO	BLT-1 1 µM	0.0472
DMSO	BLT-1 3 µM	0.0025
DMSO	BLT-1 9 µM	0.0010
DMSO	Lovastatin 5 µM	0.6629
DMSO	Lovastatin 10 µM	0.1655
DMSO	BLT-1 1 µM & Lovastatin 5 µM	0.0058
DMSO	BLT-1 1 µM & Lovastatin 10 µM	0.0021
DMSO	BLT-1 3 µM & Lovastatin 5 µM	0.0140
DMSO	BLT-1 3 µM & Lovastatin 10 µM	0.0131
DMSO	BLT-1 9 µM & Lovastatin 5 µM	0.0013
DMSO	BLT-1 9 µM & Lovastatin 10 µM	0.0011
DMSO	spheroids w non-targeting siRNA	0.1632
DMSO	spheroids w SRBI targeting siRNA	0.6998

Figure 24

control	*vs sample:*	p-value
WM3854 spheroids treated with:	WM3854 spheroids treated with:	
DMSO	2-DG 5 mM	< 0.0001
DMSO	BLT-1 1 µM	0.1844
DMSO	BLT-1 3 µM	0.0001
DMSO	BLT-1 9 µM	0.0001
DMSO	Lovastatin 5 µM	0.0012
DMSO	Lovastatin 10 µM	0.0004
DMSO	BLT-1 1 µM & Lovastatin 5 µM	< 0.0001
DMSO	BLT-1 1 µM & Lovastatin 10 µM	< 0.0001
DMSO	BLT-1 3 µM & Lovastatin 5 µM	< 0.0001
DMSO	BLT-1 3 µM & Lovastatin 10 µM	< 0.0001
DMSO	BLT-1 9 µM & Lovastatin 5 µM	< 0.0001
DMSO	BLT-1 9 µM & Lovastatin 10 µM	< 0.0001
DMSO	spheroids w non-targeting siRNA	< 0.0001
DMSO	spheroids w SRBI targeting siRNA	0.0006

7. APPENDIX

Figure 25

control	*vs sample:*	p-value
WM793b spheroids treated with:	WM793b spheroids treated with:	
DMSO	2-DG 5 mM	< 0.0001
DMSO	BLT-1 1 μM	< 0.0001
DMSO	BLT-1 3 μM	< 0.0001
DMSO	BLT-1 9 μM	< 0.0001
DMSO	Lovastatin 5 μM	< 0.0001
DMSO	Lovastatin 10 μM	< 0.0001
DMSO	BLT-1 1 μM & Lovastatin 5 μM	< 0.0001
DMSO	BLT-1 1 μM & Lovastatin 10 μM	< 0.0001
DMSO	BLT-1 3 μM & Lovastatin 5 μM	< 0.0001
DMSO	BLT-1 3 μM & Lovastatin 10 μM	< 0.0001
DMSO	BLT-1 9 μM & Lovastatin 5 μM	< 0.0001
DMSO	BLT-1 9 μM & Lovastatin 10 μM	< 0.0001
DMSO	spheroids w non-targeting siRNA	0.0044
DMSO	spheroids w SRBI targeting siRNA	< 0.0001

Figure 27

control	*vs sample:*	p-value
MCM1DLN spheroids treated with:	MCM1DLN spheroids treated with:	
DMSO	Lovastatin 5 μM	< 0.0001
DMSO	BLT-1 1 μM	0.0082
DMSO	BLT-1 1 μM & Lovastatin 5 μM	< 0.0001
DMSO	spheroids w non-targeting siRNA	0.2513
DMSO	spheroids w SRBI targeting siRNA	0.1590

Figure 29

control	*vs sample:*	p-value
1205Lu spheroids treated with:	1205Lu spheroids treated with:	
DMSO	Lovastatin 5 μM	0.2797
DMSO	BLT-1 1 μM	0.3631
DMSO	BLT-1 1 μM & Lovastatin 5 μM	0.1610
DMSO	spheroids w non-targeting siRNA	0.2071
DMSO	spheroids w SRBI targeting siRNA	0.0538

Figure 35

control	*vs sample:*	p-value
1205Lu cells w non-targeting siRNA	1205Lu cells w SR-BI targeting siRNA	0.0017
MCM1DLN cells w non-targeting siRNA	MCM1DLN cells w SR-BI targeting siRNA	0.0001

7. APPENDIX

Figure 36 d.

control	*vs sample:*	p-value
1205Lu cells w non-targeting siRNA	1205Lu cells w SR-BI targeting siRNA	< 0.0001
MCM1DLN cells w non-targeting siRNA	MCM1DLN cells w SR-BI targeting siRNA	< 0.0001
451Lu cells w non-targeting siRNA	451Lu cells w SR-BI targeting siRNA	< 0.0001

Figure 37 d.

control	*vs sample:*	p-value
1205Lu cells w non-targeting siRNA	1205Lu cells w SR-BI targeting siRNA	0.0632
MCM1DLN cells w non-targeting siRNA	MCM1DLN cells w SR-BI targeting siRNA	0.0004
451Lu cells w non-targeting siRNA	451Lu cells w SR-BI targeting siRNA	n.a.

Figure 38 d.

control	*vs sample:*	p-value
1205Lu cells w non-targeting siRNA	1205Lu cells w SR-BI targeting siRNA	0.0081
MCM1DLN cells w non-targeting siRNA	MCM1DLN cells w SR-BI targeting siRNA	0.1446
451Lu cells w non-targeting siRNA	451Lu cells w SR-BI targeting siRNA	n.a.

Figure 39 c.

control	*vs sample:*	p-value
MCM1DLN cells w non-targeting siRNA	MCM1DLN cells w SR-BI targeting siRNA	< 0.0001

Figure 40 d.

control	*vs sample:*	p-value
1205Lu cells w non-targeting siRNA	1205Lu cells w SR-BI targeting siRNA	0.0072
MCM1DLN cells w non-targeting siRNA	MCM1DLN cells w SR-BI targeting siRNA	0.0405
451Lu cells w non-targeting siRNA	451Lu cells w SR-BI targeting siRNA	0.0637

Figure 41 d.

control	*vs sample:*	p-value
1205Lu cells w non-targeting siRNA	1205Lu cells w SR-BI targeting siRNA	0.0128
MCM1DLN cells w non-targeting siRNA	MCM1DLN cells w SR-BI targeting siRNA	0.0086
451Lu cells w non-targeting siRNA	451Lu cells w SR-BI targeting siRNA	0.0159

Figure 42 d.

control	*vs sample:*	p-value
1205Lu cells w non-targeting siRNA	1205Lu cells w SR-BI targeting siRNA	0.0002
MCM1DLN cells w non-targeting siRNA	MCM1DLN cells w SR-BI targeting siRNA	< 0.0001
451Lu cells w non-targeting siRNA	451Lu cells w SR-BI targeting siRNA	0.4809